The Effect of Hydrogen and Hydrides on the Integrity of Zirconium Alloy Components

Hydride Reorientation

Author

Manfred P. Puls
Oakville, Ontario, Canada

A.N.T. INTERNATIONAL®

Advanced Nuclear Technology International
Spinnerivägen 1, Mellersta Fabriken plan 4,
448 50 Tollered, Sweden

info@antinternational.com
www.antinternational.com

Ecolabelled printed matter, 441 799

Disclaimer

The information presented in this report has been compiled and analysed by Advanced Nuclear Technology International Europe AB (ANT International®) and its subcontractors. ANT International has exercised due diligence in this work, but does not warrant the accuracy or completeness of the information. ANT International does not assume any responsibility for any consequences as a result of the use of the information for any party, except a warranty for reasonable technical skill, which is limited to the amount paid for this report.

Quality-checked and authorized by:

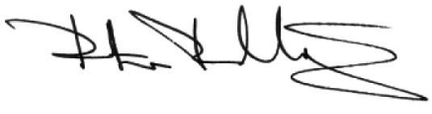

Mr Peter Rudling, President of ANT International

Contents

1 Introduction

This Stand Alone Report (SAR) provides a comprehensive review and critical analysis of studies carried out to determine the conditions governing hydride orientation in tubular components made of zirconium alloys used in nuclear reactors. It is a follow-up to a recent book by the author [Puls, 2012] entitled: The Effect of Hydrogen and Hydrides on the Integrity of Zirconium Alloy Components: Delayed Hydride Cracking. In that book, as the title emplies, emphasis was placed on establishing the physical foundations needed to understand and predict the phenomenon of Delayed Hydride Cracking (DHC). This is a phenomenon that can occur even at low hydrogen contents in high strength zirconium alloys and is little affected by the orientations and volume fractions of hydride precipitates contained in the bulk of the material.

In the very early experimental studies of the effect of hydride precipitates on the integrity of fuel cladding and pressure tube components, the phenomenon of DHC had not yet been discovered as a possible degradation mechanism. Emphasis was placed at that time on the overall fracture toughness behaviour of the material as affected by increasing volume fraction of hydride precipitates, given that this latter phase had been found to be more brittle than the zirconium alloy matrix material in which these hydride precipitates form. It was found that the orientation of hydride precipitates plays a much more important role in determining the fracture toughness of these components than does, for instance, their volume fraction. This is because, at hydrogen contents of practical importance, hydrides form as approximately linear arrays[1] of platelet-shaped microscopic precipitates with habits on or near the basal planes of the α–Zr matrix in which they form. In the highly textured fuel cladding and pressure tube components these stringers have predominantly two tube orientations: circumferential and/or radial. In the earliest investigations of zirconium alloys used in fuel cladding and pressure tubes it was found that the fracture toughness of such tubes were significantly degraded when the orientations of the hydride precipitate clusters were in the radial direction of the tube wall compared to when their orientations were in the circumferential (hoop) direction. Hence, during the early development stages of these components, efforts were directed towards finding manufacturing processes that would result in the precipitation of mostly circumferentially oriented hydride stringers in externally unstressed tubes when cooled to temperatures at which hydride precipitation occurs. However, it was also found that a sufficiently large tensile hoop stress applied during cooling in these tubes could result in the reorientation of hydride stringers from the circumferential to the radial direction accompanied by a significant reduction in fracture toughness.

Overall, as reflected in the studies covered in this SAR, the greatest concern has been with the role of hydrides on the integrity of fuel cladding tubes rather than pressure tubes because the former components absorb considerably more hydrogen to the end of their design life during residency in the reactor than do pressure tubes, even though the residence time of the former is considerably shorter. Moreover, the continual drive by the industry to achieve greater operating efficiencies by extending the length of time between refuelling has led to the need for the development of fuel cladding components capable of maintaining their structural integrity under normal and design-basis accident conditions for ever increasing volume fractions of hydrides in the material.

In recent years emphasis has also been directed at quantifying the potential for hydride reorientation in fuel cladding tubes when these tubes are removed from wet storage and transported for placement in longer-term dry storage facilities. During dry storage of spent fuel, a hoop stress is imparted on the cladding by the inner gas pressure whilst the cladding temperature decreases gradually from several hundred degrees Celsius over several decades. Under such conditions, stress reorientation of hydride precipitates to the radial direction of the cladding tube could be possible which, then, could also make possible a severe decrease in fracture toughness of the cladding material.

As noted, the underlying physical basis of the phenomenon treated here has largely been provided in the recent book by Puls [Puls, 2012] and the reader is referred to this reference for such background. The main aim of the present account, thus, is to provide a comprehensive summary and critical assessment – from the earliest up to the most recent times – of the literature information on the experimental and theoretical methods used to study the factors affecting hydride reorientation.

This SAR is organized into six main sections (equivalent to chapters in a book) with the various topics in each section treated in roughly chronological order. Section 1, given here, provides a brief introduction. Section 2

[1] Variously referred to as stringers or clusters.

summarizes the results of the earliest experimental studies on this topic. Section 3 gives an updated version of the original derivation of Ells and Puls of the theory of hydride reorientation based on classical nucleation theory. Section 4 – the longest section in this SAR, starting from the earliest to the most recent studies – deals with various applications of the Ells/Puls theoretical model to experimental data. Recent extensions to the foregoing theory are then discussed followed by accounts of other studies and methods of quantifying hydride reorientation, both in unirradiated and pre-irradiated material. A large subsection in this section is devoted to the results of *in situ* synchrotron X-ray studies. These studies have enabled real time observations of the evolution and characteristics of hydride precipitation during cooling and heating with and without external stress. Motivated by the need to interpret these results, an analysis based partially on results of Eshelby's theory of the stress state within and at the boundary of misfitting inclusions is used to explain the *in situ* observations of strain variations in hydride and matrix during heating and cooling with and without an externally applied tensile stress. Section 5 deals with theoretical computations based on the Phase Field Methodology of the evolution of hydride precipitate morphology and stress state under various thermo-mechanical cycles. These studies have been supplemented by *ab initio* atomistic models, the applications of which allow for the determination of the crystal structure and hydrogen compositions of hydride precipitates formed during the nucleation and early growth periods of hydride formation. Finally, Section 6 gives summaries of the foregoing studies, highlighting the conclusions drawn from each of these. This section is lengthier than is usually found in reports of this type, the reason for this greater length being to provide the reader with a relatively concise yet still sufficiently detailed account that it can be understood without the inclusion of all of the figures and almost all of the equations given in the preceding sections. Throughout this text, including Section 6, important findings and associated conclusions have been highlighted by placing them in italic font.

2 Early observations of factors determining hydride orientations

At the start of the development in the 1950s of zirconium alloy components for fuel cladding and pressure tube components there was concern that the presence of hydrides in these components could have deleterious influences on their mechanical properties. These concerns were initially allayed because studies had shown that even in material containing up to 1000 wppm hydrogen, the presence of the resultant large volume fraction of hydrides – which have up to this hydrogen content in these materials an approximately plate-shaped morphology when uniformly distributed – caused little reduction in their ductility. It was only when failures of some Zircaloy-2 fuel claddings irradiated at the Savanah River Plant, USA, showed that this failure had occurred in the heavily hydrogenated regions of the outer cladding where, locally, approximately 500 to 800 wppm hydrogen had accumulated and where hydrides had precipitated with their plate normals in the circumferential direction, did it become evident that hydride orientation with respect to the applied tensile stress axis could be an important factor in affecting the ductility of hydride-containing zirconium alloys. (Hydrides aligned with their plate normals in the circumferential direction are in the literature referred to as radial because, when viewed in optical micrographs of tube sections with normals either in the axial (longitudinal) or the radial directions of the tube show up on edge, elongated in the radial and axial tube directions, respectively. Similarly, hydrides oriented with their plate normals in the radial direction are referred to as circumferential hydrides as they have their plate edges elongated in the circumferential and axial directions.)

Marshall and Louthan [Marshall & Louthan, 1963] showed that failure of these irradiated fuel tubes could be attributed to the radial orientation of the hydrides in the heavily hydrogenated region. The authors noted that in all previous deformation tests hydride precipitates had been oriented circumferentially such that they were approximately aligned along the externally applied tensile stress axis, with the result that these hydrides had little deleterious effects on the material's mechanical properties.

At about the same time as the Savannah River fuel cladding failures had occurred, a similar failure, also attributed to radially oriented hydrides, was observed in a failed swaged fuel element at the Chalk River Nuclear Laboratories, Chalk River, Canada [Parry & Evans, 1962]. To explain these results Parry and Evans analysed hydride orientations in hydrogenated (100 wppm) zirconium alloy specimens (consisting of plates, wires and sections of pressure tubes) subjected to various amounts of bending strain. The authors concluded that, comparing hydride orientation in bent and unbent specimens, hydride orientation, as exhibited by the directions of the normals to the platelet-shaped faces of the hydride clusters, is governed by the strain applied to the material, both through the retained strain produced during its manufacture and through the added amount produced by bending. They concluded that zirconium hydride platelets oriented themselves along the direction along which the material is deformed, parallel to any applied tensile strains and perpendicular to any applied compressive strains. In addition, they found that there was a limiting applied strain of about 7% below which no strain orientation of the hydrides occurred.

In a parallel study restricted to specimens cut from Zircaloy-2 tubes Louthan and Marshall [Louthan & Marshall, 1963] showed – in agreement with the findings of Parry and Evans [Parry & Evans, 1962] – that alignment of the hydride precipitates in the as-received state depended on the type and magnitude of deformation experienced by the tubes during their manufacture. *Parry and Evans were the first to show that this alignment could be changed during hydride precipitation when the component is subjected to a suitably oriented and sufficiently large external stress. By comparing the hydride orientations found in tubes produced by different manufacturing routes before and after application of external tensile or compressive stresses these latter authors showed that manufacturing processes resulting in tube wall reduction (compression) during forming had the strongest tendency for hydrides to be aligned. The alignment in these tubes was with the plate normal of the hydrides oriented in the radial direction, i.e., the in-plane alignment of the hydride platelets was along the direction of plastic flow of the material experienced during the compression. Louthan and Marshall [Louthan & Marshall, 1963] found that there was a threshold stress that needed to be exceeded before reoriented hydrides were obtained in such materials during hydride precipitation under a tensile stress. This threshold stress was largest for tube manufacturing processes resulting in the greatest degree of alignment of the hydride precipitates along the tube's circumferential direction when cooled under no externally applied stresses.*

The importance that hydride orientation has on the mechanical properties – shown for the first time by Marshall and Louthan [Marshall & Louthan, 1963] – resulted in a large number of subsequent studies carried out to elucidate the factors and underlying mechanisms controlling hydride orientation in tube components during normal and abnormal service conditions. The primary practical purpose of these studies was to insure that

hydrides in as-manufactured pressure tubes and fuel claddings would be preferentially aligned along the circumferential-axial directions and would remain so during service under normal operating conditions.

In the first of these studies, Kearns and Woods [Kearns & Woods, 1966] subjected various (mostly) Zircaloy-4 tubing and a few plate materials to a wide range of thermo-mechanical treatments and examined the hydride orienting tendencies of these materials as a function of whether an external stress was applied or not during cooling. The objective of these studies was to better understand the role that underlying properties such as crystallographic texture, grain size, hydride nucleation sites and amount of cold work would have on hydride orientating tendencies. To determine the role of texture in affecting hydride alignment tendencies, Kearns conceived of two simpler measures that can be derived from the more detailed graphical measure of texture prevalent at the time given by the inverse pole representation. One of these measures was the volume fraction of crystals having their basal poles in a specified orientation direction with respect to a reference direction. The other measure, denoted by the parameter, "f_d ", where "d" is a reference direction, was the determination of the resolved fraction of basal poles of the hexagonal close packed (hcp) crystallites aligned in a given reference direction. This latter measure, which has subsequently often been referred to as the Kearns factor, has found wide use as a succinct indicator of the crystallographic texture of a component in relation to its geometry. The reference directions for the foregoing measures are usually chosen as the orthogonal directions characterizing the principal directions of a sample or component. A useful property of the Kearns factors for the three orthogonal directions of a specimen or component is that their sum must equal unity. A sample having a random distribution of grain orientations is described as having no texture. In such a sample all three grain orientations would be equally represented and therefore each of the three Kearns factors would be equal to 1/3. In Zr alloys this sum rule could be useful for sample configurations such as tubes and rolled plates becausef_d in the working (axial or longitudinal) direction is usually less than 0.1. Hence, approximate values of the Kearns factors in the other two directions could be obtained by inverse pole figure measurements of the sample with the X-ray beam oriented in only one of the two remaining orthogonal sample directions. An example showing the relationship between the inverse pole figure characterization of texture in a plate sample with the calculated volume distribution of basal poles and their associated Kearns factors is given in Figure 2-1.

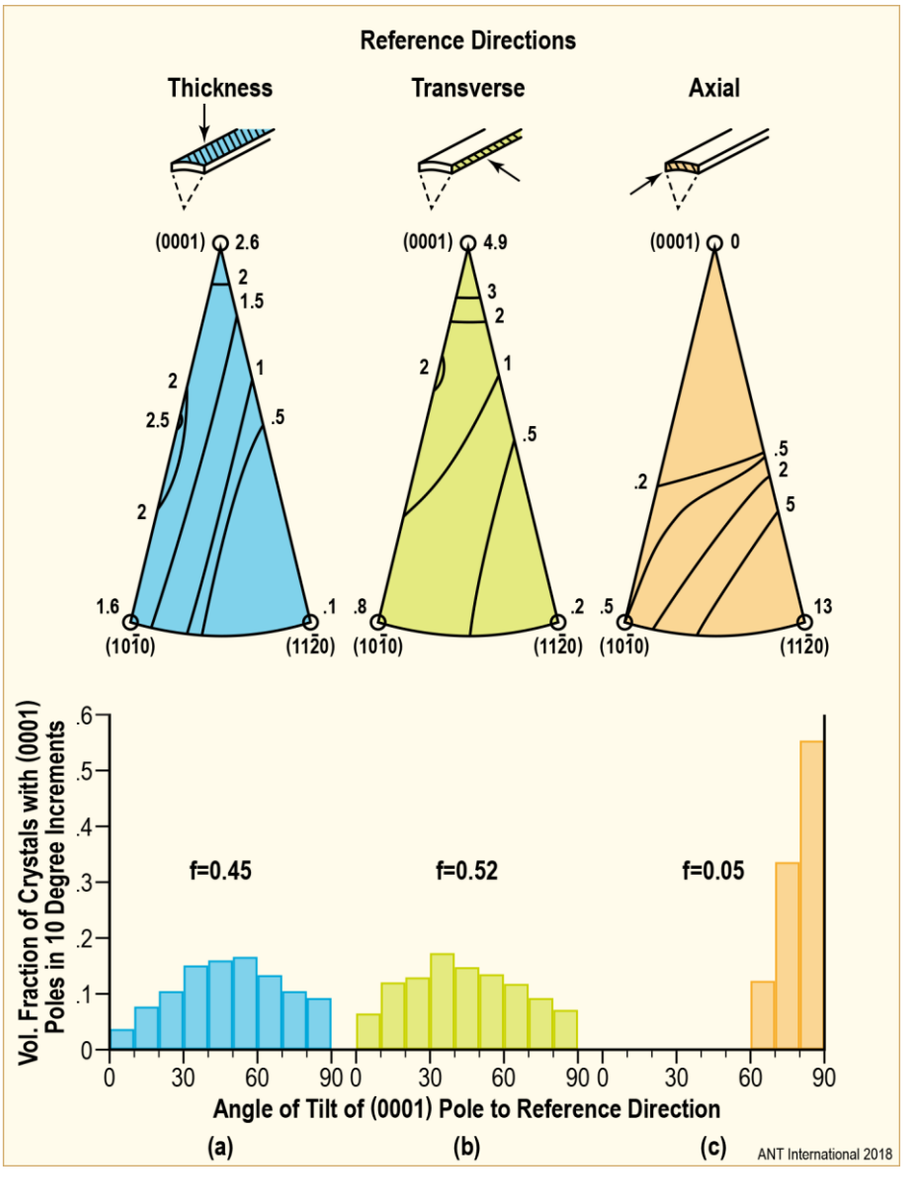

Figure 2-1: Inverse pole figure characterization of texture in tubing (from [Kearns & Woods, 1966]). Numbers on contour lines indicate orientation densities (times random) with respect to reference direction. Histograms show corresponding (calculated) volume distributions of basal poles.

Kearns and Wood [Kearns & Woods, 1966] determined that the basal pole textures in the Zircaloy materials studied depended primarily on the prior conditions of deformation rather than on subsequent annealing of the material in the alpha phase, the latter mostly altering only the orientation of poles of the $(1\ 1\ \bar{2}\ 0)_{\alpha-Zr}$ and $(1\ 0\ \bar{1}\ 0)_{\alpha-Zr}$ planes. Basal poles tend to predominate in directions perpendicular to the working directions with a difference in orientation found only in the two directions transverse to the working or rolling direction. For plates, the distributions between the two directions were roughly two thirds to one third in the thickness and transverse directions, respectively, whilst the fuel cladding tubes studied by Kearns and Woods [Kearns & Woods, 1966] generally had a greater fraction of grains oriented with their basal poles in the circumferential direction. The authors point out that a key factor in the control of texture is the ratio of the diameter to wall reduction during forming. Low values of this ratio result in a larger fraction of basal poles oriented in the thickness (i.e., radial for a tube) direction whilst high values result in a larger fraction of basal poles oriented in the circumferential direction.

As was done by Louthan and Marshall [Louthan & Marshall, 1963], the authors compared the orienting tendencies of hydrides in tubes and plates when these precipitate during cooling in the presence or absence of external stress. *As Kearns and Woods [Kearns & Woods, 1966] noted, ideally, correlation of hydride orientation with texture should be done on the basis of the spatial orientation of the hydride platelets and the appropriate*

crystallographic (habit) planes on which they reside. Thus correlating the observed macroscopic hydride orientations with the calculated Kearns factors was shown not to be very useful since the specific crystallographic orientation of each hydride platelet is hidden in the averaging procedure used in calculating these factors. The authors found, instead, that for both externally stressed and unstressed samples, hydride orientation correlated best with the volume distribution of the basal pole orientations – an example of which is given in Figure 2-2– rather than the resultant basal pole Kearns factors. Comparison of the orienting tendencies of hydrides in tubes subjected to different thermo-mechanical treatment cooled with and without applied external stress showed that an important factor in the increase in orienting tendency in externally stressed samples was the decrease in grain size and increase in fractions of grains oriented with their basal poles parallel to the stress axis. The authors' interpretation of their results was hampered somewhat, however, by the lack of available data on the habit planes of hydride precipitates and whether these differed between hydrides precipitated with or without an externally applied stress. In fact, it wasn't clear at the time whether hydride platelets favoured more than one habit plane and, if yes, whether these habit planes covered a narrow or wide range of orientations. Based on the finding from their data that hydride orienting tendency increased with decreasing grain size, Kearns and Woods [Kearns & Woods, 1966] concluded that this could only be the case if hydrides favoured a single or a narrow range of habit plane orientation(s). This conclusion differed from that by Louthan and Angerman [Louthan & Angerman, 1966] who argued that the assumption of a single or narrow range of habit planes for hydride precipitation combined with this being the same for hydride precipitation with or without application of external stress would mean that there could be no stress orienting effect. It is worth repeating Kearns and Woods' reasoning here because it demonstrates an important point regarding the usefulness of the Kearns factors in predicting the component directions that would be most favourable for hydride alignment with or without external stress. The argument is as follows.

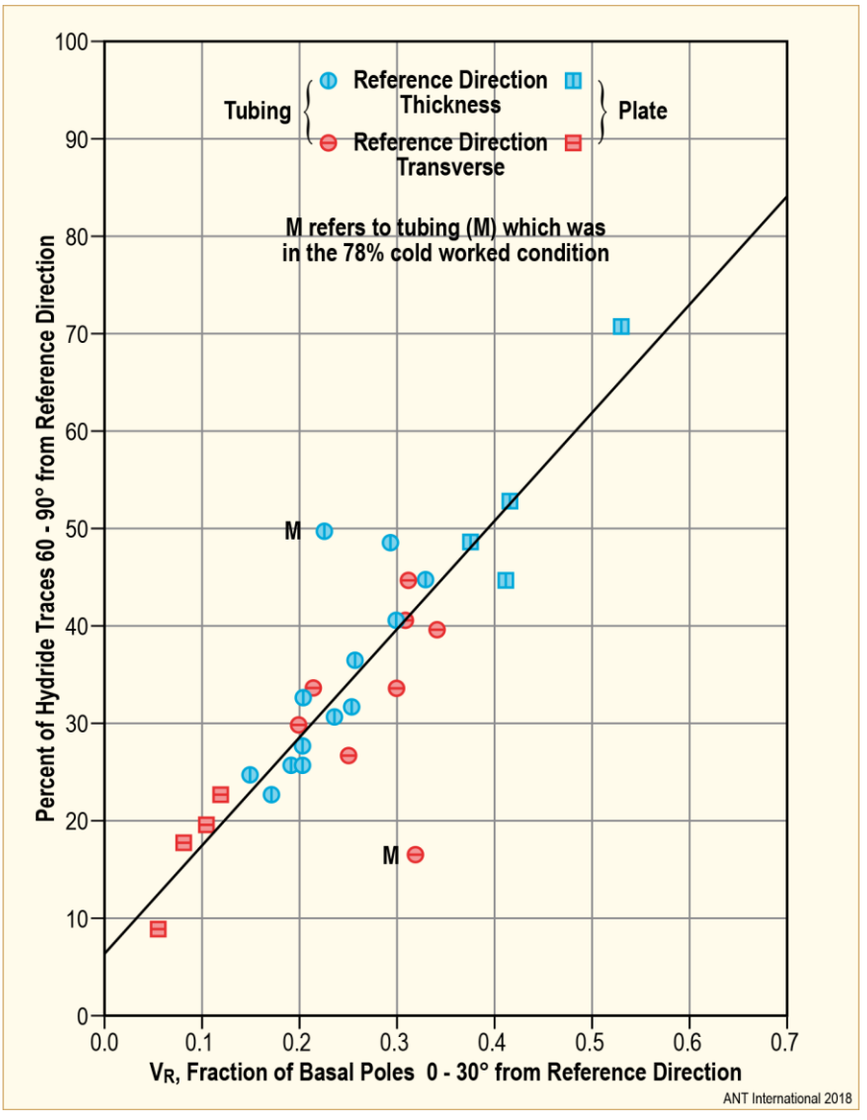

Figure 2-2: Correlation of hydride orientations with basal pole textures in samples cooled under 138 MPa uniaxial tensile stress. The solid line, labelled as average curve from Fig. 5 of the paper by Kearns and Woods [Kearns & Woods, 1966] is the correlation in unstressed samples (from [Kearns & Woods, 1966]).

Kearns and Woods [Kearns & Woods, 1966] derived a relationship between the hydrogen content in a single grain and its grain diameter by assuming each grain contained a single, plate-shaped hydride of thickness invariant with grain size. This means that for given hydrogen content in the solid, hydrogen concentration in a grain will increase as the grain size decreases. Thus, in fine-grained material, a grain containing a hydride will contain considerably more hydrogen than the average concentration in the sample. For example, for grains having an average diameter of 8 μm, a grain containing a 0.7 μm thick hydride across its diameter would contain 1300 wppm hydrogen. Thus with a sample containing a hydrogen content of 150 wppm only 10% of the grains would be occupied. *If hydrides favour only a single habit plane oriented such that the directions of hydride plate normal, matrix basal pole and external and internal (grain interaction) stress axes approximately align, then only a small fraction of the available grains would be needed for complete preferential hydride orientation.* (As we now know (for a summary discussion see Chapter 3 in Puls [Puls, 2012]), this result would depend not only on the direction and sign of the combination of internal and external tensile stress – the former of which is affected by the texture – but also on the associated hydride misfit strains that control the shape and orientation of the hydrides observed at a microscopic level.) *This means that for hydrogen contents of practical interest in components (tubes) used in nuclear reactors, only when the basal pole Kearns factor value is very low, such as in the axial direction of pressure or fuel cladding tubes, or in the rolling direction of plates, where it is generally less than 0.1, would this make hydride platelet orientation with platelet normals in this direction unlikely. For instance, the basal pole Kearns factors of pressure and fuel cladding tubes are opposite in their values for the*

circumferential and radial tube directions [Coleman & Inozemtsev, 2008; Coleman et al., 2009], being roughly 2/3 and 1/3 and vice versa, respectively, yet both tubes show similar hydride orienting behaviour under zero and non-zero externally stressed conditions. Thus in both components DHC initiation and propagation is possible on the radial-axial plane. It is somewhat ironic that the study by Kearns and Woods [Kearns & Woods, 1966], which is noteworthy for introducing the now widely used Kearns factors as a concise measure of the texture of a zirconium alloy component, also led to the conclusion that this factor has only limited utility as an indicator of the degree and direction of hydride platelet alignment with respect to the three principal directions of tubes or plates.

One unequivocal and important experimental result established by Kearns and Woods [Kearns & Woods, 1966] was that reorientation of hydrides under external stress is associated only with precipitation and does not occur under isothermal conditions. A theoretical justification as to why this is the case was first given by Ells [Ells, 1970], followed by a more refined version of this derivation by Puls [Puls, 1984a, 1986].

Parallel to the study by Kearns and Woods [Kearns & Woods, 1966], Parry [Parry, 1966] carried out tests to determine the susceptibility of cw Zr-2.5Nb pressure tube material to hydride reorientation during cooling under an applied stress. Some hydride reorientation was observed in these tests even at the lowest external stress of 110 MPa. However, for the samples containing 100 and 200 wppm hydrogen, the maximum temperature to which the samples were taken was such that during the thermal cycle there were still a substantial number of hydrides present at that temperature. This limitation on the maximum temperature of the thermal cycle was chosen in these tests because the authors' main objective was to determine the amount of hydride reorientation when cooling from the maximum pressure tube outlet temperature of the reactor, which is approximately 300°C. The report by Parry [Parry, 1966] is perhaps most noteworthy for one of the first examples showing the composite structure of hydrides in a hydride cluster extending along the pressure tube's circumferential direction in an as-received specimen. The cluster shown, reproduced in Figure 2-3, seems to fill an entire grain that is elongated, similar to all other grains visible in this section, in the circumferential direction with the individual smaller hydrides constituting this cluster arrayed as a stack of hydrides oriented at ≈45° to the circumferential direction along which the grain and the macroscopic hydride is extended. Parry [Parry, 1966] noted that the reoriented hydrides, crossing many grains, did not show such a composite structure. Both the studies of Kearns and Woods [Kearns & Woods, 1966] and Parry [Parry, 1966] showed that there were no hydrides with plate normals in the longitudinal direction of the tube in as-received or in longitudinally stressed tube specimens for tensile stresses up to 160 MPa, consistent with the close to negligible number of grains having basal poles oriented in this direction.

Figure 2-3: One of the earliest micrographs [Parry, 1966] showing the composite structure of a hydride cluster (transverse section of a Zr-2.5Nb pressure tube cooled under no external stress).

The study by Parry [Parry, 1966] was followed a year later by two papers by Marshall [Marshall, 1967a, 1967b], one dealing with the influence of fabrication history on stress reorientation of hydrides in Zircaloy tubing and the other dealing with how different tube fabrication processes control the hydride orientations in externally

unstressed tubes, respectively. The usefulness of these results is somewhat limited, however, because the author did not relate the results to the texture of the material, interpreting them, instead, in terms of presumed different dislocation structures produced by different fabrication procedures.

It is evident from the foregoing that no uniform interpretation on hydride orienting tendencies had emerged in relation to hydride habit planes, crystallographic texture and the presence or absence of residual and externally applied stress. To help clear up this uncertainty, Schelzke [Schelzke, 1969] focussed his experimental study on the effect that changes in texture have on the orienting tendencies of hydrides in the presence or absence of externally applied stress in hydrogenated, cold-worked, thin-walled Zircaloy tubes. *A statistical treatment of the observed traces of hydride platelets in as-received tube specimens as evidenced from metallographic sections normal to one of the three principal tube directions (axial, circumferential and radial) showed that hydride platelets generally occupied habit planes with normals ranging from 5 to 20° from the basal pole orientation. It was observed that hydrides were reoriented by external stress, but only when located in those grains having their basal pole direction oriented within the foregoing narrow angular range with respect to the stress axis. Within this narrow range of stress application, the hydride platelet traces were observed to align themselves parallel to the stress direction under compression and perpendicular to the applied stress direction under tension. In as-received material no hydrides had precipitated with their normals in the axial tube direction, consistent with the very small number of grains having basal poles oriented in this direction. The preferred hydride habit plane orientations determined in Schelzke's work are in agreement with the findings of Babayak [Babayak, 1967] and Westlake [Westlake, 1968] for the same alloys. The orientation of the hydrides in the as-received state was interpreted qualitatively by Schelzke [Schelzke, 1969] as being a consequence of residual stresses produced in the grains, the sign, magnitude and direction of which was influenced by the orientation of a particular grain with respect to the cold working direction of the tube. Qualitative interpretation of the foregoing experimental results led to the conclusion that crystallographic texture plays a dual role in influencing hydride orientation. One role is that there must be a sufficient number of grains with normals parallel to the hydride habit plane normal and the direction of internal and/or external stress. The other role is that texture affects the direction and magnitude of internal stress in each grain produced during the plastic deformation processes imposed during the manufacture of the tube.* In the thin-walled, fine-grained Zircaloy tubes investigated by Schelzke [Schelzke, 1969], hydride precipitation was mostly intra-granular; thus the foregoing conclusions are restricted to tubes in which this precipitation mode is predominant. Schelzke [Schelzke, 1969] found that annealing of these tubes up to 500°C resulted in no changes in the orienting tendencies of hydrides in externally unstressed tubes. However, from 550°C and above, hydrides in externally unstressed tubes became increasingly more randomly oriented. This was attributed by the author as occurring as a result of the consequence of two factors: the reduction in internal stresses and a change in basal pole texture to a more random distribution in the radial-circumferential plane. *Ells [Ells, 1968], in his review of hydride precipitation in zirconium alloys, noted that another effect of texture in influencing the magnitude and direction of residual stresses of individual grains is the anisotropy of thermal expansion, suggesting that this could result in stresses as high as 138* MPa *in some grain orientations when cooled from 400°*C *to ambient temperature.* In connection with this, Ells [Ells, 1970] noted a recent paper in which a theoretical explanation for stress orienting of $Fe_{16}N_2$ precipitates was developed by Li [Li, 1967], anticipating the application by Ells of this model by Li in quantifying the extent of hydride reorientation as a function of stress applied during precipitation.

It can be seen from the foregoing studies that already by the end of the 1960s, a number of key observations concerning hydride orientations in tubes had been established. These observations are:

a) Hydrides formed under slow cooling conditions show up as irregularly shaped elongated stringers when viewed at optical magnifications. (A hydride stringer is defined here as a collection of linear features, the thickness, length and distribution of which depends on the material's texture, hydrogen content and cooling rate.)

b) In externally unstressed tubes, hydride stringers are preferentially oriented with their traces in the circumferential/axial tube directions. The shapes and orientations of the broad outlines of these stringers are similar to those of the grains in which they are contained. Selected observations indicate that these transverse stringers consist of a collection of clusters of short individual hydrides tilted ≈45° to the circumferential tube direction in the circumferential-radial plane.

c) Stress applied during hydride precipitation produces hydride stringers oriented with their traces perpendicular to the direction of tensile stress and parallel to the direction of compressive stress.

d) Stress applied during isothermal hold after a cool down (during which there would be no further hydride precipitation) does not affect the existing distribution of hydride orientations.

e) Reorientation of hydride stringers from circumferential to radial direction by an external tensile stress applied in the circumferential direction during hydride precipitation requires that the applied stress exceed a threshold stress. Above this threshold stress value, the proportion of reoriented hydride stringers increases with increase in the magnitude of the external tensile stress.

f) The smaller hydride platelets making up a stringer all resided on similar, preferred habit planes with respect to the α–Zr matrix grains in which they are located. The individual hydride habit planes are the same irrespective of whether the macroscopic orientations of the stringers were changed with application of an external stress.

g) In commercial α– and α/β–zirconium alloys (Zircaloys and Zr-2.5Nb, respectively) the habit planes of hydride platelets – as deduced from optical observations of hydride stringers – are oriented 5 to 20° from the basal pole direction of the α–Zr matrix grains in which they form. This result is consistent with hydride habit planes of $\{1\ 0\ \bar{1}\ 7\}_{\alpha-Zr}$ (≈ 14° from the basal pole direction) determined subsequently in these alloys.

h) Based on the information given in items a) to f), it is concluded that the observed preferred circumferential orientation of hydride stringers in externally unstressed, cold-worked, fine-grained material occurs because of the presence of internal tensile stress generated in the radial tube wall direction in grains oriented with their basal poles directed in the radial direction. It is conjectured that these internal tensile stresses are produced during the reduction in wall thickness of the tubes during the cold working step provided that the cold working is such as to result in only a small reduction in diameter. In this case, plastic flow in the tube is directed in the circumferential direction.

i) The fraction of hydrides that can preferentially orient under a tensile stress in a given direction is limited by the availability of grains having favourable basal pole orientations. In general, the basal pole fraction in any direction that would be limiting for complete preferential hydride orientation would depend on the total volume fraction of hydrides at the precipitation temperature and on the grain size. In tubes in which the Kearns factor is generally less than 0.1 there are insufficient grains with basal pole orientations in the axial direction for noticeable stress-reorientation of hydrides with their platelet normals pointing in this direction.

With the exception of the study by Kearns and Woods [Kearns & Woods, 1966], the foregoing studies investigated hydride orientation and reorientation under stress after only a single precipitation cycle.

Missing from these foregoing experimental findings is a mechanistic understanding of how stress (strain) affects hydride orientation in zirconium alloy tubes. Louthan and Marshall's [Louthan & Marshall, 1963] qualitative explanation for the stress orienting effect was that a hydride platelet oriented with its normal in the direction of applied tensile stress brings about a lowering of the energy of the system because the less dense hydride provides an extension of the system in the direction of the applied stress that is greater than the elastic extension produced by the stress on the matrix that it replaces. Not clear in this explanation is exactly how the authors envisioned the energy of the system to be lowered by this extension. Parry's [Parry, 1966] interpretation for the stress orienting was that hydride formation under tensile stress results in a reduction in overall internal stresses in the system with the inference that orientation of the hydride with its platelet normal in the stress direction maximizes this effect. Although there may be such an effect for material deforming elastic-plastically, this is not the first order contribution to the lowering of the energy produced by stress orienting. In fact, within a linear elastic model of the solid, a simple rationale and corresponding mathematical relationship for the energy change produced by stress orienting had already been developed by Eshelby [Eshelby, 1957, 1961] for the general case of a misfitting precipitate spontaneously transforming from the matrix under an external stress. Eshelby [Eshelby, 1957, 1961] called this energy change the interaction energy. Eshelby [Eshelby, 1957, 1961] points out that within the continuum, linear elastic description of a solid, the stress fields generated by the misfitting inclusion and the external load are linearly-additive. Hence, there is no cross-term between the two stress fields in this approximation. The internal energy of the system in this approximation is changed only by the self-energy of the inclusion when brought in from an external source or spontaneously produced during a phase transformation. However, this actually results in an increase in the total strain energy of the solid – regardless of the sign of the inclusion's misfit strains – whilst the interaction energy is simply the work done by the resultant movement of the external load as it is displaced at the surface of the specimen by the strains produced there when a volume of matrix material in the interior of the system is transformed to that of a misfitting inclusion. The strains of the inclusion evaluated at the surface of a finite specimen correspond to the stress-free (also referred to as transformation or eigen-) strains of the misfitting inclusion. Unfortunately, conceptually incorrect or ambiguous statements along the lines given by Louthan and Marshall [Louthan & Marshall, 1963] as to the reason for hydride stress orienting have persisted in the literature up to the present.

3 Theory of hydride stress orienting based on classical nucleation models

3.1 Overall theoretical development

The foundations of the foregoing stress orienting models of Ells [Ells, 1970] and Puls [Puls, 1984a, 1986] are derived from classical nucleation models of liquid-gas and liquid-liquid systems of Vollmer and Weber [Vollmer & Weber, 1926]. By classical is meant that – starting from the embryonic state of the new phase – there is a finite difference in structure, state and/or composition between nucleus and parent phase with a sharp interface between the two. For a system held at constant temperature below the solvus temperature, formation of the new phase is thought to occur by random statistical fluctuations of clusters (embryos) of varying sizes in which the fluctuations have produced solute compositions close to those of the equilibrium coexistence compositions between bulk quantities of the two phases. Because of the presumed sharp interface between the two phases, surface energy is created. This surface energy makes an increasing contribution to the total Gibbs free energy change for formation of the embryo as it increases in size up to a maximum value above which further increases in size result in a diminishing contribution of the surface energy change to the change in total Gibbs free energy for precipitate formation. The critical size for formation of a stable nucleus for a given undercooling below the equilibrium (bulk property) solvus is the size at which the changes in surface energy result in a maximum in Gibbs free energy change.

The earliest applications of the foregoing models to solid-solid transformations of two-component, crystalline metallic solids were mostly to substitutional solid solutions. In such systems diffusion of the two components of the solid is by a vacancy mechanism and generally involves the diffusion of both solute and solvent species at temperatures when the transformation is kinetically feasible. In substitutional solid solutions the difference in atomic radii is generally small with the result that the stress-free misfit strains (i.e., the relative differences in sizes) between the unconstrained states of daughter and parent phases are also small. In addition, with solute/solvent diffusion governed by a vacancy mechanism, at temperatures where such diffusion is rapid the misfit strains between nucleus and matrix phases is often reduced by diffusion to negligible levels by vacancy accumulation along the interphase boundary, resulting in an incoherent interface between nucleus and matrix. This is not the case expected for the Zr-H system for which one can approximate the lattice Zr atoms as being immobile with only the interstitially located H atoms in the lattice being mobile. This assumption is the basis for the classical nucleation model described in the following.

The theory for hydride stress orienting given by Puls [Puls, 1984a, 1986] follows closely the methodology developed by Sauthoff for substitutional solid solutions [Sauthoff, 1975, 1976, 1977]. The purpose of the latter author's study was to determine which of the stages of nucleation, growth and coarsening played the dominant role in stress orienting of tetragonally misfitting Au-rich, plate-shaped precipitates in the Fe-Mo-Au alloy. Unlike the initial study of stress orienting for misfitting precipitates developed by Li for the nucleation stage subsequently adopted by Ells [Ells, 1970] for the nucleation and growth stages of hydride precipitates, Sauthoff's general relationships dealt with the effect of stress on all three stages of precipitate evolution: nucleation, growth and coarsening. Moreover, Sauthoff assumed that the precipitates formed would be coherent, or partially coherent, such that they would retain at least some of their tetragonal misfit strain with the matrix. The following is a brief outline of the Ells/Puls model for hydride orientation under stress in Zr and its alloys, updated to account for the solvus relationships derived in [Puls, 2012].

In classical nucleation theory the nucleation rate is given by

Equation 3-1:

$$J^* = Z\beta^* \frac{N}{c_H^\beta} exp\left(-\frac{\Delta G^*}{k_B T}\right) exp\left(-\frac{\tau}{t}\right)$$

where J^* = time-dependent nucleation rate (the superscript $*$ denotes quantities evaluated at the size of the critical nucleus)

Z = Zeldovich non-equilibrium factor ($\approx 10^{-2}$ to 10^{-1})

β^* = rate at which atoms are added onto the critical nucleus

N = number of atomic nucleation sites per unit volume

c_H^β = atom (or mole) solute to solvent ratio (H/Zr in our case) in the critical nucleus (where β designates the precipitate phase, which for hydrides could be either the δ, γ or ε phase)

ΔG^* = free energy of activation for critical nucleus formation

τ = incubation time

t = isothermal reaction (hold) time

$k_B T$ = product of Boltzmann constant and absolute temperature, respectively

In Equation 3-1, the Zeldovich factor accounts for the fact that some supercritical nuclei decompose and that N is an over estimate of the actual number of critical nuclei that can be formed at any one time.

It is assumed in Equation 3-1 that the system has been abruptly brought to a state of super-saturation determined by the magnitude of the under-cooling from the equilibrium solvus which is the solvus corresponding to bulk quantities of the two phases at the isothermal hold temperature. This means that at the start of the isothermal hold time there would exist few, if any, metastable clusters of the precipitate phase. One would then expect there to be an incubation time, τ, before any critical nuclei would be formed after which there would be a short transient period of increasing nucleation rate followed by a regime during which there would be a constant (steady-state) increase in precipitate clusters. This steady state production of nuclei eventually would change to a decreasing, transient rate, terminating when the solute has been reduced to its equilibrium value.

The incubation time in Equation 3-1 is approximated by Russell [Russell, 1971] as:

Equation 3-2:

$$\tau = (2\beta^* Z^2)^{-1}$$

For hold times much greater than the incubation time, i.e., $t \gg \tau$, the bulk of the nuclei are formed at a constant, steady state rate, and it is over this regime that a meaningful comparison of the difference in nucleation rate for hydride platelets of different orientations with respect to an applied stress is obtained. That is, during steady state nucleation, the condition for the incubation time factor, $exp\left(-\frac{\tau}{t}\right) \rightarrow 1$, is assumed in Equation 3-1. With this assumption, the steady state nucleation rate, J_{ss}^*, is given by:

Equation 3-3:

$$J_{ss}^* = Z\beta^* \frac{N}{c_H^\beta} exp\left(-\frac{\Delta G^*}{k_B T}\right)$$

To determine the steady state nucleation rate, the factors Z and β^* need to be evaluated in addition to ΔG^*.

The Zeldovich factor is given by Russell [Russell, 1968] as:

Equation 3-4:

$$Z = \left[\frac{1}{2\pi k_B T} \cdot \left(\frac{\partial^2(\Delta G^o)}{\partial n^2}\right)_{n^*}\right]^{-1/2}$$

where n = number of atoms in an embryo

n^* = number of atoms in the critical nucleus

ΔG^o = Gibbs free energy change for the formation of a cluster of n solute atoms

The rate, β^*, at which atoms join the critical nucleus is given by Russell [Russell, 1970] as:

Equation 3-5:

$$\beta^* = \frac{S^* c_H^\alpha}{d^4} D$$

where S^* = disordered area of the critical nucleus (i.e., the area of the nucleus over which single solute atoms could be added)

D = appropriate diffusivity

c_H^α = atom (or mole) solute (H) to solvent (Zr) ratio in the matrix phase

d = distance of one lattice parameter

The definition of S^* takes account of cases where hydride nuclei form on preferred habit plane(s) producing an ordered (coherent) interface along which single atoms arriving by diffusion cannot be added.

An explicit expression for $\beta^*$for homogeneous nucleation of a disc-shaped nucleus at its critical dimensions was derived by Russell [Russell, 1970] as:

Equation 3-6:

$$\beta^* = 2\pi a^{*2} c_H^o N \frac{D_H^v}{d}$$

where a^* = radius of the disc at its critical dimensions

c_H^o = atom fraction of solute (H) in the supersaturated solution of the α–Zr phase; this is equivalent to c_H^α in Equation 3-5, but denoted by c_H^o here to indicate that in a closed system, cooling from a temperature at which all hydrides had been dissolved, it is the total hydrogen content in the solid

N = defined in the list below Equation 3-1

D_H^v = volume diffusion coefficient of the solute (H)

d = jump distance of solute (H) in the matrix (α–Zr) phase

The derivation of the critical nucleation energy for a material also subjected to external stress is given in Appendix A Here we summarize the results obtained. The notation used in the original publication [Puls, 1984a, 1986] has been changed in this text to be consistent with that used in this writer's recent book on DHC [Puls, 2012]. Only the treatment for plate-shaped δ–hydride precipitates is repeated here as these represent the most frequently observed final shapes and phase. For ease of calculations of the strain energy contributions to the change in Gibbs free energy upon formation of a hydride nucleus, the shape of the nucleus is approximated by an oblate spheroid of minor axis, *c*, and major axis, *a*. An oblate spheroid is not a suitable shape for accounting for the possibility that there are abrupt differences in the surface energy depending on the orientation of the surface. Thus for the purposes of accounting for the surface energy contributions to the total Gibbs free energy change, the shape of the nucleus is approximated by a disc of radius, *a*, and thickness, 2*c*, and assigning different surface energy values for the faces (γ_c) and the edge (γ_i) of a nucleus having such shape. The disc is assumed to be oriented in an individual grain such that its face normal is parallel to the basal pole direction of the α–Zr matrix grain in which it is located. That is, the habit plane of the hydride nucleus is assumed to have the following crystallographic orientation relationship: $\{0\ 0\ 0\ 2\}_{\alpha-Zr} \approx \parallel (1\ 1\ 1)_\delta$ and $[1\ 1\ \bar{2}\ 0]_{\alpha-Zr} \parallel (1\ \bar{1}\ 0)_\delta$. These orientation relationships correspond to those observed experimentally for hydride precipitate sizes considerably greater than those of critical nuclei. When these orientation relationships are achieved by an invariant plane strain transformation, it is obvious that the habit plane facet is a coherent interface. It is further assumed that this facet is also coherent with the matrix when the transformation has been achieved by a pure lattice strain transformation. That is, it is assumed that the choice of transformation mode affects only the transformation strains of the hydride nucleus – and hence its strain energy – but not significantly its surface energy. In Puls' original treatment [Puls, 1984, 1986] only the latter – pure lattice strain transformation case – was specifically addressed, although the treatment is sufficiently general to include the possibility of different transformation modes and, hence, transformation strains and interphase surface energies.

The change in total Gibbs free energy of formation of a δ hydride disc-shaped nucleus, for which the nucleus strain energy is determined – for ease of calculation – by assuming that it has the shape of an oblate spheroid *(sph)* inclusion of volume, $V_{sph} = (4/3)\pi a^2 c$, is given by:

Equation 3-7:

$$\Delta G = \frac{4}{3}\pi a^2 c\left(\Delta g^{hyd}_{chem} + \Delta g^{hyd}_{strain} + \Delta g^{hyd}_{int}\right) + 2\pi a^2 \gamma_c + 4\pi a c \gamma_i$$

where Δg^{hyd}_{chem} = change in chemical Gibbs free energy of the hydride phase from its equilibrium (incoherent) solvus composition (i.e. excluding energy contributions from coherency misfit strains between hydride and matrix) and when the H composition in the α–Zr phase is in excess of the equilibrium solvus composition

Δg^{hyd}_{strain} = change in strain energy of hydride precipitate and matrix produced by a misfitting, coherent hydride precipitate

Δg^{hyd}_{int} = interaction energy with internal or external stresses produced when a hydride precipitate forms or dissolves in the presence of these stresses

γ_c = coherent surface energy between hydride precipitate and matrix

γ_i = incoherent surface energy between hydride precipitate and matrix

All of the energies within the brackets are per unit volume whilst the surface energies are per unit area. Note that with the foregoing definition, Δg^{hyd}_{chem} is negative when the α–Zr lattice is supersaturated in hydrogen (i.e., has a greater value) with respect to its equilibrium solvus composition. For nucleation to be possible, this energy must be sufficiently negative to overcome the positive surface and self-strain energies of nucleus formation plus any positive interaction energies.

As shown in Appendix A, the dimensions and, hence, the critical Gibbs free energy changes beyond which stable nuclei are achieved is obtained by determining the extremum of the Gibbs free energy change given by Equation 3-7.

Assuming a size-independent eccentricity, ε^*, for the critical nucleus, as shown in Appendix A, the critical nucleation energy, ΔG^*, for a δ–hydride disc-shaped precipitate is:

Equation 3-8:

$$\Delta G^* = \frac{2\pi}{3}\frac{\bar{\gamma}_p^3}{\left[\varepsilon^*\left(-\Delta g'^{hyd}_{chem} - \Delta g^{hyd}_{strain}(iso) - \varepsilon^* \Delta g^{hyd}_{strain}(aniso) - \Delta g^{hyd}_{int} + c^{\delta}_H \Delta g^{H}_{int}\right)\right]^2}$$

with the total surface energy of the precipitate (p), $\bar{\gamma}_p$, given by:

Equation 3-9:

$$\bar{\gamma}_p = \gamma_c + 2\varepsilon^* \gamma_i$$

and the critical length by:

Equation 3-10:

$$a^* = \frac{\bar{\gamma}_p}{\varepsilon^*\left(-\Delta g'^{nucl}_{chem} - \Delta g^{hyd}_{strain}(iso) - \varepsilon^* \Delta g^{hyd}_{strain}(aniso) - \Delta g^{hyd}_{int} + c^{\delta}_H \Delta g^{H}_{int}\right)}$$

where $\varepsilon^* = c^*/a^* = \gamma_c/\gamma_i$ is the eccentricity of the hydride precipitate at its critical dimensions.

In Equation 3-8 and Equation 3-10, the chemical free energy for hydride nucleus formation, $\Delta g'^{hyd}_{chem}$, is defined by

Equation 3-11:

$$\Delta g_{chem}^{nucl} = \frac{c_H^{\delta}}{\overline{V}_{Zr}^{\alpha-Zr}} RT_n ln\left(\frac{c_H^{s,eq}(\boldsymbol{\sigma})}{c_H^{o}}\right)$$

where c_H^{δ} = H/Zr concentration in the critical nucleus (assumed to be the same as the equilibrium composition of δ–hydride precipitates at the (α + δ)/δ phase boundary in equilibrium with the α–Zr phase as given in Zr-H phase diagrams applicable to macroscopic quantities of each phase)

R = gas constant

T_n = absolute value of the hold temperature at which the nucleation rate is being determined corresponding to a chosen undercooling from the incoherent solvus

$\overline{V}_{Zr}^{\alpha-Zr}$ = molar volume of nucleus per mole Zr prior to transformation

$c_H^{s,eq}(\boldsymbol{\sigma})$ = H/Zr concentration in the α–Zr phase at the solvus composition for incoherent (non-misfitting and, hence, stress free) hydride precipitates at temperature, T_n, subjected to internal and external stresses, $\boldsymbol{\sigma}$

c_H^{o} = H/Zr concentration in the supersaturated α–Zr phase

The concentrations, c_H, in Equation 3-11 are defined by the general relation $c_H = r_H/\beta_{pha}$, where r_H is the H/Zr ratio concentration and β_{pha} is the maximum number of energetically equivalent interstitial sites per Zr atom in a given phase.

The strain energy is based on an approximate expression by Christian [Christian, 1965] valid when $c/a \ll 1$ (i.e., for thin, platelet-shaped precipitates):

Equation 3-12:

$$\Delta g_{strain}^{hyd} = \frac{E}{1-\nu}\Delta^2 + \frac{E}{1-\nu}\frac{\pi}{2}\frac{c}{a}\left[\Delta\cdot\xi + \frac{1}{4(1+\nu)}\xi^2\right]$$

where E = elastic modulus

ν = Poisson's ratio

Δ = isotropic component of hydride transformation strains

ξ = hydride transformation strain in the direction of the plate face normal in excess of the isotropic component

In Equation 3-12 the term involving shear strains in the plane of the plate has been omitted from Christian's original expression for reasons explained in Appendix A. The strain energy in Equation 3-12 has been separated into isotropic (iso) and anisotropic ($aniso$) components given from Equation 3-12, respectively, by:

Equation 3-13:

$$\Delta g_{strain}^{hyd}(iso) = \frac{E}{(1-\nu)}\Delta^2$$

Equation 3-14:

$$\Delta g_{strain}^{hyd}(aniso) = \frac{E}{(1-\nu)}\frac{\pi}{2}\left[\Delta\cdot\xi + \frac{1}{4(1+\nu)}\xi^2 + \frac{1}{8}\frac{(2-\nu)}{(1+\nu)}s^2\right]$$

and, hence, the total strain, $\Delta g_{strain}^{hyd}(total)$, is given by:

Equation 3-15:

$$\Delta g^{hyd}_{strain}(total) = \Delta g^{hyd}_{strain}(iso) + \varepsilon \Delta g^{hyd}_{strain}(aniso)$$

The interaction energies, Δg^{hyd}_{int} and Δg^{H}_{int} are given by:

Equation 3-16:

$$\Delta g^{hyd}_{int} = -\frac{\sigma_{ij} e^{T}_{ij}}{r^{\delta}_{H}}$$

Equation 3-17:

$$\Delta g^{H}_{int} = -\sigma_{ij} \lambda_{ij}$$

where σ_{ij} = stress matrix

e^{T}_{ij} = hydride transformation strain matrix

r^{δ}_{H} = H/Zr ratio at the $(\alpha + \delta)/\delta$ phase boundary corresponding to the tie-line composition for a given temperature extending from the $\alpha/(\alpha + \delta)$ solvus phase boundary to the $(\alpha + \delta)/\delta$ phase boundary;

λ_{ij} = lambda strains defined by $\lambda_{ij} = \partial e_{ij}/\partial r^{\alpha}_{H}$, where the e_{ij} are lattice strains produced by an increment, δr^{α}_{H}, of H/Zr ratio; hence these strains have units of strain/r^{α}_{H}

In most cases $\left|-\Delta g^{hyd}_{int} + c^{\delta}_{H} \Delta g^{H}_{int}\right| \ll \left|-\Delta g'^{nucl}_{chem} - \Delta g^{hyd}_{strain}(iso) - \varepsilon^{*} \Delta g^{hyd}_{strain}(aniso)\right|$ and ΔG^{*}can be approximated by:

Equation 3-18:

$$\Delta G^{*} = \frac{2\pi}{3} \frac{\bar{\gamma}^{3}_{p}}{\left[\varepsilon^{*}\left(-\Delta g'^{nucl}_{chem} - \Delta g^{hyd}_{strain}(iso) - \varepsilon^{*} \Delta g^{hyd}_{strain}(aniso)\right)\right]^{2}} - \frac{4}{3}\pi \left\{ \frac{\varepsilon^{*}\left[-\Delta g^{hyd}_{int} + c^{\delta}_{H} \Delta g^{H}_{int}\right] \bar{\gamma}^{3}_{p}}{\left[\varepsilon^{*}\left(-\Delta g'^{H}_{chem} - \Delta g^{hyd}_{strain}(iso) - \varepsilon^{*} \Delta g^{hyd}_{strain}(aniso)\right)\right]^{3}} \right\}$$

Expressing Equation 3-18 in terms of the critical nucleus volume at zero stress:

Equation 3-19:

$$V^{*}_{o} = \frac{4}{3}\pi \varepsilon^{*} (a^{*}_{o})^{3}$$

with a^{*}_{o} and ε^{*} given by:

Equation 3-20:

$$a^{*}_{o} = \frac{\bar{\gamma}_{p}}{\varepsilon^{*}\left(-\Delta g'^{nucl}_{chem} - \Delta g^{hyd}_{strain}(iso) - \varepsilon^{*} \Delta g^{hyd}_{strain}(aniso)\right)}$$

Equation 3-21:

$$\varepsilon^{*} = \frac{\gamma_{c}}{\gamma_{i}}$$

the following approximate expression is obtained for the critical nucleation energy:

Equation 3-22:

$$\Delta G^* = \Delta G_o^* - V_o^*\left[-\Delta g_{int}^{hyd} + c_H^\delta \Delta g_{int}^H\right]$$

where ΔG_o^* is the critical nucleation energy at zero external stress given by:

Equation 3-23:

$$\Delta G_o^* = \frac{2\pi}{3}\frac{\bar{\gamma}_p^3}{\left[\varepsilon^*\left(-\Delta g_{chem}^{nucl} - \Delta g_{strain}^{hyd}(iso) - \varepsilon^* \Delta g_{strain}^{hyd}(aniso)\right)\right]^2}$$

with the value of ΔG^* given by Equation 3-22 and Equation 3-23, the steady-state nucleation rate in a specimen under external stress, $\boldsymbol{\sigma}$, can then be written as:

Equation 3-24:

$$J_{ss,\boldsymbol{\sigma}}^* = J_{ss,o}^* exp\left\{\frac{V_o^*\left[-\Delta g_{int}^{hyd} + c_H^\delta \Delta g_{int}^H\right]}{k_B T}\right\}$$

with $J_{ss,o}^*$, the nucleation rate at zero external stress, given by:

Equation 3-25:

$$J_{ss,o}^* = Z\beta_o^* \frac{N}{c_H^\delta} exp\left(-\frac{\Delta G_o^*}{k_B T}\right)$$

with

Equation 3-26:

$$\beta_o^* = 2\pi a_o^{*2} c_H^o N \frac{D_H^v}{d}$$

Equation 3-24 shows that the nucleation rate in an externally stressed material is approximately the nucleation rate under zero stress multiplied by an exponential factor that depends (in a closed system) on the difference in interaction energy resulting from hydrogen added to or removed from solution with this corresponding amount of hydrogen obtained from dissolving or forming hydrides, respectively.

The interaction energy for hydride formation in Equation 3-24 is given by Equation 3-16. This interaction energy has been derived with the sign convention in which tensile stress is positive. Hence, $-\Delta g_{int}^{hyd} = \left(\sigma_{ij} e_{ij}^T\right)/r_H^\delta$ is positive for hydride formation under applied tensile stresses since the hydride transformation strains are positive. Thus, if $\left|\Delta g_{int}^{hyd}\right| > \left|c_H^\delta \Delta g_{int}^H\right|$, external tensile stress enhances the nucleation rate compared to its rate at zero external stress. A similar result for the effect of stress on nucleation rate was derived by Ells [Ells, 1970] and Sauthoff [Sauthoff, 1976] except that the isotropic factor, $-\frac{c_H^\delta}{\bar{V}_{Zr}^{\alpha-Zr}} p_h \bar{V}_H^{\alpha-Zr}$, equivalent to the anisotropic factor, $c_H^\delta \Delta g_{int}^H$, in this treatment was left out. This factor accounts for the fact that in experiments where the sample is under a uniform external stress and closed to ingress of hydrogen from an external source – which is generally the case in stress orienting experiments – the source of hydrogen to form hydrides must come from hydrogen in solution under the same external stress. Hence, this shows that only if there were a difference in partial molar volumes or transformation strains between hydrogen in solution and in hydride is there an effect of external stress on the steady state nucleation rate. Based on the present data for the partial molar volumes of hydrogen in α Zr and δ hydride, $\bar{V}_H^{\alpha-Zr}$ and $\bar{V}_H^{\delta-hyd}$, respectively, where $\bar{V}_H^{\delta-hyd}$ is another way (for isotropic transformation strains) to express the molar volume change on forming hydride, there is a small difference in magnitude between these two volumes, depending on temperature. Consequently, the hydride nucleation rate under external stress would differ somewhat from that in externally unstressed material. However, there would be no effect of external stress on hydride orientation during nucleation if the transformation strains of hydrogen in solution and in hydride precipitates were isotropic. In fact, the transformation strains of both hydrogen in solution and hydride are anisotropic which means that the nucleation rate under stress depends on the orientation of the hydrides and hydrogen atoms in solution. Hydrides aligned with their plate normals in the direction of an applied external tensile stress would have lower negative interaction energy and, hence, greater nucleation rate, than those aligned in the other two orthogonal directions. Thus, for the most general case, account must also be taken of the anisotropy of the

transformation strains of H atoms in solution in the hcp α–Zr matrix via the relations given by Equation 3-17. Thus, with the hydride and hydrogen interaction energies given by Equation 3-17 and Equation 3-16, respectively, Equation 3-22 becomes:

Equation 3-27:

$$\Delta G^* = \Delta G_o^* - V_o^*\left[\left(\sigma_{ij}e_{ij}^T\right)/r_H^\delta - c_H^\delta\sigma_{ij}\lambda_{ij}\right]$$

and, hence, Equation 3-24 becomes:

Equation 3-28:

$$J_{ss,\sigma}^* = J_{ss,o}^* exp\left\{\frac{V_o^*\left[\left(\sigma_{ij}e_{ij}^T\right)/r_H^\delta - c_H^\delta\sigma_{ij}\lambda_{ij}\right]}{k_B T}\right\}$$

It is further evident from Equation 3-24 *and* Equation 3-28 *that the potency of the stress orienting effect during hydride nucleation depends on the magnitude of the critical nucleation volume at zero external stress. From* Equation 3-19*,* Equation 3-20 *and* Equation 3-21*, the magnitude of this volume depends on the surface energies, the undercooling from the incoherent solvus and the strain energy of the nucleus.*

It is to be noted that aside from trivial changes in notation, the development given in the foregoing differs somewhat from that in the original treatment by Puls [Puls, 1984a, 1986] as follows:

- The molar volume used to convert partial molar self-strain and interaction energies of hydride precipitates (nuclei) to energies per unit volume is now correctly given as the partial molar volume of Zr in the α–Zr phase, as compared to previous uses of the partial molar volume of hydride per mole hydride. This change has no effect on the expressions obtained to calculate the critical nucleus volume since the volumes used to convert partial molar energies to energies per unit volume are, in each case, consistent with each other and, hence, self-cancelling.
- The change in chemical Gibbs free energy has been formulated so that it represents the difference in chemical energy between the precipitate (nucleus) phase and the supersaturated parent phase as opposed to the opposite formulation in the original treatment. This change has no quantitative impact on the final result as the resultant difference in sign between the two formulations in relation to the signs of the self-strain and interaction energies has been properly accounted for in each case.
- The hydrogen (solute) concentration variable, c_H^α or c_H^δ, has been changed from mole or atomic fraction or H/Zr ratio, r_H, to the latter concentration normalized by the factor, β_{pha}. This factor gives the maximum number of effective equivalent interstitial sites in a given hydride phase. The value of 1.5 for this factor for the δ–hydride phase at the $(\alpha + \delta)/\delta$ phase boundary is deduced from the experimental temperature-composition phase diagram at the lowest temperature of measurement. With r_H/β as the choice of concentration variable, the hydrogen concentration in the Zr-H system now has similar bounds from zero to one as does the solute concentration in binary substitutional solid solutions. As a result, previous derivations of the chemical Gibbs free energy change developed for the formation of precipitate nuclei formed from a supersaturated solution of the solute-dilute parent phase in systems of binary substitutional solid solutions can be directly applied to the Zr-H system. However, in the earliest derivations for this chemical free energy change by Puls [Puls, 1984a, 1986] it was incorrectly assumed that the appropriate hydrogen concentration variable is the hydrogen/zirconium ratio, r_H^δ (denoted there by x). In addition, following Carpenter [Carpenter, 1973], the upper bound for the terminal value of the hydrogen/zirconium atom or mole ratio of the hydride phase that is in equilibrium with the dilute solution α–Zr phase was given as 1.66 whereas a more accurate estimate should have been $x \equiv r_H^\delta = 1.5$. As a result, overall, there are some differences in the numerical values of the differences between the hydride and hydrogen interaction energies between the two derivations.

Implicit in the foregoing assumptions concerning the calculation of the critical nucleation energy, is that smaller sized embryos would grow to the dimensions of the critical nucleus along the same morphological path. This point was made by Johnson and co-workers [Johnson et al., 1975] in relation to evaluating the second partial derivative of ΔG^o with respect to n in Equation 3-4. These authors point out that this derivative needs to be taken along the morphological path traversed by embryos as they increase in size to that of the critical nucleus. For a spherical nucleus this is straightforward since the embryos would be able to maintain their spherical shape throughout this formation path. This would not be the case for embryos culminating in critical nuclei observed at the micro scale level having preferred habit planes, as these generally have needle- or plate-shaped morphologies. In this case the existence of facets on the preferred habit plane should make these surfaces immobile to growth in the direction normal to this plane by the

addition of single atoms arriving by volume diffusion [Johnson et al., 1975]. It would seem however if, rather than by volume diffusion, the evolution of the embryos to critical nuclei dimensions occurs by cooperative movements, such as for instance by an invariant plane strain transformation – as in a martensitic transformation – then increases in the thickness of plate-shaped embryos and nuclei would be possible through the cooperative movements of successive planes above and/or below the facets of existing embryos or nuclei. However, unlike a purely structural transformation that can rapidly form by this mechanism, such as the formation of martensite, the structural component of hydride nucleus formation needs to be accompanied by the transfer of a large number of hydrogen atoms from the H-dilute matrix to the H-concentrated precipitate phase. So far, it has not been established at what stage of the phase transformation this transfer of atoms occurs (for instance, before, during or after the cooperative movement of the α–Zr lattice). This uncertainty in the exact mode of the phase transformation is not unlike the still on-going controversy concerning the transformation mechanism of the much more extensively studied bainite transformation in low carbon steels [Fielding, 2013] in which both a structural and a compositional change is required. The principal difference between these two types of phase transitions (aside from a difference in crystal structure) is that the bainite formation requires the rejection of interstitial carbon atoms to achieve its bulk equilibrium composition when it forms, rather than an increase in interstitial hydrogen atoms in the case of hydride formation. *As is shown further on, this lack of knowledge concerning at what stage of the transformation hydrogen transfer from matrix to nucleus occurs creates an uncertainty in the appropriate misfit strains between hydride nucleus and matrix that are applicable for the purpose of quantifying the degree of hydride reorientation during the nucleation stage of hydride formation.*

Finally, for calculating the effect of stress on hydride nucleation it would appear, at first glance, not to be necessary to have numerical estimates of the pre-exponential factors in Equation 3-3 given by Equation 3-4 to Equation 3-6 if these factors are not affected by the presence or absence of external stress. However, evaluation of the pre-exponential factor requires an estimate of the undercooling from the solvus sufficient to achieve an observable nucleation rate in laboratory scale experiments when comparing the efficacy of homogeneous versus heterogeneous nucleation. As is shown further on, such different nucleation rates at a given undercooling result in different potencies for the effect of stress on hydride orientation and, hence, both the pre-exponential and exponential parameters in Equation 3-3 need to be numerically evaluated.

Johnson and co-workers [Johnson et al., 1975] derived expressions for nuclei having a range of different facetted morphologies, comparing their results with the simplest case of a spherical nucleus. To derive these expressions, the authors assumed that the process of evolution of a facetted nucleus through its embryonic form to its critical state by diffusional growth can be deduced from the conceptually simpler reverse process of precipitate dissolution. The authors justified the equivalences between these two processes on the basis of the principle of time reversal [Tisza & Manning, 1957]. This principle states that an isothermal process taking place by statistical fluctuations follows the same average path in the forward as in the reverse direction. Applying this methodology to the case of hydride nucleation requires assuming that during this stage of hydride formation there is no hysteresis between nucleus formation and dissolution, i.e., in a statistical mechanical sense the probability of transfer of hydrogen atoms to and from a hydride precipitate having dimensions ranging from being equal to, to less than its critical dimensions is the same. Experimental results of solvus determinations show, however, that there is hysteresis between hydride formation and dissolution. Whether this hysteresis between the temperature for hydride formation and dissolution observed on a macro scale also applies to the nucleation stage of hydride formation and dissolution is difficult to ascertain on the basis of present experimental results. To begin with, however, it would be useful to know the nucleation rate that is prevalent at the earliest detection of hydride formation in some of the most commonly used techniques for solvus determination. This is evaluated in the following Section 3.2.

3.2 Evaluation of nucleation rate under zero applied stress

Most experiments to determine the hydride solvus consist of monitoring the value of a parameter that has high sensitivity to the start or completion of the phase transformation during continuous cooling and heating of samples containing a known quantity of total hydrogen. It may be that the sensitivities in these experiments to phase transformations is such the hysteresis determined between hydride formation and dissolution is only representative of the phase transformation stage during which the hydride precipitates have grown to sizes greater than those at the nucleation stage.

In such a case a recent review of the possible origins of hysteresis, Puls [Puls, 2012] showed that one source of hysteresis during both the hydride formation and dissolution stages could be the entropy produced during the phase transformation because the thermodynamic barrier to phase transformation involves overcoming a macroscopic (i.e., finite) energy barrier that is too large to be surmounted by thermal fluctuations alone. It is implicit in the following application of the nucleation stage of hydride formation that this is not the case in the specific example chosen in the following.

The numerical estimate of the nucleation rate under zero external stress is made using Equation 3-25 with Equation 3-26. For the case of nuclei embryos having plate-shaped or oblate spheroidal shapes growing with constant aspect ratio, this is obtained from the expression for the critical semi-major radius of the oblate ellipsoid given by Equation 3-20 to Equation 3-21, the corresponding critical nucleation barrier given by Equation 3-23 and the addition rate of hydrogen atoms into a hydride embryo given by Equation 3-26. It is assumed that these equations are applicable to both homogeneous and heterogeneous nucleation with the differences between the two arising from differences in the values for the hydride surface energies, the effective strain energy and the number of nucleation sites.

Before proceeding with these calculations it is useful to estimate the nucleation rate that would be sufficient for the onset of hydride formation to be detectable in experimental determinations of the solvus during cooling starting from a temperature at which all hydrides had previously been dissolved. The data of Pan and co-workers [Pan et al., 1996] are used for this purpose since the authors of this study went to some length to determine, for given hydrogen content, the conditions of maximum temperature, hold time at temperature and subsequent cooling rate resulting in the lowest temperature for the onset of hydride formation. The hydride formation solvus corresponding to these cases was denoted as TSSP1 and interpreted as representing the solvus for hydride nucleation. From the plots of the variation of the dynamic elastic modulus with temperature it seems that deviations from a linear variation with temperature of hydrogen in solution under a cooling rate of 2°C/minute would first become detectable when about ≈ 1 wppm/°C of hydrogen atoms had been transferred from solution in the α–Zr matrix to hydride precipitates. In the initial analysis by Puls [Puls, 1984a], physical parameters in the steady state nucleation rate expression were chosen that would produce what was thought at that time to be a detectable nucleation rate of $\approx 1 \times 10^{17}$ nuclei/($\mathrm{m^3 s^{-1}}$). However, no attempt was made in that study to convert this nucleation rate to an experimentally detectable change in wppm H in solution per unit temperature reduction. This is done in the following using, as an example, one of the results given in Table 4 of Puls [Puls, 1984a].

For Zircaloy-2 with hydrogen content of 150 wppm the data of Slattery [Slattery, 1967] gives a TSSP temperature of 567 K. Assuming this to be the nucleation temperature, a critical nucleus volume, $V_o^* = 5.253 \times 10^{-27} \mathrm{m^3}$ was obtained for δ–hydride precipitates, corresponding to a nucleation rate of $J_o^* = 8.602 \times 10^{16}$ nuclei $\mathrm{m^{-3} s^{-1}}$. In these calculations it was assumed that the ratio of H to Zr atoms in the hydride is a constant (i.e., independent of the temperature at which nucleation occurs) and equal to 1.66. Using this factor, the rate of transfer of hydrogen atoms, r_H, from solution to critical δ–hydride nuclei is given by $\dot{r}_H = 1.66 \times 5.253 \times 10^{-27} \times 8.602 \times 10^{16} = 7.501 \times 10^{-10}$ $\mathrm{s^{-1}}$. Converting this concentration variable to wppm per second, $\dot{w}_H$, yields 8.223×10^{-6} wppm $\mathrm{s^{-1}}$. We now apply this result to the experiments of Pan and co-workers [Pan et al., 1996], which were carried out at a cooling rate of 3.333×10^{-2} °C $\mathrm{s^{-1}}$ (2°C $\mathrm{min^{-1}}$). Dividing $\dot{w}_H$ by this cooling rate indicates that the change in hydrogen concentration from solution to hydride at TSSP would be 2.467×10^{-4} wppm H/°C. This conversion rate is about a factor of 10^4 too small to be detectable in this type of experiment. Thus one can conclude from this analysis that at the temperature at which TSSP1 is observed in the Pan and co-workers' experiments there would have to be a corresponding nucleation rate of $\approx 10^{20}$ nuclei $\mathrm{m^{-3} s^{-1}}$. Hence, in the following analysis, various combinations of values for chemical, strain and surface energies were chosen that would result in such a targeted nucleation rate.

We start by estimating the change in chemical free energy given by Equation 3-11 for a sample containing 100 wppm H. We assume that the nucleation temperature, T_n, is given by the TSSP1 temperature corresponding to this hydrogen content. In order to determine the chemical free energy at this temperature, we need to determine what the equilibrium (i.e., incoherent) solvus relationship is. Because of the large hysteresis, this relationship cannot be determined experimentally since both of these solvi have been shown to be affected by this hysteresis. It needs to be pointed out that true hysteresis is not the result of the super saturation needed below the equilibrium solvus during the nucleation stage to overcome the energy barrier produced by surface energy. This undercooling during the nucleation stage is generally present in all first order phase transformations. The nucleation barrier – which ceases to be of importance when macroscopic proportions of the two phases are present – differs from hysteresis because it can be overcome – given sufficient time – through thermal fluctuations whereas overcoming a hysteresis barrier is only possible once a sufficiently large, finite thermodynamic driving force has been applied. There is currently no overall consensus on the origin of hysteresis. Flanagan and co-workers [Flanagan et al., 1995] have reviewed this topic from the perspective of trying to understand hysteresis in hydrogen-metal systems by examining attempts to quantify and explain hysteresis observed in those and other solid state reactions. A summary of this review, applicable to the Zr-H system, is given in the book by [Puls, 2012]. Here we make use of two proposals to account for hysteresis, both of which are then used to derive a theoretical expression for the incoherent (equilibrium) solvus using experimentally determined solvi for terminal dissolution (TSSD) and onset of (conventionally referred to as terminal) hydride precipitation (TSSP1).

<u>Derivation of chemical energy driving nucleation based on considerations derived from a finite energy barrier model of solvus hysteresis</u>

The first approach is based on a purely thermodynamic assessment of the data combined with the conjecture that the hysteresis arises because the phase transformation in both directions requires overcoming a macroscopic energy barrier. As noted in the foregoing, such a barrier cannot be overcome by thermal fluctuations alone as assumed in classical nucleation theory. The need to overcome a finite energy barrier results in finite growth of the new phase, once the driving force is high enough to overcome it. Such finite precipitate growth or dissolution produces entropy, and this entropy is deemed to be at least one possible source of hysteresis between the solvi for hydride formation and dissolution in the Zr-H system. Flanagan and co-workers [Flanagan et al., 1995] reasoned that the barrier needing to be overcome is the same in each direction and therefore that the reference (incoherent, equilibrium) solvus should be located approximately halfway between the experimentally determined solvi for hydride dissolution and precipitation. Assuming that hysteresis has numerically negligible effect on the vibrational contribution to the change in Gibbs free energy during phase transformation, then the enthalpy for the equilibrium solvus is obtained from the experimentally determined enthalpies of formation and dissolution solvi by taking the average or square root of the product of these two enthalpies. This approach has physical significance provided the pre-exponential in the usual van't Hoff fit to the solvus data has the same value for all three solvi.

Using the data of Pan and co-workers [Pan et al., 1996], it is seen that two bounding solvi – designated as TSSP1 and TSSP2 – were determined for hydride formation. Assuming, as did the authors, that TSSP1 is the solvus for hydride formation detected during the hydride nucleation stage whilst TSSP2 is the solvus detected during the hydride growth stage, then one could argue that the difference in enthalpies in a van't Hoff plot of the data between TSSP2 and TSSD – i.e., in plots of $ln\, c_H^s \;\; vs \; 1/T(\mathrm{K})$ to the data – true hysteresis is reflected in the difference in the enthalpies of TSSP2 and TSSD, whilst the difference in enthalpies of TSSP2 and TSSP1 reflects the undercooling from the hypothetical equilibrium solvus required for hydride nucleation. For a physically meaningful comparison we use the fit to the data of Pan and co-workers [Pan et al., 1996] determined by Shi and co-workers [Shi et al., 1995] listed in Table 3-1 that is based on a common value for the pre-exponential term. The enthalpy of formation for the equilibrium solvus, ΔH_E, is then derived from the enthalpies for hydride precipitation, ΔH_{P2}, determined from the TSSP2 data and for hydride dissolution, ΔH_D, determined from the TSSD data, using the relation, $\Delta H_E = -\sqrt{\Delta H_{P2} \cdot \Delta H_D}$. The result is $\Delta H_E = -29\,953\ \mathrm{J\,K^{-1}mol^{-1}}$ H, listed in Table 3-1. With these parameters, at a hydrogen content of 100 wppm, the equilibrium (TSSE) and TSSD, TSSP1 and TSSP2 solvi temperatures listed in Table 3-2 are obtained. From these results, the equilibrium solvus concentration at the assumed nucleation temperature, T_n, for material with hydrogen content of 100 wppm derived from the TSSP1 data, is equal to 61.6 wppm. Thus at the nucleation temperature, the α–Zr phase containing 100 wppm of hydrogen atoms in solution is supersaturated by ≈ 38 wppm, yielding a chemical driving energy, $-\Delta g'^{H}_{chem} = 1.584 \times 10^2\ \mathrm{J\,m^{-3}}$. Some of this energy is used up to overcome the strain energy generated by the coherent hydride nucleus. For anisotropic transformation strains, the strain energy depends on the aspect ratio, ε, of the hydride nucleus, decreasing with decrease in this ratio. Hence, from Equation 3-23 for ΔG_o^*, decreasing this ratio will increase the net energy in the denominator and reduce the nucleation barrier. However, Equation 3-23 for ΔG_o^* was derived assuming that hydride embryos grow to their critical dimensions with constant aspect ratio, which is what one would expect during the nucleation stage in which case the surface energy dominates the magnitude of the nucleation barrier – and hence its shape – assuming that the surface energy differs with orientation of the precipitate's surface. At constant aspect ratio the effective surface energy, $\bar{\gamma}_p$, depends only on the chosen value for the coherent surface energy; i.e., it is independent of ε^* for a given γ_c. Moreover, variations in this parameter have a greater effect on the magnitude of the nucleation barrier than do variations in the strain energy because the former has a cubic dependence compared to an inverse square dependence for the latter. Thus, given a chosen undercooling from the equilibrium solvus and, hence, $-\Delta g'^{H}_{chem}$, the choice of the magnitude of γ_c is the most critical parameter in achieving a nucleation rate that is experimentally observable.

Table 3-1: Enthalpies of dissolution and formation for TSSD, TSSP1 and TSSP2 derived from a fit of the experimental data of Pan and co-workers [Pan et al., 1996] assuming a common value for the pre-exponential term, $A = 3.9153 \times 10^4$ wppm. The corresponding value for TSSE was derived assuming $\Delta H_E = -\sqrt{\Delta H_{P2} \cdot \Delta H_D}$.

Hydride Solubility Expressions (wppm)	Enthalpies in Solubility Expressions (J mol^{-1} H)
$c_H^s(TSSD) = A \cdot \exp(\Delta H_D/RT)$	$\Delta H_D = -31\,000$
$c_H^s(TSSP1) = A \cdot \exp(\Delta H_{P1}/RT)$	$\Delta H_{P1} = -27\,7040$
$c_H^s(TSSP2) = A \cdot \exp(\Delta H_{P2}/RT)$	$\Delta H_{P2} = -28\,942$
$c_H^s(TSSE) = A \cdot \exp(\Delta H_E/RT)$	$\Delta H_E = -29\,953$
	© ANT International 2018

4 Applications of the Ells/Puls and other theories of hydride stress orienting

4.1 Earliest applications of the Ells/Puls theory

4.1.1 Hydride stress orienting in Zr-2.5Nb material (Hardie and Shanahan, 1975)

The first application of the Ells hydride reorientation model by others to experimental data was carried out by Hardie and Shanahan [Hardie & Shanahan, 1975]. These authors carried out stress reorientation experiments in tensile specimens produced from two sources of Zr-2.5Nb material: rolled plate material and flattened pressure tube material. A problem in determining the stress orienting potency in the flattened tube material was, however, that the straightening process produced alternating macroscopic residual tensile and compressive stress zones through the thickness of the wall of the tube. In an earlier study of straightened tube specimens [Hardie & Shanahan, 1974] the authors determined that the maximum residual tensile stress occurred in a thin layer starting at the outer diameter (OD) tube wall surface and the maximum residual compressive stress occurred in a layer starting from the inner diameter (ID) tube wall surface. In specimens hydrogenated after straightening, it was found in externally unstressed specimens that the hydride distribution just at the OD surface consisted of a mixture of radial and circumferentially oriented hydrides whilst the hydride distribution at the ID surface consisted of mostly circumferential hydrides. The authors referred to these two regions as zones of mixed and stringer hydride orientations, respectively. In comparison, in hydrogenated, externally unstressed tube material that had not been straightened, the predominant hydride orientation was circumferential across the entire tube wall thickness. Measurements of the radial hydride distribution as a function of increasing applied circumferential tensile stress throughout both the mixed and the stringer zones gave a sigmoidal variation of % radial hydride fraction versus applied stress. The saturation level of % radial hydride fraction varied with the amount of total hydrogen content dissolved at the temperature at which the external stress was applied during cool down. To achieve close to 100% radial hydrides required that the temperature at which external stress was applied during cool down exceed the terminal solubility limit for hydride dissolution for the given total hydrogen content in the specimen.

To compare their results with the predictions of the Ells model the authors fitted their data for $R_x^{rad}(\sigma)$ (denoted by $R\,_{\boldsymbol{\sigma}}^{rad}$ by Hardie and Shanahan) to the mathematical form of the Ells equation using the relation:

Equation 4-1:

$$R_x^{rad}(\sigma) = R_o exp(B)$$

where R_o, B = fitting constants

σ = uniaxial tensile stress applied during the thermal cycle

With this approach R_o accounts for the effect of residual stresses in the specimen through the fraction of radial hydride orientation obtained when cooled over the same temperature range under zero externally applied stress. From Equation 4-1 $F_x(\sigma, \%)$ is given by:

Equation 4-2:

$$F_x(\sigma, \%) = 100\frac{R_o exp(B\sigma)}{1 + R_o exp(B\sigma)} \equiv \frac{100}{1 + \frac{1}{R_o} exp(-B\sigma)}$$

An example of comparison between the experimentally determined dependence of $F_x(\sigma, \%)$ as a function of applied tensile stress with that predicted by Equation 4-2 is reproduced here in Figure 4-1. The figure shows that there is excellent agreement between the two, thus providing support for the validity of the physical mechanism for hydride stress re-orientation that has led to the plotted mathematical form. In Figure 4-2 and Figure 4-3 similar plots of fits of Equation 4-2 to the data as those given in Figure 4-1 are shown, but without the addition of the associated data points.

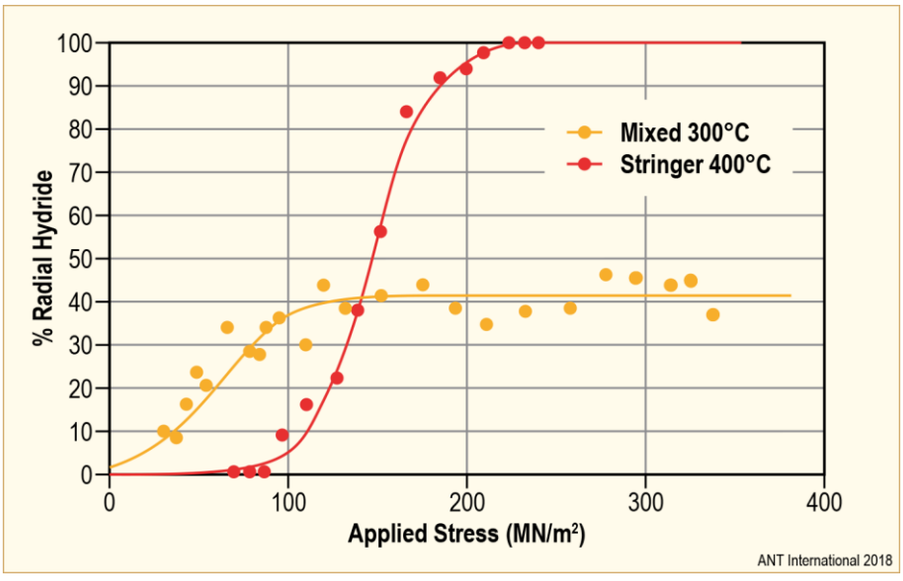

Figure 4-1: Plots of the % radial hydrides ($F_x(\sigma, \%)$) in a Zr-2.5Nb flattened tube specimen containing 100 wppm H for two different maximum temperatures from which the specimens were cooled as a function of uniaxial tensile stress applied in the tube circumferential direction (MN/m² ≡ MPa) (Series C specimen). Maximum temperatures from which the specimens were cooled are indicated in the figure (from [Hardie & Shanahan, 1975]).

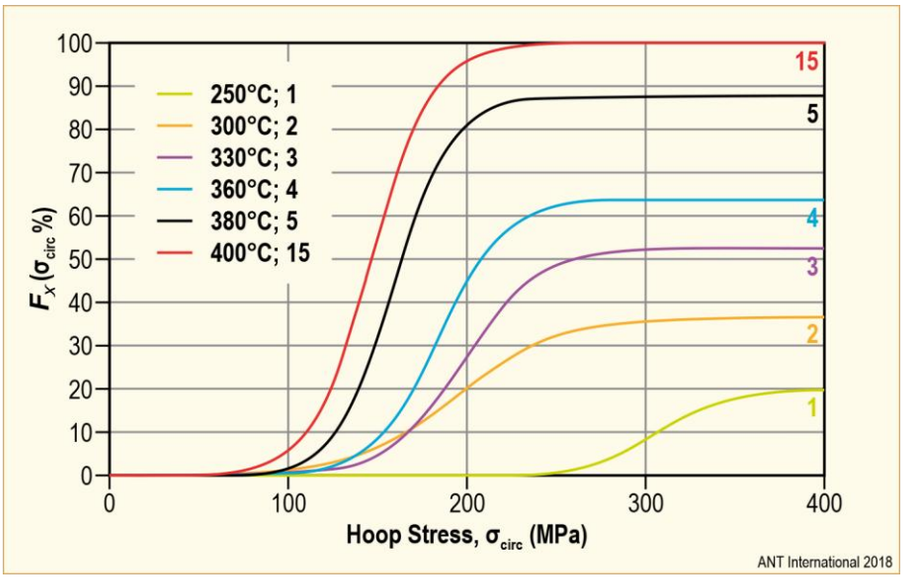

Figure 4-2: Curve fits to data of % radial hydrides ($F_x(\sigma_{circ}, \%)$) versus uniaxial externally applied tensile stress in the tube's circumferential direction for different maximum temperatures from which the specimens were cooled (from [Hardie & Shanahan, 1975]). The data used in these fits were of specimens from the ID stringer zone of flattened Zr-2.5Nb pressure tube material, all with hydrogen content of 100 wppm. The ID stringer zone is a region of maximum macroscopic residual compressive stress in the material. The number beside each curve corresponds to the specimen number in Table 2 of [Hardie & Shanahan, 1975] and to the number given in the legend showing the maximum temperature from which each of the specimens was cooled.

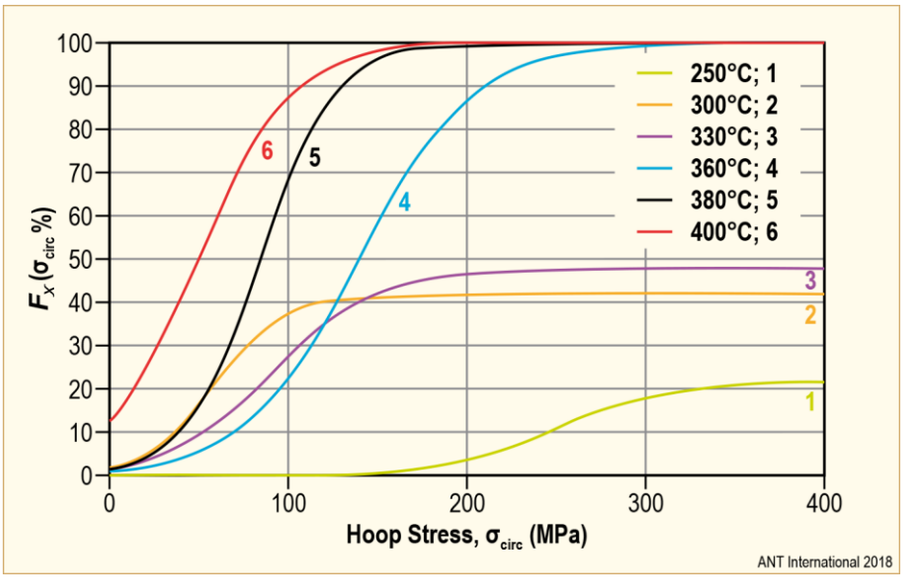

Figure 4-3: Curve fits to data of % radial hydrides ($F_x(\sigma_{circ.}\ \%)$) versus uniaxial externally applied tensile stress in the tube's circumferential direction for different maximum temperatures from which the specimens were cooled (from [Hardie & Shanahan, 1975]). The data used in these fits were of specimens from the OD mixed zone of flattened Zr-2.5Nb pressure tube material, all with hydrogen content of 100 wppm. The OD zone is a region of maximum macroscopic residual tensile stress. The number beside each curve corresponds to the specimen number in Table 1 of [Hardie & Shanahan, 1975] and to the number given in the legend showing the maximum temperature from which each of the specimens was cooled.

Note that for all of the fits given in Figure 4-2 there is an apparent lower threshold stress before there is a noticeable increase in hydride reorientation. The data for these plots were taken from the stringer zone of the flattened specimens (zone of maximum macroscopic residual compressive stress). On the other hand, for the fits plotted in Figure 4-3 – except for the data at 250°C – no lower threshold stress is indicated. The data for these plots were taken from the mixed zone of the flattened specimens (zone of largest macroscopic residual tensile stress). For the results from the stringer zone it can be seen from Figure 4-2 *that the apparent lower threshold stress (and, correspondingly, also the upper threshold stress) increases with decrease in maximum hold temperature*. For specimens with the same hydrogen content, a decrease in maximum hold temperature corresponds to a decrease in nucleation temperature. When the maximum temperature is less than TSSD, only the % of hydrogen content that is dissolved is reoriented during cooling, which accounts for the decrease of F_x in the upper plateau region with decrease in maximum temperature for these specimens, all containing 100 wppm hydrogen. There is a similar trend for the results shown in Figure 4-3 for specimens from the mixed zone between the highest and the lowest maximum temperature employed, but in this case some results give the same value for the upper threshold stress (specimens 6 and 5) or a reversal (specimens 3 and 2) in the sequence with reduction in temperature. It is also evident from Figure 4-3 that the higher is the starting radial hydride fraction in a specimen the steeper is the increase in F_x with increase from zero of the externally applied tensile stress.

Concentrating on two cases of specimens with hydrogen content of 100 wppm and a temperature of 400°C at which the external uniaxial stress is applied – i.e., hydrogen content and temperature of stress application exceeding the corresponding TSSD temperature – Table 4-1 gives the values of the constants obtained for these cases by Hardie and Shanahan [Hardie & Shanahan, 1975]. These values are compared with the theoretically estimated value of B determined from the data of Table 3-2 and the indicated ΔE_{int} value. The theoretical plot was obtained assuming that R_o in Equation 4-2 corresponds to the case of $F_x(\%)$ equal to 2% radial hydrides when the specimen is cooled under zero externally applied stress.

Table 4-1: Experimentally and theoretically determined parameters in Equation 4-2 for specimens containing 100 wppm H.

Source	Stressing (Nucleation) Temperature (°C)	$10^3 R_o$	B (10^{-6} Pa)
Experimental – Mixed Zone	400	148	0.038
Experimental – Stringer Zone	400	0.49	0.037
Theoretical†	(285)	204	0.030
†Calculated using Equation 3-42 to Equation 3-44 with $\Delta E_{int} = 0.115\sigma_{circ}$ and the data for V_o^* and T_n given in Table 3-2			

The results summarized in Table 4-1 show reasonable agreement between the experimentally and theoretically determined exponential factors, B. Reasonable agreement is also obtained for the pre-exponential factors, R_o, between the experimental and theoretical results for which, in both cases, the starting radial hydride fraction was approximately the same (≈ 3%) – as observed in the experimental example and assumed in the theoretical one. The R_o factor for the experimental results from the stringer zone is considerably less compared to those of the other two cases as it incorporates the effect of the macroscopic internal residual compressive stress produced by the flattening procedure.

4.1.2 Hydrides in Zircaloy: Interactions between tensile stress and hydride morphology (Bai and co-workers, 1994)

The second application of the Ells model to hydride stress re-orientation data was by Bai and co-workers [Bai et al., 1994]. These authors based the analysis of their experimental results of hydride orientation in recrystallized and annealed (RXA) Zircaloy-4 sheet material on the theoretical version given by Puls [Puls, 1984a, 1986] using the simplified expression given by Equation 4-1. Tensile specimens were prepared from the Zircaloy-4 sheet material such that the tensile axis of the specimen was in the sheet's transverse direction. Figure 4-4 shows a comparison of the 'natural' and stress re-oriented orientations of hydrides in the sheet with those in a fuel cladding tube. The crystallographic texture of the specimens was similar to that in tubes, having Kearns factors of 0.65, 0.22 and 0.13 in the normal, longitudinal and transverse directions of the specimen's coordinate system. The 'natural' orientations of the plate-shaped hydrides in the tensile specimens correspond to the in-plane transverse (circumferential) orientation of the plate-shaped hydrides in the tube, whilst the stress re-oriented hydrides in the specimen correspond to radial hydrides in the tube. Hydride orientations were determined using Scanning Electron Microscopy (SEM) coupled with an image analyser. The particle orientation was defined by the angle made by the average direction of hydride segments in a cluster with the stress axis. The ratio of perpendicularly oriented hydrides (radial hydrides) was given by the percentage of hydrides having orientation angles from 0° to 30° to the total number of hydrides of all orientations. The application of the stress orienting model to their results is noteworthy in that the authors tried to account for the effect of internal grain interaction stresses produced during the forming process. Stresses and associated dislocation densities were obtained by X-ray diffraction (XRD) and Transmission Electron Microscopy (TEM). An additional feature of the stress orienting tests was that gaseous hydrogenation of the specimens at 400°C was done while a tensile stress was maintained on the (tapered) specimens. After hydrogenation to a specific H content, the specimens were cooled under stress at a rate of 1.4°C/min and the hydride orientations along the specimen length (and, hence, at different values of stress) were determined. The authors defined two tensile stress thresholds for hydride orienting: a lower threshold, σ'_{th}, which gives the applied tensile stress at which the hydride orientation first starts to change and an upper threshold, σ''_{th}, at which nearly all of the hydrides have stress reoriented. For the RXA material analysed with this hydride reorientation model, these stresses were obtained as 95 and 170 MPa, respectively. Both inter- and intra-granular hydrides were observed.

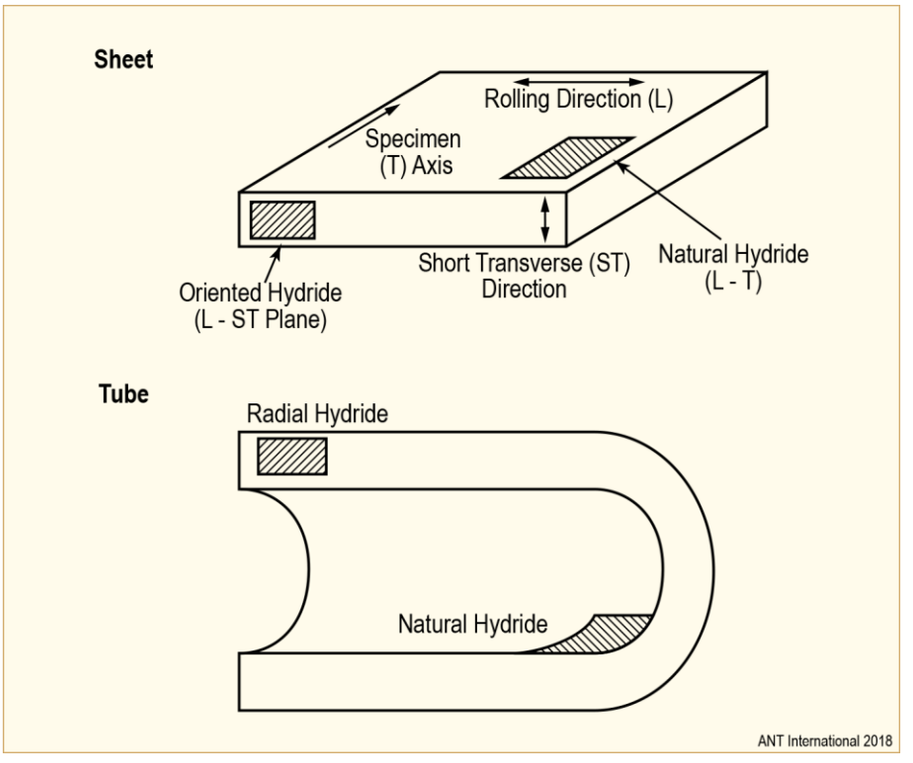

Figure 4-4: Schematic of comparison of hydride orientation correspondences and orientation of the "natural" (zero external stress) hydrides in tube versus sheet material. The latter material was used to study hydride orientation with and without external stress (from [Bai et al., 1994]).

In applying the model to their results, the authors start with the original version of the nucleation rate expression, the modified version of which is given here by Equation 3-42 leading, via Equation 3-42 to Equation 3-45, to an expression for the ratio, $F_x(\sigma)$, under a uniaxial tensile stress of the number of radially aligned versus total number of hydrides. For the externally unstressed, but residually stressed material the authors find from experiment that $F_x(\sigma_{res}) = 0.30$. $F_x(\sigma_{res})$ and, hence, the associated $R_x^{rad}(\sigma_{res})$, correspond to the case of externally unstressed material containing internal residual stresses left over from the rolling process. From the general relation between F_x and R_x^{rad} given by Equation 3-35 this would be equivalent to $R_x^{rad}(\sigma_{res}) = 0.43$ or $1/R_x^{rad}(\sigma_{res}) = 2.33$. However, the authors modify the relation given by Equation 3-36 by taking account of the following experimental observations. The first is that in the residually stressed material the circumferential hydrides were located at either grain boundaries or within grains, but the radial hydrides were mostly located only at grain boundaries oriented perpendicular to the transverse (tube circumferential) direction. The second observation is that after cooling under an externally applied circumferential stress, most of the reoriented radial hydrides were located predominantly at inter-granular sites oriented in the radial direction. This suggested to the authors that the additional, radially oriented hydrides produced as a result of cooling under an external stress came at the expense of the circumferentially oriented hydrides produced when cooling under zero external stress, regardless of whether these were located at grain boundaries or within the grains.

To account for the foregoing experimental observations in the theoretical description of the Ells/Puls stress reorientation model, the authors modified the original expression derived by Puls [Puls, 1984a, 1986] for $N_x^{rad}(\sigma)$ (N_r in the notation of the authors, where the aligned hydrides are referred to as radial ('r') hydrides) by choosing two different values for the critical nucleation volume, one for inter-granular nuclei, $V^*_{o,inter}$, the other for intra-granular nuclei, $V^*_{o,intra}$, in the exponential term and weighting these volumes according to the observed distribution of reoriented hydrides, giving

Equation 4-3:

$$N_x^{rad}(\sigma) = N_x^{rad}(0)\exp(A)$$

Equation 4-4:

$$A = F_x^{eff}\left[\frac{(0.7 \times V_{o,inter}^{*} + 0.3 \times V_{o,intra}^{*}) \cdot E_{int}^{rad}}{k_B T}\right]$$

whilst $N_x^{circ}(\sigma)$ is given by:

Equation 4-5:

$$N_x^{circ}(\sigma) = N_x^{circ}(0)\exp(B)$$

Equation 4-6:

$$B = \left(\frac{1 - F_x^{eff}}{2}\right)\left[\frac{\left(V_{o,inter}^{*} + V_{o,intra}^{*}\right) \cdot E_{int}^{circ}}{k_B T}\right]$$

where $F_x^{eff} = F_x(\sigma) - F_x(0)$

$F_x(0)$ = radial hydride fraction at zero externally applied stress

$V_{o,inter}^{*} = 4.3 \times 10^{-27}\,\mathrm{m}^3$ for the inter-granular hydride nucleus volume

$V_{o,intra}^{*} = 15 \times 10^{-27}\,\mathrm{m}^3$ for the intra-granular hydride nucleus volume

Hence at $T = 400°\mathrm{C}$ – assuming isotropic transformation strains for hydrogen in α–Zr and pure lattice strain transformation strains derived by Carpenter [Carpenter, 1973] for hydride precipitates – the authors obtained for $F_x(\sigma) = N_x^{rad}(\sigma)/(N_x^{rad}(\sigma), + N_x^{circ}(\sigma))$ the following expression:

Equation 4-7:

$$F_x(\sigma) = \frac{1}{1 + 2.33 \cdot exp(B - A)}$$

Equation 4-8:

$$B - A \approx [-1.8 \times 10^{-8} F_x(\sigma)(\sigma_{circ}^{ext} + \sigma_{circ}^{res})]$$

No mention was made on what physical basis the two values of the critical volumes were obtained, nor why there is a weighting factor on these volumes seemingly obtained from the experimentally determined value for $F_x(\sigma)$ giving the fraction of radial hydrides. Note that in Bai and co-workers' formulation, $F_x(\sigma)$ is now also contained in the exponential expression, which means that Equation 4-7 becomes an implicit relation of $F_x(\sigma)$.

The total circumferential stress in the interaction energy expression is a net stress (in the authors' notation this is called an effective stress): $\sigma_{circ}^{net} = \sigma_{circ}^{ext} + \sigma_{circ}^{res}$ given by the vector sum of externally applied and internally imposed residual grain interaction stresses, the latter having values at 400°C of –25, –5 and 100 MPa along, respectively, the specimen's tensile, transverse and thickness (short transverse) directions (corresponding, respectively, to the circumferential, radial and axial tube directions). The result is:

Equation 4-9:

$$F_x(\sigma) = \frac{1}{1 + 2.33 \cdot exp[-1.8 \times 10^{-8} F_x(\sigma) \cdot (\sigma_{circ}^{ext} - 25)]}$$

As with the original treatment by Puls [Puls, 1984a, 1986], the assumed isotropic hydrogen interaction energy term has dropped out of Equation 4-7 and Equation 4-8. The physical origin of the factor 2.33 in Equation 4-7 and Equation 4-8 is not made clear. Numerically it has the same value as $1/R_x^{rad}(0)$, which is defined by the authors as the ratio of circumferential to radial hydrides when there are no externally applied stresses acting on the material. However, according to the Ells/Puls model, $1/R_x^{rad}(0)$ in Equation 4-7 should be the foregoing ratio when neither external nor internal stresses are acting on the material. It would appear, therefore, that the ratio used by the authors implicitly accounts for the effect of internal stress on the fraction of circumferential to

radial hydrides and, hence, is not the appropriate ratio to use in Equation 4-9, which explicitly accounts for the effect of residual stress on hydride orientation in the exponential expression.

Figure 4-5 shows a comparison with the experimental results of the variation of radial hydride fraction, $F_x(\sigma)$, versus applied external tensile stress as predicted by Equation 4-9. As the authors note, the model over estimates the orienting efficiency at the lower stresses and under estimates it at the higher stresses. Still, overall, there is good correspondence between the predictions and the experimental results.

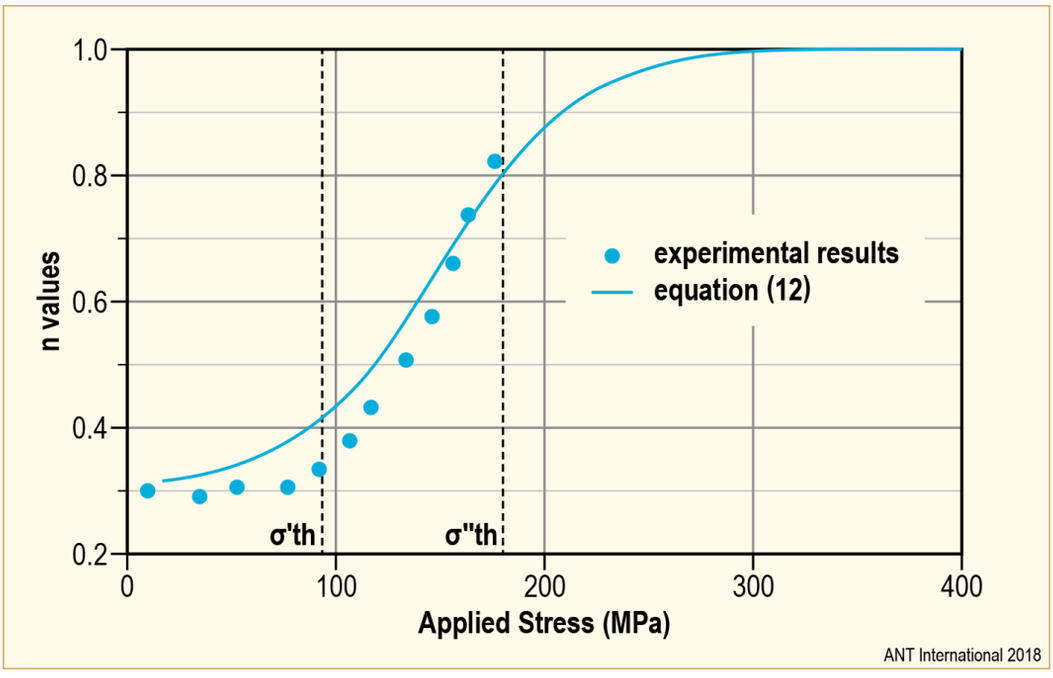

Figure 4-5: Plot showing comparison between model predictions and experimental results (from [Bai et al., 1994]). The solid line, marked equation (12) in the plot, is the model prediction based on Equation 4-9. The '*n* values' given by the vertical axis are equivalent to $F_x(\sigma)$ as defined in this text.

It has to be said, in reviewing the foregoing derivation of the practical form of the Ells/Puls model given by Equation 4-9, that some steps in Bai and co-workers' derivation of this equation seem at odds with the physical basis of the Ells/Puls model. To start with, the Ells/Puls model does not contain the term F_x as an argument in the exponentials in the expressions for the number of radial and circumferential hydrides formed under stress as given by the authors in Equation 4-7 and Equation 4-9. In addition, as noted in the foregoing, in the Ells/Puls model the pre-exponential in Equation 4-7 and Equation 4-9 should be the ratio $N_x^{circ}(0)/N_x^{rad}(0)$ in the absence of <u>any</u> stress acting on the material whereas the experimental value used by the authors implicitly accounts for the effects of residual stress on this ratio.

4.2 More recent applications of the Ells/Puls hydride reorientation theory

For Zr-2.5Nb pressure tube material, the pickup rate of hydrogen has been found to be sufficiently slow that it was not expected – even close to end-of-design life of the pressure tubes – that hydrides would be present in pressure tubes during normal operating temperatures. Hence very few studies subsequent to that of [Hardie & Shanahan, 1975] were initially carried out to determine the threshold stress for radial hydride formation. Moreover, because of the uncertainty introduced by the presence of a varying residual macroscopic stress produced through the wall thickness when using tapered tension specimens produced from flattened pressure tube material, some of these subsequent studies – applied to pressure tubes – used a different criterion for determination of the radial hydride reorientation threshold stress. The approach used to determine this threshold stress, however, does not readily lend itself to comparison with predictions of the Ells/Puls hydride reorientation theory. The results of these subsequent tests on pressure tube material are reviewed in Sections 4.4.1 and 4.4.2, whilst only studies on fuel cladding material are reviewed in this section.

For fuel cladding material, the increasing demands for high burn-up fuel has resulted in increasing number of studies being carried out focussed on quantifying the effects of radial hydrides as potentially causing failure of the fuel cladding under thermo-mechanical loading conditions thought to be present during abnormal reactor operation and during the transport and dry storage of spent fuel.

The reason for the need for these studies in fuel cladding is that in high-burn-up fuel the higher hydrogen content, increased corrosion (hence, wall thinning), higher level of radiation damage, higher decay heat in the fuel at comparable cooling time and higher fission gas pressure (hence, higher cladding stress) compared to those of lower-burn-up fuel, would influence the propensity for formation of radial hydrides and, hence, failure of the cladding.

Current U.S. regulations for storage (10 CFR 72) and transportation (10 CFR 71) of Spent Nuclear Fuel (SNF) are designed primarily i) to maintain sub-criticality and to ensure that radiation doses are less than regulatory limits; ii) that fuel rod storage casks provide adequate fuel confinement and containment; and iii) that the fuel is retrievable. As the discharged fuel burn-up level increases, SNF Zircaloy-4 (Zry-4) cladding may become more susceptible to brittle failure under normal conditions and under postulated accident conditions that could occur during handling, storage, and transportation. Although cladding failure is not prohibited by federal regulations, such failure and gross fuel dispersal may compromise the foregoing regulatory requirements, and increase operational exposure and clean-up cost.

In the following we concentrate (in chronological order) on studies of radial hydride formation in fuel cladding in which applications to extant theoretical models were made.

4.2.1 Hydride stress orienting in recrystallized Zircaloy-2 sheet (Sakamoto and Nakatsuka, 2006)

Sakamoto and Nakatsuko [Sakamoto & Nakatsuko, 2006] carried out a study to examine the effects of texture, hydrogen content, thermal cycling and hydride morphology on the threshold stress to reorient hydrides in unirradiated RXA Zircaloy-2 sheets. As shown in Figure 4-6, the effect of texture on the threshold stress was determined by machining tensile specimens along four different directions having orientations of 0, 30, 60 and 90° with respect to the rolling direction of the plate material. Table 4-2 shows the variation of the texture in the three orthogonal sheet directions of rolling, width and transverse directions (RD, WD and TD, respectively). It can be seen from the values of these Kearns factors that there is approximate similarity in the magnitudes of these factors between the sheet and fuel cladding material, with the WD and RD corresponding to the circumferential and axial directions of the fuel cladding material, respectively.

Table 4-2: Kearns parameters, f_{axial}, f_{circ}, f_{rad}, for the RD, WD and TD, respectively, of the plate. The designation of these Kearns factors as corresponding to the axial, circumferential and radial directions of fuel cladding tubes was made by Sakamoto and Nakatsuka [Sakamoto & Nakatsuka, 2006] on the basis that these factors have closely similar magnitudes in the indicated plate directions.

	f_{axial} (RD)	f_{circ} (WD)	f_{rad} (TD)
Sheet A	0.074	0.210	0.718
Sheet B	0.050	0.237	0.718

Similar to the approach of Hardie and Shanahan [Hardie & Shanahan, 1975] the effect of stress on hydride orientation was determined using tapered tensile specimens cut from the plate but in the latter case with stressing axes at various angles to the rolling direction. The material was charged with hydrogen ranging from 61 to 668 wppm. The specimens were subjected to thermal cycles ranging from 290 to 150 or 360 to 160°C. Holding time at the maximum temperature was one hour and cooling rate was less than 1°C/min. After the tests, the specimens were sectioned and examined metallographically to determine the hydride orientation as a function of distance (stress) along the tapered specimen. The usual parameter, F_x, was used to quantify the fraction of radial hydrides in the specimen with x corresponding, in this case, to the fraction of hydrides oriented within 40° of the normal direction. The value of $F_x(\sigma_{res}) \equiv F_{40}(\sigma_{res})$ was ≈ 0.03 for the hydrogenated specimens prior to the reorientation tests.

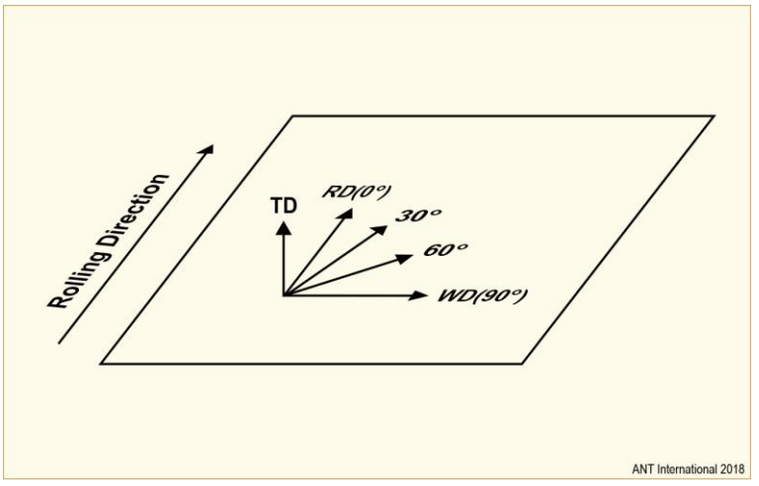

Figure 4-6: Direction of tapered specimens cut from Zircaloy-2 rolled plate (from [Sakamoto & Nakatsuko, 2006]). TD, RD and WD in the figure refer to the transverse, rolling and width directions, respectively.

Figure 4-7 shows that the fraction of radial hydrides, $F_x(\sigma)$, formed by cooling under an external stress of 160 MPa increases according to the angle the tensile specimen makes with the rolling direction (ranging from 0 to 90°). The results from these four specimen directions can be considered as being equivalent to applying a uniaxial tensile stress in a tube specimen ranging from being directed along the axial to the circumferential direction of the tube. As the texture starts out at a very low value for the RD specimen and only reaches a value of ≈ 0.20 for the WD specimen, it is not surprising that the authors find that there is an effect of texture on threshold stress for 'radial' hydride formation in these types of tests of specimens having fairly high hydrogen content. It is seen from Figure 4-8 – showing only the results for the WD specimen (specimen direction at 90° to the rolling direction) – that there appears to be a threshold stress of about 80 MPa before this effect on specimen orientation (and, hence, Kearns factor) manifests itself. The authors note that this is the case for all specimen orientations. Figure 4-8 also shows that the results obtained do not depend on hydrogen content in the sample. It is seen, however, from the steep increase in the trend of $F_x(\sigma)$ versus applied stress at 160 MPa that this stress is less than the saturation value. That is, one would expect from the Ells/Puls theory, the data of [Hardie & Shanahan, 1975], and the steep increase in $F_x(\sigma)$ versus applied stress at 160 MPa that there is an applied stress, greater than 160 MPa, at which the change in $F_x(\sigma)$ versus applied stress flattens out and the fraction of reoriented ('radial') hydrides would be close to unity (at least for all specimens with hydrogen content such that all of the hydrides would have been dissolved at the maximum temperature to which the samples were taken).

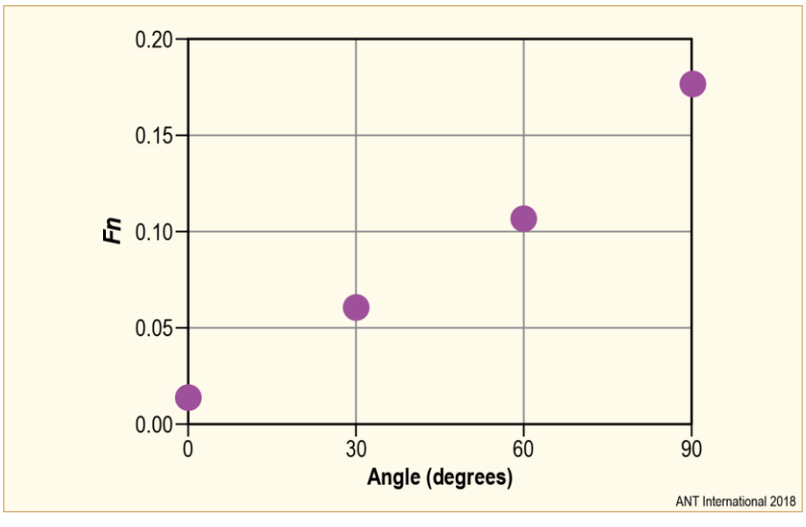

Figure 4-7: Texture dependence of $F_x(\sigma)$ (denoted by *Fn* in the figure) (fraction of radial hydrides) of specimens oriented as indicated in Figure 4-6, containing 60 to 90 wppm hydrogen, loaded at 160 MPa and cycled through the temperature range from 355 to 160°C five times (from [Sakamoto & Nakatsuko, 2006]).

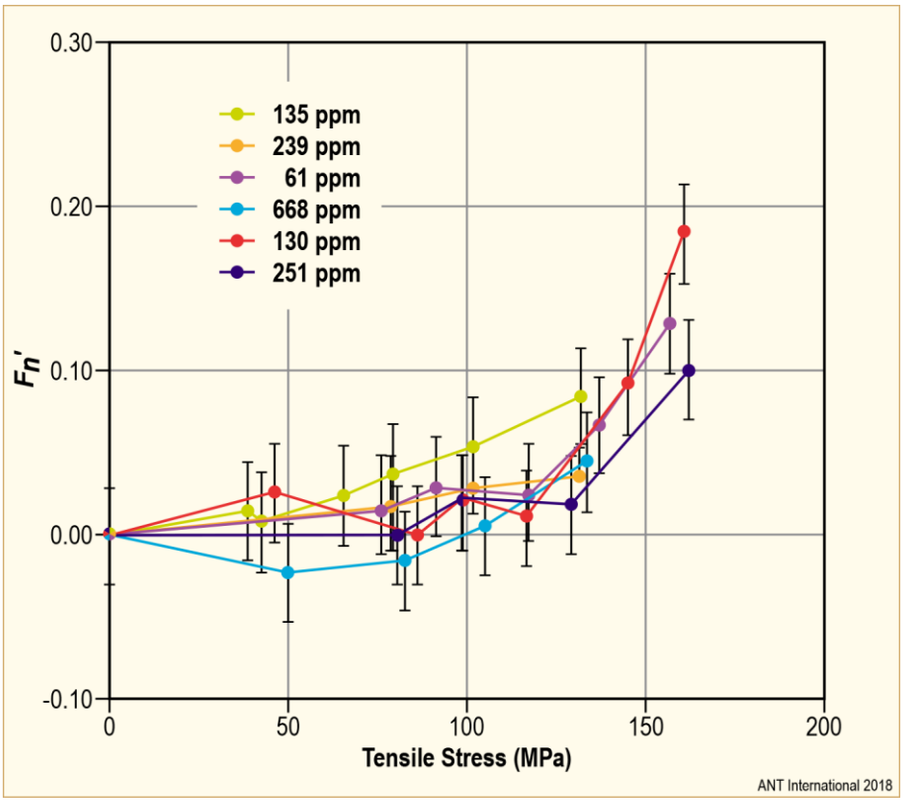

Figure 4-8: Applied stress dependence of $F_x'(\sigma)$ (fraction of 'radial' hydrides relative to the value of $F_x(0)$ at zero load with the former denoted by *Fn'* in the figure) cycled five times between 355 to 160°C with an externally applied tensile stress of 160 MPa for specimens containing 61, 130 and 251 wppm hydrogen and with an externally applied tensile stress of 130 MPa for specimens containing 135, 239 and 668 wppm hydrogen. All tests were done with specimens oriented in the WD (from [Sakamoto & Nakatsuko, 2006]).

The trends in the data of [Sakamoto & Nakatsuka, 2006] at applied stress values below about 80 MPa are similar to those of Bai and co-workers [Bai et al., 1994] in the range from zero to about 100 MPa applied tensile stress in the latter's case. This suggests that there are residual stresses acting in the WD that must be overcome before the external stress increases the probability for 'radial' hydride formation sufficiently for their increase to become observable. The authors show that a good fit between data and the predictions of the Ells model is only obtained when the existence of such residual stresses is accounted for in the model. Plotting the data in terms of R_x, related to F_x according to Equation 3-45 or Equation 3-46 (without the factor 100 when F_x is given as a fraction between zero and one), a good fit to these data is obtained with a numerical fit of the basic Ells expression (in the notation of this text): $R_x^{rad}(\sigma) = A \cdot exp(B \cdot \sigma \cdot cos^2\,\theta)$ – where A and B are fitting constants and θ is the angle between the stress direction and the normal to the hydride platelets – by adding a threshold stress term to this expression that accounts for the residual stress in the specimen. The result is as follows:

Equation 4-10:

$$R_x^{rad}(\sigma) = R_x^{rad}(0) + \alpha \cdot exp[\beta \cdot (\sigma - \sigma_{th}) \cdot cos^2\theta]$$

with $\alpha = 0.007$, $\beta = 0.5$ MPa^{-1}, the good fits shown in Figure 4-9 are obtained when setting $\sigma_{th} = 76$ MPa for the data from tensile specimens produced from sheet A and $\sigma_{th} = 79$ MPa for the data from tensile specimens produced from sheet B which results in $cos^2\theta = 0.0981$. The value chosen for the parameter, $R_x^{rad}(0)$, was not given by the authors. However, it can be obtained from the foregoing data and the general relation between F_x and R_x given by Equation 3-36. Choosing $\sigma_{th} = 79$ MPa, then, yields $R_x^{rad}(0) \cong 0.021$.

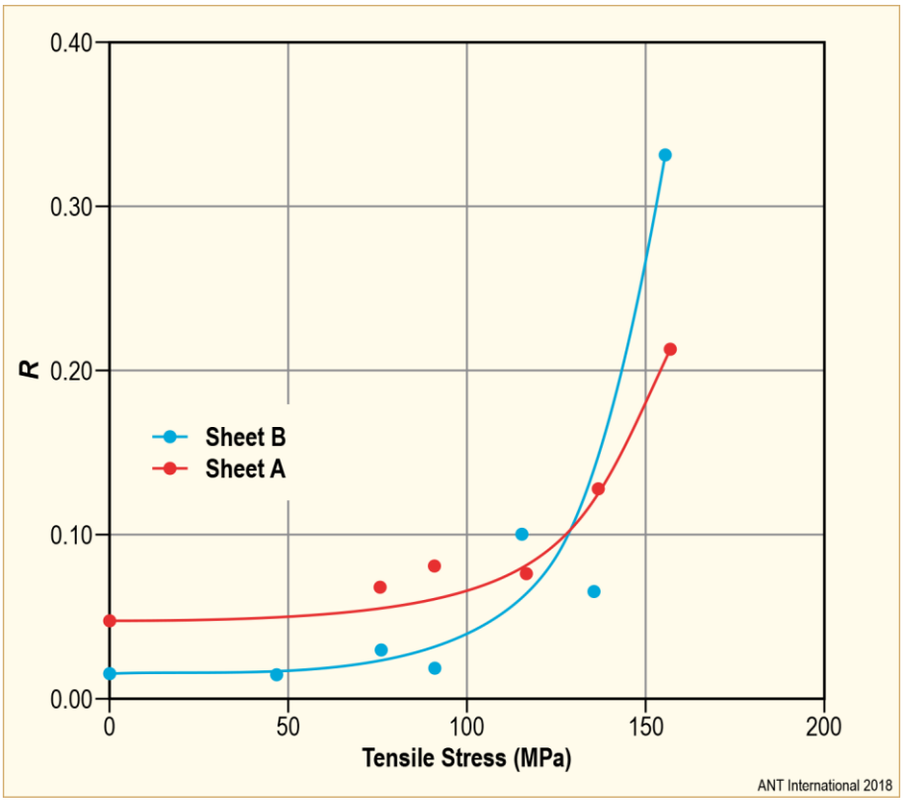

Figure 4-9: Applied stress dependence of R_{σ} (ratio of fraction of 'radial' to 'circumferential' hydrides; denoted by *R* in the figure) for specimens cut in the WD from two different sheets (A and B). The solid and dashed lines represent fits to the data using the general expression derived from the Ells model given by Equation 4-10 in which account was also taken of presumed residual compressive stresses acting in the tensile loading direction of these WD-oriented specimens. Residual compressive stresses of –76 and –79 MPa were assumed for specimens taken from sheets A and B, respectively (from [Sakamoto & Nakatsuko, 2006]).

To extract an upper hydride reorientation threshold stress from the fit to the data given by Equation 4-10, it is useful to plot this equation in terms of $F_x(\sigma)$, which is related to $R_x^{rad}(\sigma)$ according to $F_x(\sigma) = R_x^{rad}(\sigma)/(1 + R_x^{rad}(\sigma))$. The result is shown in Figure 4-10 where the abscissa is given in terms of the external stress acting on the hydrides. The negative of the latter stress was taken by Sakamoto and Nakatsuka to be the lower threshold stress for hydride reorientation. *Physically, the lower threshold stress is the externally applied tensile stress above which the fraction of reoriented hydrides first starts to increase from its as-received value of* $R_x^{rad}(0) \cong 0.021$. From the plot of Figure 4-10, *an upper threshold stress can also be defined since, at values of* $F_x(\sigma)$ *close to unity, the variation of* $F_x(\sigma)$ *versus Net Stress changes little with stress.* Assuming this point to correspond to $F_x(\sigma) = 0.97$, the upper threshold stress for hydride reorientation obtained from the fitted model is approximately 231 MPa. This seems reasonable with an assumed residual compressive stress of 80 MPa since the fraction of radial hydrides in the externally unstressed state is $F_x(\sigma) \cong 0.03$. If all hydride orientations were found within the radial-circumferential plane (i.e., grains oriented with basal pole normals oriented in the axial direction), because of the low Kearns factor for grain orientations in the axial direction, without any internal residual stress the orientation of the hydrides would be randomly distributed between the circumferential and radial directions (or, perhaps, distributed according to the Kearns factor ratios of grain orientations in the circumferential and radial directions). The experimental observation, however, is that the fraction of radial hydrides is $F_x(0) \cong 0.03$ and approximately remains at this level until the externally applied tensile stress reaches 79 MPa. From the Ells/Puls model one would expect the fraction of radial hydrides to gradually and continuously increase from its internally unstressed value as the externally applied stress is increased from zero. However, as seen by the good numerical fit of the model to the experimental data, this increase in radial hydride fraction is quite small and within experimental uncertainty up to an external increase in stress of 79 MPa. It should be noted that one uncertainty in applying this model is the experimentally unknown value of radial hydride fraction produced with the specimen under both zero internal and external stresses.

5 Theoretical evaluations of hydride precipitate morphology and stress orienting based on Phase Field Methodology

5.1 Introduction

In recent years, advances in numerical modelling and computing power have made it practical to use the Phase Field Methodology (PFM) as a convenient physical basis for numerical evaluations of microstructural changes. The particular advantage of the PFM is that it requires the simultaneous solution of only a few sets of equations in order to follow – and graphically map – the heterogeneous evolution with time of the microstructure from some non-equilibrium state. Tracking a particular microstructural evolution is made possible with this methodology through the introduction of "order" parameters, η_p, the numerical values of which describe the evolution of various uniquely identifiable features, p, of the microstructure. These parameters may or may not have a macroscopic physical meaning. Their values are chosen so that each is restricted to vary in value between zero and one. For instance, in modelling the formation of β phase precipitates from a previously homogeneous system consisting of α parent phase in a binary solid the order parameter is η_p = 1 and 0 for the β and α phases, respectively, and would vary between values $0 < \eta_p < 1$ over some distance between the interfaces of these two phases. A number of order parameters, p, might be needed to distinguish between different variants, for instance, different orientations of the β phase in relation to the crystallographic directions of the α phase. As indicated in the foregoing, in the PFM the order parameters do not change discontinuously between matrix and precipitate. The distance over which the order parameter varies between the two phases determines the width of the interface. The phase field, then, refers to the set of values that the η_p order parameters take throughout the chosen volume. In this method, the total free energy, F, of the system is described in terms of the η_p parameters and their gradients plus equations for mass (composition), heat conduction and stress state. The order parameter is generally a non-conserved variable compared to other variables such as solute/solvent concentrations needed for the complete description of the free energy of the system. Concentrations are conserved variables and, as a result, the mathematical formulations for their temporal and spatial evolution are different compared to those for any non-conserved order parameters. A feature of this methodology is that the order parameters vary in value over some width at the α/β interfaces. As result, the PFM is often referred to as a diffuse interface model, in contradistinction to models in which the interface is taken as being atomistically sharp. Sharp interface models are thought to provide a closer representation of interfaces in real systems. However, tracking the evolution of such interfaces requires more equations compared to what is required with the PFM, particularly for complex shapes. This feature makes the solution of sharp interface models prohibitive except for highly simplified cases. PFMs could also deal with sharp interface boundaries, but the need for a corresponding sharp increase in the order parameters that would be required to describe such a sharp interface in the PFM comes at the cost of increase in computational time, which scales with the dimensions of the simulation.

It is usual in solving these types of problems with the PFM to use the time dependent Ginsburg-Landau type equation for the evolution of the non-conserved order parameters and the corresponding Cahn-Hilliard-type equation for the diffusion of the conserved solute parameter. Both of these equations, in their original form, were developed quite some ago to describe the evolution of certain types of second order (critical) phase transitions. The distinguishing feature of critical phase transitions compared to first order phase transitions is that, unlike the latter, in which there are abrupt finite changes in some of the thermodynamic variables of the system, such as the composition of the precipitating phase during the phase transformation, the onset of a critical phase transformation is characterized by the gradual, continuous disappearance or appearance of one or more thermodynamic variables – the order parameters – which become zero at the phase transition point (the critical point). In critical phase transitions, near the critical point, only small changes in the order parameter(s) (which could, for instance, also be a concentration variable) are required to change the state of the system drastically. This means that the phase transformation manifests itself through the formation of gradients of composition or order parameters, accompanied by increasing fluctuations of these composition or order parameters as the critical point is approached. To mathematically describe these effects the governing equations need to account for these gradients in order parameters and/or composition. In the case of the Ginsburg-Landau equation this theory was originally developed – based on Landau's theory of second order phase transitions – to provide a phenomenological description of the transition from normal to superconductivity. In the case of the Cahn-Hilliard equation it was developed to describe spinodal decomposition of binary fluids having a miscibility gap as such systems exhibit critical behaviour at the consolute point of the phase field. Spinodal decomposition is predicted to occur in this case when the system is cooled to temperatures within the two-phase region of the phase diagram for average compositions that are inside the locus (the spinodal) defining the condition at which

the second derivative of the free energy is zero. The difference between the two equations is that in the Ginsburg-Landau equation the evolution of the system is described in terms of non-conserved order parameters, whilst in the case of the Cahn-Hilliard equation it is described in terms of a conserved compositional variable. In both original applications of these equations the physical problems to which they were applied required the use of only one order parameter. However, in general, both structural and compositional variables are needed to track the evolution of a system as it evolves from its non-equilibrium to its equilibrium state. Note that when the Cahn-Hilliard equation is applied to the evolution of a first order phase transformation, the compositional gradient term takes on the role of the surface energy term as given in classical nucleation models in the latter of which the change in composition and surface boundary between the two phases is abrupt. It also means that the interface in the Cahn-Hilliard equation has a finite composition gradient, i.e., it is diffuse. The combined use of these two equations, in which both structural (non-conserved) and compositional (conserved) variables are simultaneously tracked makes it possible to graphically solve for and represent the two or three dimensional evolution of the phase transformation throughout the volume considered, with the important benefit that there is no need to specify *a priori* the morphology of the precipitates as they form or dissolve.

5.2 Cahn-Hilliard model of an incoherent, isotropic thermodynamic system

In the original treatment of Cahn and Hilliard for an incoherent, two-component isotropic system of volume, V, the Helmholtz free energy, F, is approximated by the sum of the Helmholtz free energy, $f'(c)$, per unit volume of a homogeneous system of composition, c, plus a gradient energy term defined as the difference between homogeneous and heterogeneous (actual) free energy density, $\kappa(\nabla c)^2$, *viz.* [Cahn & Hilliard, 1959]:

Equation 5-1:

$$F = \int_V [f'(c) + \kappa(\nabla c)^2 + \cdots]dV$$

with

Equation 5-2:

$$\kappa = -[\partial^2 f/\partial c \partial \nabla^2 c]' + \frac{1}{2}[\partial^2 f/(\partial|\nabla c|)^2]'$$

where the prime indicates that the spatial derivatives are to be evaluated at the limit of small ∇c and $\nabla^2 c$ so that κ is approximately independent of the compositional gradients. Equation 5-1 and Equation 5-2 were derived by assuming that deviations from homogeneity of an initially homogeneous system can be expressed as a Taylor series expansion about the homogeneous state, f_o, [Cahn & Hilliard, 1958]. For a cubic lattice, or an isotropic continuum, the free energy density is invariant to the symmetry operations of reflection and rotation about a four-fold axis. This means that, to second order, the Taylor expansion of f reduces to:

Equation 5-3:

$$f(c, \nabla c, \nabla^2 c, \ldots) = f_o(c) + \kappa_1 \nabla^2 c + \kappa_2 (\nabla c)^2 + \cdots$$

Hence, the total free energy is given by

Equation 5-4:

$$F = \int_V [f_o(c) + \kappa_1 \nabla^2 c + \kappa_2 (\nabla c)^2 + \cdots]dV$$

in which the volume integral of the gradient energy term, $\kappa_1 \nabla^2 c$, can, by the divergence theorem, be reduced to

Equation 5-5:

$$\int_V (\kappa_1 \nabla^2 c)dV = -\int_V (d\kappa_1/dc)(\nabla c)^2 dV + \int_S (\kappa_1 \nabla c \cdot n)dS$$

Since it is always possible to choose a boundary of integration such that $\nabla c \cdot n = 0$, the surface integral in Equation 5-5 vanishes, leaving only the first volume integral term. Hence the term $(\kappa_1 \nabla^2 c)$ in Equation 5-4 can be replaced with $(d\kappa_1/dc)(\nabla c)^2$ and with $\kappa = -d\kappa_1/dc + \kappa_2$, the total Helmholtz free energy reduces to the volume integral given by Equation 5-1 with κ given by Equation 5-2.

Cahn and Hilliard point out [Cahn & Hilliard, 1959] that Equation 5-1 and Equation 5-2 should hold for any composition fluctuation capable of describing the full range of composition fluctuations resulting in the decomposition of a homogeneous phase into a two-phase mixture ranging from classical nucleation to spinodal decomposition. In the case of classical nucleation, the composition fluctuations are large in degree (amplitude) but small in (spatial) extent. Such fluctuations lead to phase separations for which there is a sharp interface (and hence large gradients) in the order parameters and composition between the two phases. As a result there is a finite (but still microscopic) energy barrier that needs to be overcome for a critical nucleus to form. Given a suitable definition of the surface energy to account for the excess gradient energy generated by the sharp interface, this is the case described by the classical nucleation model. In the spinodal decomposition case the fluctuations are small in degree but large in extent with the result that in this case there is no energy barrier other than a diffusional one for the spontaneous formation of the second phase. The compositions in the phase diagram at which this is possible are when the Gibbs free energy derivatives with respect to composition, $(\partial^2 G/\partial c^2)_{P,T} < 0$. The locus at which $(\partial^2 G/\partial c^2)_{P,T} = 0$ is referred to as the spinodal inside of which spinodal decomposition is possible. Between the spinodal and the bimodal – the latter being the locus of composition versus temperature at which the two phases are in equilibrium (i.e., the phase field locus in an incoherent mixture) – the system is metastable since finite (but still microscopic) composition fluctuations are required to overcome a finite energy barrier (the critical nucleation energy) for phase separation to occur.

Note that, unlike in the classical nucleation model where the structural characteristics and the composition of the nucleus and the surrounding parent phases are assumed to have the values of the bulk phases in equilibrium with each other (i.e., as given by the phase diagram), in the Cahn-Hilliard model of nucleation and growth, the chemical free energy, strain energy and surface (gradient) energy changes need to be determined for structural (order parameter) and composition variables having values other than those given by the equilibrium phase diagram. *Since free energy values away from the equilibrium state of the system are rarely known, this is one of the weaknesses of this model for quantitative application when applied to phase transformations under conditions conforming more closely to the classical nucleation model of phase separation.*

5.3 Application of PFM to hydride precipitates in zirconium

Shi and co-workers were the first to apply the PFM to simulate the morphological development and orientation of hydride precipitates in externally stressed and unstressed zirconium material. The earliest such paper is that of Ma and co-workers [Ma et al., 2002]. In this paper the shape and orientation of γ–hydride precipitates forming during their nucleation and growth stages with or without externally applied stress is evaluated. This study was restricted to the formation of the γ–hydride phase because the symmetry in the transformation strains of this phase with respect to the α–Zr matrix [Carpenter, 1973] allows the problem to be solved in two dimensions. γ–hydride precipitates have a face-centred-tetragonal crystal structure lying on the $(1\ 0\ \bar{1}\ 7)_{\alpha-Zr}$ planes of the matrix, which are within 15° of the $(0\ 0\ 0\ 1)_{\alpha-Zr}$ pole. Observed in the basal, $(0\ 0\ 0\ 1)_{\alpha-Zr}$, plane of the matrix they appear needle-like with axes along the three equivalent $\langle 1\ 1\ \bar{2}\ 0\rangle_{\alpha-Zr}$ directions. The objectives of the authors' study were to determine the shapes, distributions and orientations of these precipitates with or without an externally applied uniaxial tensile stress. To simplify the modelling in this first attempt at using the phase field method for this type of system the authors assumed that the polycrystalline material has grains of only one orientation with respect to the externally applied stress and that any effects of grain boundaries are ignored. In effect, this means that the modelled system consisted of a single crystal.

For the complete description of the γ–hydride phase formation in this case, three long range order parameters, $\eta_1(r,t)$, $\eta_2(r,t)$, $\eta_3(r,t)$, were needed to account for the three possible $\langle 1\ 1\ \bar{2}\ 0\rangle_{\alpha-Zr}$ directions along which the γ–hydride precipitates can lie. As in the case of the classical nucleation model, the energies involved in the evolution of the multi-phase microstructure consist of the sum of the change in chemical free energy of the system in its *incoherent* state, the formation of the total interfacial energy between the two phases, the strain energy of matrix and precipitates produced by the transformation strains of the precipitates throughout the volume of the system and the work done by external or internal stresses as a result of changes in hydrogen in solution in the matrix and phase fraction of hydride precipitates. In the mathematical formulation of the change in free energy from its unstable homogeneous state to its stable heterogeneous state, all of these energy changes and work terms are given as a function of changes of the field variables, $c_H(r,t)$ and $\eta_p(r,t)$ with time, t, and

position, r. The temporal evolution of the microstructure (i.e., the spatial and morphological development of the hydride precipitates and the hydrogen atoms in the α–Zr matrix were determined from the simultaneous solutions of the Ginzburg-Landau type equation for the long range order parameters, $\eta_p(r,t)$, and the Cahn-Hilliard type equation for the diffusion of the hydrogen concentration, $c_H(r,t)$[19].These equations have the general form, respectively:

Equation 5-6:

$$\frac{\partial \eta_p(r,t)}{\partial t} = -L_p \frac{\delta F}{\delta \eta_p(r,t)} + \zeta_p(r,t)$$

Equation 5-7:

$$\frac{\partial c_H(r,t)}{\partial t} = M\nabla^2 \frac{\delta F}{\delta c_H(r,t)} + \xi(r,t)$$

where L_p = kinetic coefficient characterizing the structural relaxation, $\eta_p(r,t)$

M = kinetic coefficient giving the diffusion mobility of hydrogen in solution;

F = total free energy of the system that, depending on what variables are held constant, is either the Helmholtz or the Gibbs free energy

$\zeta_p(r,t), \xi(r,t)$ = Langevin random noise terms

$\eta_p(r,t)$ = Long-range order parameter as function of position, r, and time, t

The Langevin random noise terms are related to the chemical fluctuations in the long range order parameter(s) and in the composition, respectively and have a Gaussian distribution, satisfying the fluctuation-dissipation theorem [Lifshitz &Pitaevskii, 1980]. In the explicit formulation of F it is important to recognize that this function actually represents a change in energy from some reference state.

Since, unlike in the original formulations of Cahn and Hilliard [Cahn & Hilliard, 1958, 1958], there are now also order parameters as well as concentration variables required in describing the phases, Equation 5-1 becomes:

Equation 5-8:

$$F = \int_V \left[f\left(c_H(\eta_p(r))\right) + \sum_{p=1}^{\nu} \frac{\kappa_p}{2} \left(\nabla \eta_p(r)\right)^2 + \frac{\kappa_c}{2} (\nabla c_H)^2 \right] d^3r + E + W$$

where κ_p $(or\ \alpha_p)$ = gradient energy coefficient of the order parameters

κ_c $(or \beta)$ = gradient energy coefficient of the hydrogen concentration

E and W = total strain energy and work term contributions, respectively, to the free energy

Explicit expressions for these in the general case and for the Zr-H system are given in Sections 5.3.1 to 5.3.3. The total interfacial surface energy, γ, of the system is the excess free energy associated with the gradient energy terms and the change in chemical free energy between the homogeneous and the heterogeneous state, which is given by:

[19] Although the rate dependent Equation 5-7 is now generally referred to as the Cahn-Hilliard equation, it is only the $\delta F/\delta \eta_p(r,t)$ term in that equation that was originally derived by Cahn and Hilliard in the usual references cited concerning this equation.

Equation 5-9:

$$\gamma = \int \left[f(c_H, \eta_p) - f_o(c_H) + \sum_{p=1}^{\nu} \frac{\alpha_p}{2} \left(\nabla \eta_p(r) \right)^2 + \frac{\beta}{2} (\nabla c_H)^2 \right] d^3 r$$

where

Equation 5-10:

$$f_o(c_H) = f\left(c_H^{\gamma}, \eta_{po}(c_H^{\gamma}) \right) + \frac{f\left(c_H^{\gamma}, \eta_{po}(c_H^{\gamma}) \right) - f(c_H^{\alpha}, \eta_p = 0)}{c_H^{\gamma} - c_H^{\alpha}} (c_H^{o} - c_H^{\alpha})$$

where $c_H^{\gamma} = c_{H,eq}^{\gamma}$ = hydrogen concentration at incoherent equilibrium of the γ–hydride precipitate phase

$c_H^{\alpha} = c_{H,eq}^{\alpha}$ = hydrogen concentration at incoherent equilibrium of the α–Zr matrix phase

c_H^{o} = average hydrogen concentration in the system

(It is implicitly assumed in the following derivation applied to the formation of γ–hydride precipitates that this phase is an equilibrium one, despite the preponderance of experimental evidence indicating that it is a metastable one.)

The authors used a Landau-type polynomial expression for the expansion of the chemical free energy about the equilibrium (incoherent) composition values $c_{H,eq}^{\alpha}$ and $c_{H,eq}^{\gamma}$ of hydrogen in the matrix and γ–hydride phases, as follows:

Equation 5-11:

$$f(c_H, \eta_P) =$$

$$\frac{A_1}{2}(c_H - c_{H,eq}^{\alpha})^2 + \frac{A_2}{2}(c_H - c_{H,eq}^{\gamma}) \sum_{p=1}^{\nu} (\eta_p^2) - \frac{A_3}{4} \sum_{p=1}^{\nu} (\eta_p^4) + \frac{A_4}{6} \sum_{p=1}^{\nu} (\eta_p^6) +$$

$$A_5 \sum_{q \neq p}^{\nu} \eta_p^2 \eta_q^2 + A_6 \sum_{p \neq q, p \neq r}^{\nu} \eta_p^4 (\eta_q^2 + \eta_r^2) + A_7 \sum_{p \neq q \neq r}^{\nu} \eta_p^2 \eta_q^2 \eta_r^2$$

The constants A_1 to A_7 are phenomenological coefficients with the values of A_1 to A_4 mainly determining the two minima compositions, $c_{H,eq}^{\alpha}$, for which $\eta_p(\boldsymbol{r}, t) = 0$ and $c_{H,eq}^{\gamma}$, for which $\eta_p(\boldsymbol{r}, t) = 1$ or -1, in the chemical free energy variations whilst the proper choice of the remaining constants, A_5 to A_7 ensures that two (or three) different hydride variations cannot grow at the same location. Note that *the concentrations at the two minima are the phase field concentrations of the two phases in incoherent equilibrium.* All effects of coherency strains on phase field compositions are assumed contained in the elastic strain energy contribution to the total energy, expressions for which are given in the following. *Strictly speaking no experimental results exist in the Zr-H system which precisely gives the foregoing concentrations since the usual experimental phase field data contain both the effects of coherency strains and hysteresis.*

5.3.1 Summary of Khachaturyan and Shatalov theory of coherency energy changes arising from size mismatches between atoms and lattice mismatches between matrix and precipitate phases

In addition to the chemical free energy changes and corresponding spatial gradients in composition and order parameters, account must be taken of coherency energy changes arising from size mismatches between atoms and from lattice mismatches between matrix and precipitate phases. Some time ago Khachaturyan and Shatalov (KS) [Khachaturyan & Shatalov, 1969] developed a general formalism to express the change in total mechanical

energy of a system evolved from a previously homogeneous state to a heterogeneous mixture of coherent misfitting inclusions. (Inclusions – as defined by Eshelby [Eshelby, 1957] – are misfitting particles having the same elastic constants as the surrounding matrix.) These misfitting particles impose transformation strains, $e_{ij}^{T}(r)$, on the body. (Note that these transformation strains are sometimes also referred to as incompatibility strains to express the fact that they are not produced by internal or external sources of stress in the body but are the result of phase transformations in which there are differences in volumes and/or shapes between the transformed and original phases, or the results of the introduction of misfitting point defects such as atoms, vacancies and interstitials.) Locally, the transformation strains imposed by these inclusions result in strains that vary with distance from their source locations and differ depending on whether inclusion and matrix deform according to elastic or elastic-plastic constitutive relationships.

A detailed description of the KS theory is given in Khachaturyan's book [Khachaturyan, 2008]. In this derivation based on a continuum, linear elastic model of a solid body of finite volume, V, and stress-free boundaries, the total mechanical energy of such a body in which inclusions with transformation strains, $\varepsilon_{ij}^{T}(p)$ of types, p, are introduced, is given as the linear sum of two parts, one arising from the spatially homogeneous, the other from the spatially heterogeneous parts of the strains produced in the body by these transformation strains.

The spatially homogenous component is, in addition, made up of two parts, one giving the sum of the self-energies of the inclusions, the other the relaxation energy of the body under static equilibrium when these inclusions are inserted coherently into the body. The strain energy contribution from the self-energies of the inclusions is the linear sum of the individual self-energies. This is given by:

Equation 5-12:

$$E_{self} = \frac{1}{2}\sum_{p=1}^{\nu} V_p C_{ijkl}\, e_{ij}^{T}(p) e_{kl}^{T}(p)$$

where C_{ijkl} = elastic constants

V_p = volume of a single inclusion (corresponding to the original volume of the material transformed to the p^{th} inclusion)

ν = number of inclusions of type, p

(Note that Khachaturyan [Khachaturyan, 2008] and other authors use the notation e_{ij}^{o} and σ_{kl}^{o} for the transformation strains and stresses.)

During the relaxation, each inclusion initiates lattice displacements in its vicinity that are opposed by the elastic response of the inclusion and the remainder of the body. This relaxation energy is approximated in Khachaturyan's derivation [Khachaturyan, 2008] by a power series in the relaxed strains, $e_{ij}(\boldsymbol{r})$ giving the relaxation energy per unit volume, $f_{relax}(\boldsymbol{r})$, as follows:

Equation 5-13:

$$f_{relax}(\boldsymbol{r}) = \frac{1}{2} C_{ijkl} e_{ij} e_{kl} - \sigma_{kl}^{T}(\boldsymbol{r}) e_{ij}$$

where $\sigma_{kl}^{T}(\boldsymbol{r})$ and C_{ijkl} are equivalent to the first and second order expansion coefficients of the power series.

The total relaxation energy – to second order in the relaxed strains – is then obtained by integration of $f_{relax}(\boldsymbol{r})$ over the volume of the body, giving:

Equation 5-14:

$$E_{relax} = \int_{V} \left[\frac{1}{2} C_{ijkl} e_{ij} e_{kl} - \sigma_{kl}^{T}(\boldsymbol{r}) e_{ij}\right] dV$$

In the further development of Equation 5-14, the heterogeneous nature of the multi-connected, multi-variant medium is mathematically expressed through the relation:

Equation 5-15:

$$e_{ij}^{T}(\boldsymbol{r}) = \sum_{p=1}^{\nu} \tilde{\theta}_p(\boldsymbol{r}) e_{ij}^{T}(p)$$

where $\tilde{\theta}_p$ is a shape function, defined by Khachaturyan [Khachaturyan, 2008] as being equal to unity inside and zero outside of each inclusion of type, p. The shape function specifies the location and shape of each inclusion associated with a particular transformation strain. With the shape function defined in this way, Equation 5-15 describes a body containing inclusions of different types (characterized by their transformation strains) separated from the material surrounding it by a sharp interface.

With elastic stress related to elastic strain according to the standard relation:

Equation 5-16:

$$\sigma_{ij}(\boldsymbol{r}) = \frac{\delta E_{elast}}{\delta e_{ij}(\boldsymbol{r})} = -\sigma_{ij}^{T}(\boldsymbol{r}) + C_{ijkl} e_{kl}$$

The strain, $e_{ij}^{T}(\boldsymbol{r})$, corresponding to the stress-free state, is determined from Equation 5-16 by setting $\sigma_{ij}(\boldsymbol{r}) = 0$ giving:

Equation 5-17:

$$-\sigma_{ij}^{T}(\boldsymbol{r}) + C_{ijkl} e_{kl}^{T}(\boldsymbol{r}) = 0$$

Substituting $\varepsilon_{kl}^{T}(\boldsymbol{r})$ given by Equation 5-15 into Equation 5-17, then, yields the definition of $\sigma_{ij}^{T}(\boldsymbol{r})$:

Equation 5-18:

$$\sigma_{ij}^{T}(\boldsymbol{r}) = \sum_{p=1}^{\nu} \tilde{\theta}_p(\boldsymbol{r}) \sigma_{ij}^{T}(p)$$

where

Equation 5-19:

$$\sigma_{ij}^{T}(p) = C_{ijkl} e_{kl}^{T}(p)$$

Substituting Equation 5-18 into Equation 5-14, the relaxation strain energy is given by:

Equation 5-20:

$$E_{relax} = \int_{V} \left[\frac{1}{2} C_{ijkl} e_{ij} e_{kl} - \sum_{p=1}^{\nu} \sigma_{ij}^{T}(p) \tilde{\theta}_p(\boldsymbol{r})\, e_{ij} + \right] dV$$

The relaxation strain energy contains terms linear in strain because of the presence of internal sources of strain (the transformation strains) that are not produced as a result of internally or externally applied stresses. In a body in mechanical equilibrium, these sources of strain retain their source strengths and generate relaxed strains, e_{ij}, in the body that are non-zero.

In the further development of the relaxation strain energy expression, Khachaturyan [Khachaturyan, 2008] separated the total strains in the body into two linearly additive components: a homogeneous component, given by $\bar{e}_{ij}$, which is the source of all the macroscopic volume and shape changes of the body as determined at the outer boundary and a remaining heterogeneous component, given by $\delta e_{ij}(\boldsymbol{r})$, producing no overall changes in volume and shape of the body. Mathematically the relationship between these strains is expressed by:

Equation 5-21:

$$\delta e_{ij}(\boldsymbol{r}) = e_{ij}(\boldsymbol{r}) - \bar{e}_{ij}$$

with the condition

Equation 5-22:

$$\int_V \delta e_{ij}(\boldsymbol{r})\, dV = 0$$

The homogeneous component, given by $\bar{e}_{ij}$ follows from the mechanical equilibrium condition of a finite body for which the external surfaces of the body are stress free (in the absence of any externally applied stresses or strains). These homogeneous strains are denoted with a bar across them to indicate that they are averaged strains, approximately uniform throughout the body, independent of the locations of the inclusions and, hence, having no spatial dependence. Because of the latter property, these strains are sometimes also referred to as non-configurational strains.

With the separation of the strains into the foregoing two components, defined by Equation 5-21 and Equation 5-22, the total relaxation strain energy is now given by the linear sum of the homogeneous and heterogeneous components, *viz.*,

Equation 5-23:

$$E_{relax}^{total} = E_{relax}^{hom} + E_{relax}^{heter}$$

Equation 5-24:

$$E_{relax}^{hom} = \frac{V}{2} C_{ijkl} \bar{e}_{ij} \bar{e}_{kl} - \sum_{p=1}^{\nu} V_p \sigma_{ij}^{T}(p) \bar{e}_{ij}$$

Equation 5-25:

$$E_{relax}^{heter} = \int_V \left[\frac{1}{2} C_{ijkl} \delta e_{ij} \delta e_{kl} - \sum_{p=1}^{\nu} \sigma_{ij}^{T}(p) \Delta\tilde{\theta}_p(\boldsymbol{r}) \delta e_{ij} \right] dV$$

where $\Delta\tilde{\theta}_p$ in Equation 5-25 is given by the relation:

Equation 5-26:

$$\Delta\tilde{\theta}_p(\boldsymbol{r}) = \tilde{\theta}_p(\boldsymbol{r}) - \frac{V_p}{V}$$

The relation:

Equation 5-27:

$$\int \tilde{\theta}_p(\boldsymbol{r}) dV = V_p$$

which follows from the definition of $\tilde{\theta}_p(\boldsymbol{r})$, was employed for the derivation of Equation 5-23 to Equation 5-25.

Now the relaxation energies given by Equation 5-23 to Equation 5-25 depend on two sets of internal parameters: the components of the homogeneous strains, $\bar{e}_{ij}$, and the local elastic displacements, $\boldsymbol{u}(\boldsymbol{r})$. The latter are related to the heterogeneous strains by the standard relationship between displacements and strains, *viz.*,

Equation 5-28:

$$\delta e_{ij} = \frac{1}{2}\left(\frac{\partial u_i}{\partial r_j} + \frac{\partial u_j}{\partial r_i} \right)$$

The equilibrium expressions of the relaxation energies, given by Equation 5-23 to Equation 5-25, are obtained through the mechanical equilibrium conditions:

Equation 5-29:

$$\frac{\partial E_{relax}^{total}}{\partial \bar{e}_{ij}} = 0$$

Equation 5-30:

$$\frac{\partial E_{relax}^{total}}{\partial u_i(\boldsymbol{r})} = 0$$

Taking the derivatives given by Equation 5-29 of the relaxation energy given by Equation 5-23 to Equation 5-25 and equating the result to zero gives:

Equation 5-31:

$$VC_{ijkl}\bar{e}_{kl} - \sum_{p=1}^{\nu} V_p \sigma_{ij}^T(p) = 0$$

This result can be written, making use of the relation for $\sigma_{ij}^T(p)$ given by Equation 5-19:

Equation 5-32:

$$\bar{e}_{ij} = \sum_{p=1}^{\nu} w_p e_{ij}^T(p)$$

where w_p is the volume fraction, V_p/V, of inclusions of type, p. *Equation 5-32 shows that elastic relaxation involves homogeneous strain and, moreover, that the associated shape and volume change of the body is proportional to the volume fraction of the inclusions contained in the body.*

Substituting the relaxed value of homogeneous strain given by Equation 5-32 into Equation 5-23, the total homogeneous component of relaxation strain energy is given by:

Equation 5-33:

$$E_{relax}^{homo} = -\frac{V}{2}\sum_{p=1}^{\nu}\sum_{q=1}^{\nu} C_{ijkl} e_{ij}^T(p) e_{kl}^T(q)\, w_p w_q$$

The derivation for the heterogeneous component of the relaxed strain energy involves taking the derivative given by Equation 5-30 of the relaxation strain energy expression given by Equation 5-25. As this derivation is rather lengthy, involving expressing the results in terms of Fourier transforms, the reader is referred to Khachaturyan's book [Khachaturyan, 2008] for the details. A key feature of this derivation is the recognition – following from the definition of the heterogeneous strains – that the local displacements, $\boldsymbol{u}(\boldsymbol{r})$, vanish at the free surface. The result, in terms of Fourier transforms, for the heterogeneous elastic relaxation energy is given by:

Equation 5-34:

$$E_{relax}^{heter} = -\frac{1}{2}\sum_{p=1}^{\nu}\sum_{q=1}^{\nu}\int \frac{d^3k}{(2\pi)^3} B_{pq}(n)\left\{\Delta\tilde{\theta}_p(\boldsymbol{r})\right\}_{\boldsymbol{k}}^{*}\left\{\Delta\tilde{\theta}_q(\boldsymbol{r})\right\}_{\boldsymbol{k}}$$

where

Equation 5-35:

$$B_{pq}(n) = n_i \tilde{\sigma}_{ij}^T(\boldsymbol{k})\Omega_{jk}(n)\tilde{\sigma}_{kl}^T(\boldsymbol{k})n_l$$

or, in vector notation,

6 Summary and Conclusions

The summary and conclusions given here are longer than one would normally expect to find in a report of this type. It was felt, however, that the information provided up to this point – covering the totality of the field from its inception to its present time – is so varied and complex that a concise but yet sufficiently detailed summary was in order. The aim was to provide a reasonably self-contained account that, nevertheless, provided sufficient detail for its content to be readily understood without reference to any of the figures, tables and almost all equations given in the preceding sections. Because this section is still quite lengthy, it has been subdivided into subsections that correspond to similar ones given in the preceding sections.

6.1 Early Work

From early studies carried out at the start of nuclear reactor development in the 1950s to the end of the 1960s, a number of key observations concerning hydride orientations in tubes had already been established. These observations are:

a) Hydrides formed under slow cooling conditions show up as irregularly shaped elongated stringers when viewed at optical magnifications. (A hydride stringer is defined here as a collection of closely clustered smaller platelet-shaped hydride precipitates, the thickness, length and distribution of which depend on the material's texture, hydrogen content and cooling rate.)

b) *In externally unstressed tubes manufactured for reactor application, hydride stringers are preferentially oriented with their traces in the circumferential/axial tube directions.* The shapes and orientations of the broad outlines of these stringers are similar to those of the grains in which they are contained. Selected observations indicate that these transverse stringers consist of a collection of clusters of short individual hydrides, frequently tilted ≈ 45° to the circumferential tube direction in the circumferential-radial plane.

c) Uniaxial tensile stress applied during cooling over temperature ranges where hydride precipitation occurs produces hydride stringers oriented with their traces perpendicular to this stress and parallel to the direction of compressive stress.

d) Stress applied during isothermal hold after a cool down (during which there would be no further hydride precipitation) *does not affect the existing distribution of hydride orientations.*

e) Reorientation of hydride stringers from circumferential to radial direction by an external tensile stress applied in the circumferential direction during hydride precipitation requires that the applied stress exceed a threshold stress. Above this threshold stress value, the proportion of reoriented hydride stringers measurably increases with increase in the magnitude of the external tensile stress.

f) The smaller hydride platelets making up a stringer were found to reside on similar, preferred habit planes with respect to the α–Zr matrix grains in which they were located. The individual hydride habit planes are the same irrespective of whether the macroscopic orientations of the stringers were changed with application of an external stress.

g) In commercial α– and α/β–zirconium alloys (Zircaloy and Zr-2.5Nb, respectively) the habit planes of hydride platelets – as deduced from optical observations of hydride stringers – are oriented 5 to 20° from the basal pole direction of the α–Zr matrix grains in which they form. This result is consistent with hydride habit planes of $\{1\ 0\ \bar{1}\ 7\}_{\alpha\text{–}Zr}$ (≈ 14° from the basal pole direction) determined subsequently in these alloys.

h) Based on the information given in items a) to f), it was concluded that the observed preferred circumferential orientation of hydride stringers in externally unstressed, cold-worked, fine-grained material occurs because of the presence of internal tensile stress generated in the radial tube wall direction in grains oriented with their basal pole oriented in the radial direction or compressive stress in the circumferential direction of grains with their basal poles oriented in the circumferential direction. It is conjectured that these internal tensile or compressive stresses are produced during the reduction in wall thickness of the tubes during the cold working step under conditions resulting in only a small reduction in tube diameter. In this case, plastic flow in the tube would be directed in the circumferential direction.

i) The fraction of hydrides that can preferentially orient under a tensile stress in a given direction is limited by the availability of grains having favourable basal pole orientations. In general, the basal pole fraction in any direction that would be limiting for complete preferential hydride orientation would

depend – in addition to the grain size – on the total volume fraction of hydrides at the precipitation temperature. In tubes in which the Kearns factor is generally less than 0.1 there are insufficient grains with basal pole orientations in the axial direction for stress-reorientation of hydrides with their platelet normals pointing in this direction.

6.2 Theoretical Model

For the determination of hydride nucleation rate under zero stress an expression was developed based on classical nucleation theory. The classical model involves developing an expression for the increase in Gibbs free energy of formation of a hydride nucleus of critical dimensions. To account for the effect of stress on the resultant change in critical nucleation energy, an approximate solution (see Equation 3-18 to Equation 3-28) was derived that applies when the change in net interaction energies for hydride formation of a nucleus of critical size is much less than the sum of the changes in chemical and strain energies for this formation. In this case, the total Gibbs free energy change for hydride nucleus formation is simply the sum of the Gibbs free energy change for nucleus formation under zero stress plus the Gibbs free energy change for formation under stress. In the classical model, the nucleation rate is proportional to an exponential term with exponent given by the total Gibbs free energy change of formation of a nucleus of critical size divided by the usual product of Boltzmann constant and absolute temperature at the nucleus formation temperature. Hence, in this approximation the nucleation rate is proportional to the product of the usual hydride nucleation rate expression under zero stress multiplied by an additional exponential term with exponent given by the product of the volume of the critical nucleus under zero stress times the net interaction energy change for formation of this nucleus. In a closed thermodynamic system the net interaction energy change is given by the interaction energy change for hydride formation minus the interaction energy change under the same stress for removal of hydrogen in solution to form this hydride. The latter interaction energy change was modified from the original solution by Puls to account for the anisotropy of the transformation strains of hydrogen in solution. This anisotropy arises from the crystallographic anisotropy of the interstitial sites of the hcp α–Zr lattice in which the hydrogen atoms reside.

The approximate solution of the Ells/Puls model for hydride nucleation under non-hydrostatic stress predicts that an increase in the volume of the critical nucleus increases the potency of the effect of stress on hydride reorientation, but with an associated decrease in nucleation rate. A corollary to this is that when the rate of increase in hydrogen supersaturation is slow, such as at very slow cooling rates or for hydrogen diffusion to local regions of elevated stress or decreased temperature, the potency for hydride reorientation is increased. The magnitude of the critical nucleation volume depends on the hydride's surface energy, the increase in chemical driving energy with decrease in temperature below the incoherent solvus (or, conversely, with increase in hydrogen concentration above the incoherent solvus) and the strain energy of the nucleus. The latter depends on the shape of the critical nucleus and its transformation strains with these transformation strains depending, in turn, on temperature and hydrogen composition of the critical nucleus with the hydrogen composition of the latter also depending on temperature.

The model predicts that during precipitation hydride reorientation under a uniaxial tensile stress would occur when the net interaction energy change for the reoriented hydrides is less than that for hydride orientation under zero external stress.

If the difference in interaction energy change for hydride formation and hydrogen removal under the same stress is positive then application of an external tensile stress enhances the nucleation rate compared to the nucleation rate at zero external stress. However, this is the case only if there is a difference in partial molar volumes or transformation strains between hydrogen in solution and in hydride precipitates. The earliest models developed to account for the effect of stress on hydride orientation as given by Ells, and for other materials by Sauthoff, neglected to include the change in interaction energy of hydrogen atoms removed from solution to form hydrides or, in the model by Sauthoff, Au solute atoms removed from solution to form Au-rich precipitates. The subsequent treatment by Puls included this term but assumed that the transformation strains of the removed hydrogen atoms in solution are isotropic. In this case, the theory predicts that there would be no difference in the strength of the stress orienting effect, whether or not the contribution to the net interaction energy of the removal of hydrogen in solution is included. This is because, if hydrogen atoms in solution have isotropic transformation strains, there is no difference in interaction energy for the removal of these atoms regardless of the orientation of the external stress with respect to the orientation of the hydrides. Therefore the predictions for the interaction energy difference between unreoriented and reoriented hydrides are the same in both the original Ells and subsequent original Puls hydride nucleation models.

In estimates of the potency of stress reorientation the inclusion of the anisotropy of the transformation strain matrix of hydrogen in solution means that the contribution to the interaction energy arising from the removal of

hydrogen atoms in solution affects the difference in interaction energies between circumferentially and radially oriented hydrides. However, inclusion of this interaction energy term also creates an uncertainty in the predictions of the model for the magnitude of the stress reorienting effect since it results in the prediction that there could be two possible bounding solutions. One bounding solution is based on the assumption that hydrogen removed from solution for hydride formation in a given grain comes from either the same grain or from near-by grains having identical orientations with respect to the direction of the externally applied stress (i.e., they are part of the same (closed) thermodynamic system). Alternatively, a larger interaction energy difference for hydride reorientation is achieved if the hydrogen atoms required for forming the hydride nuclei are assumed to come predominantly from grains in which the chemical potential of hydrogen in solution (diffusible hydrogen) is greater than it is in the grains in which the reoriented hydrides are formed.

In summary, preferential, stress assisted hydride reorientation during nucleation occurs because the transformation strains of hydrogen in solution and hydride precipitates are anisotropic with the governing anisotropy being that of the transformation strains of the hydride precipitates. Hydrides aligned with their plate normals in the direction of a uniaxial tensile stress are predicted to have lower negative interaction energy and, hence, greater nucleation rate, than those aligned in the other two orthogonal directions.

For the simplest case of a material having a crystallographic texture consisting of only two sets of grain orientations, one set of grains having basal poles oriented in the radial direction, the other set of grains having basal poles oriented in the circumferential direction, the present model for stress assisted hydride reorientation shows that when the source of hydrogen in solution to form hydrides comes from the same set of grains in which the hydride precipitates are formed, the difference in interaction energies for hydride formation in the two sets of grains is much reduced compared to the case if the transformation strains of the hydrogen atoms in solution had isotropic symmetry. In this latter case only the transformation strains for hydride formation enter into the difference in interaction energy between the two orientations. A similar result as the latter is, however, also obtained when taking account of the anisotropy of the transformation strains of hydrogen atoms in solution when these atoms come from grains that have their basal poles at right angles to the grains in which preferential, stress-driven hydride precipitation occurs.

It is evident from the foregoing that there can be large quantitative differences in the predictions for the orienting potency of hydride precipitates under stress depending on the differences in magnitudes of the three dilatational components of transformation strains for hydride formation. Two sets of transformation strain matrices are in current use in the literature. The set with the least amount of anisotropy is derived assuming hydride formation occurs via a pure lattice strain transformation. The other set with the greatest amount of anisotropy was derived assuming that hydride formation occurs via an invariant plane strain transformation. In this case all of the volumetric strain for hydride formation is directed in the direction of the hydride precipitate's plate normal with the other two transformation strains in the plane of the plate approximately equal to zero. No direct experimental evidence exists to verify which of these two proposed sets of transformation strains occurs in reality. Further on, results of atomistic models of hydride formation are discussed that attempt to shed light on this uncertainty.

Both sets of transformation strain matrices predict that under a uniaxial tensile stress directed in the circumferential direction of a tubular component there would be an increase in temperature at which radial hydrides (hydrides with their normals in the circumferential direction) first precipitate compared to the precipitation temperature of hydrides when there is no uniaxial tensile stress. The largest increase in temperature is obtained when assuming that hydride formation occurs via an invariant plane strain transformation. For this case the model predicts that radially oriented delta hydride precipitates would form at higher temperatures than circumferentially oriented precipitates. For example, for a uniaxial tensile stress of 200 MPa, the shift in precipitation temperature at 300°C from that of an unstressed material is ≈ 4°C. Such a large temperature shift is at, or slightly greater than, the uncertainty of most solvus determination techniques and should therefore be detectable. However, this large shift was calculated for material for which it was assumed that there are only two sets of sharply defined grain orientations at 90° to each other. Actual materials do not have such a sharply defined texture and the integrated temperature shift over all grain orientations may not be detectable in such materials based on the sensitivities of present methods of solvus determinations. These methods effectively provide values for the onset of hydride precipitation that represents an average over all orientations. This point is explored in more detail in Section 5.2 in which the results of recent synchrotron X-irradiation studies by Vizcaíno and co-workers are presented.

One often used experimental approach to quantifying the degree of hydride orientation has been to define a parameter, F_x, giving the ratio of the number of hydride platelets whose edges make traces having angles, φ, between 0 to x degrees from some reference direction, divided by the total number of hydrides of all

orientations between 0° and 90° from this reference direction. For tubular specimens in which case the number of radial hydrides formed is of importance for predicting the fracture toughness of the component, the reference direction chosen is the radial direction. These hydrides or hydride clusters are described as being non-aligned because the orientations of their platelet edges are perpendicular to the direction of the hoop stress in pressurized tube components. In the case considered in the following this means that radial hydrides are non-aligned hydrides under a circumferentially oriented external tensile stress. In terms of the model for hydride reorientation under stress an expression for F_x is derived assuming that in relating the experimentally determined parameter, F_x, to theoretically predicted one it is useful to define a parameter, R_x^{rad}, given by:

Equation 6-1:

$$R_x^{rad} = N_x^{rad}/N_x^{circ}$$

where N_x^{rad} = number of hydrides having φ values in the range 0 to x degrees from the radial direction

N_x^{circ} = number of hydrides with their orientations in the range x to 90 degrees from the radial direction

From the definition of F_x we have that:

Equation 6-2:

$$F_x = N_x^{rad}/(N_x^{rad} + N_x^{circ})$$

Dividing both numerator and denominator in this relation by N_x^{circ} then yields:

Equation 6-3:

$$F_x = R_x^{rad}/(1 + R_x^{rad})$$

A theoretical estimate of R_x^{rad} and, hence, F_x, is obtained from the nucleation rate expressions by assuming that the number of hydrides that have grown to observable size at a given temperature are proportional to their nucleation rate.

A theoretical evaluation of the dependence of F_x versus stress shows that F_x follows a sigmoidal variation with stress which means that, at low stress, F_x follows an exponential increase with stress that, at the point of steepest increase in this dependence, becomes a decreasing function of stress. Because of this exponential dependence, mathematically, there are no finite values of stress between zero and infinity at which there is no change in F_x and, hence, there are no mathematical criteria giving threshold stress values below and above which there are no further changes in F_x. However, for practical purposes, given the generally very gradual increase in F_x with stress at low stress values and, conversely, a similar very gradual decrease at high stress values, engineering lower and upper threshold stress values can be defined for practical applications. An example would be to choose for the lower threshold stress the value at which F_x has increased from 0 to 2 or 3% and for the upper threshold stress the value at which F_x has reached 98%. From the sigmoidal dependence of F_x versus stress one could also expect that for a given set of environmental conditions the magnitudes of the lower and upper threshold stress values are linked such that an increase in the lower threshold stress also means that there would be a corresponding increase in the upper threshold stress. This linkage, for the most part, is evident in the various fits of the theory to experimental results, as discussed in the following.

6.3 Early applications of the Ells/Puls model of hydride reorientation

The studies of Shanahan and Hardie, which were carried out on hydrogenated, flattened pressure tube material in which the flattening procedure produced macroscopic regions of residual stress of opposite signs, were the first to provide results showing that the functional dependences of F_x versus stress predicted by the theory are, indeed, followed by the experimental results. The experimental results also show that for specimens having the same nominal total hydrogen content there is an effect of maximum hold temperature on the lower and upper threshold stress values for hydride reorientation with the lower threshold stress (and, correspondingly, upper threshold stress) increasing with decrease in maximum hold temperature.

Experimental results of Sakamoto and Nakatsuka on plate material show that F_x increases very little with stress over a range of stress values at low stress to a much greater extent than would be predicted by the theory assuming that only an externally applied uniaxial tensile stress were acting on the specimen. The authors attributed this to the existence of internal regions of residual compressive stress directed in the circumferential direction of the specimen and thus acting in opposition to the externally applied uniaxial tensile stress in this direction. The presence of this residual stress would also explain why in specimens cooled from above the solvus under no external stress, $F_x(\sigma,\%) \approx 2\%$; i.e., that most of the hydride stringers had oriented with their edges oriented in the circumferential direction when cooled under zero external stress. The negative of this residual compressive stress was taken by Sakamoto and Nakatsuka as the value of the lower threshold stress for hydride reorientation because the inclusion of this residual stress in that directions resulted in extending the region of F_x having an experimentally undetectable increase in F_x versus applied external stress, in accord with their experimental results. Physically, with this choice, the lower threshold stress corresponds to the externally applied uniaxial tensile stress above which the fraction of reoriented hydrides shows a detectable increase from its as-received value of $R_x^{rad}(0) \cong 2\%$. Although the range of applied stress was insufficient to show the onset of the decreasing half of the sigmoidal dependence of F_x with stress, an upper threshold stress could similarly be defined corresponding to $F_x(\sigma,\%) \approx 98\%$. It can be shown from the Ells/Puls model that the effect of the presence of the residual compressive stress in the circumferential direction on the upper threshold stress value would be to increase this stress by the same amount as that for the lower threshold stress.

To interpret their experimental data via the Ells/Puls model, Chu and co-workers focussed on the difference in undercooling, ΔT, as a function of decreasing solution temperature as a key parameter controlling the reorientation ratio. Therefore they expressed the theoretical results in the following form (repeat of Equation 4-14):

Equation 6-4:

$$F_x(\sigma,\%) = \frac{100}{\left(1 + 49 \cdot exp\left[-\frac{D \cdot \sigma}{(\Delta T)^3 T}\right]\right)}$$

whilst also accounting in the experimental determination of $F_x(\sigma,\%)$ for the reduction in the total number of hydrides that could be reoriented for a given solution temperature and total hydrogen content in the specimen. That is, the total number of hydrides of all orientations in the denominator of $F_x(\sigma,\%)$ is based on the dissolution solvus concentration at the solution temperature.

An evaluation was carried out by this writer for three solution temperatures of 450, 400 and 350°C assuming that each of these solution temperatures corresponds to the equilibrium (incoherent) solvus temperature. For simplicity, it was assumed in the modelling that the solution temperature is then equivalent to T_{TSSD}, thus defining the hydrogen content in the specimen. Hence ΔT would be the difference between the TSSD and TSSP temperatures with the TSSP temperatures determined from those experimental results that detect the onset of hydride nucleation. The correlations of Pan and co-workers were used to determine ΔT because these authors had determined a range of TSSP loci. The curve having the lowest precipitation temperatures, designated as TSSP1, was assumed to represent the locus of solvus temperatures at the onset of hydride nucleation. *Based on these TSS correlations it is seen that the difference in temperature between hydride dissolution and precipitation increases with decreasing hydrogen content (Figure 4-12) with the result that lower and upper threshold stresses also increase with increasing hydrogen content.*

When the expression for $F_x(\sigma,\%)$ given in the foregoing is plotted versus circumferential stress *assuming a constant value for ΔT for all dissolution temperatures, there is a shift to the left in the sigmoidal curves with decreasing dissolution temperature, although this shift is smaller than the shift to the right for the case of ΔT increasing with decrease in dissolution temperature.* In the former case there is now a decrease of the hoop stress at the upper threshold value of $F_x(\sigma,\%) = 98\%$ and little change in the hoop stress at the lower threshold value of $F_x(\sigma,\%) = 3\%$ because all $F_x(\sigma,\%)$ values at the three solution temperatures were pinned to $F_x(\%) = 2\%$ at zero external tensile stress.

Overall it can be seen (Figure 4-12 and Figure 4-13) that the foregoing fitted Ells/Puls hydride stress re-orientating expression for $F_x(\sigma,\%)$ – with fitting constants to experimental data assumed independent of temperature – always predicts a similar direction of shift with hydrogen content for both the lower and the upper engineering threshold stress limits, with the amount of shift for these limiting values depending on the steepness of the dependence of $F_x(\sigma,\%)$ versus stress at the lower and upper threshold stress values.

From the trend in the model predictions of the efficacy of a given applied external stress in producing radial hydrides, it can be seen that this efficacy increases with increase in solution temperature, provided all hydrides had been taken into solution at the highest temperature of the thermo-mechanical cycle.

6.4 Extensions of the Ells/Puls hydride model for hydride stress reorientation

Based on the Ells/Puls model of stress assisted hydride reorientation during nucleation, Massih and Jenkvist developed a solution methodology for hydride stress reorientation capable of accounting for the simultaneous variation in hydride volume fraction and orientation during continuous cooling under a uniaxial tensile stress. The results of this study show that nucleation rate increases with decrease in critical nucleation volume whilst (Equation 4-21) orienting potency increases with increase in critical nucleation volume. Thus at the start of the spike in the fraction of radially oriented hydrides with times, at 2 900 s, the critical nucleation volume varies rapidly and is largest at the beginning compared to a subsequent rapid drop – with corresponding increase in nucleation rate – over the following 200 s. The result is that the hydride orienting potency (and, hence, fraction oriented) is largest at the start of the spike but drops rapidly over this time interval during further cooling until a quasi-steady-state supersaturation level is achieved throughout the remaining cooling stage during which there is little change in nucleation rate (and, hence, critical nucleation volume) corresponding to little change in orienting potency.

Qin and co-workers developed a modified version of the Ells/Puls hydride reorientation model to predict the effect that grain boundaries have on hydride nucleation and orientation potency under an external uniaxial tensile stress. The authors based their theoretical formulation closely on the classical study of Johnson and co-workers in which it was shown that the existence of planar facets along the interface between nuclei and matrix produces coherent interfaces whilst the interfaces at the edges are incoherent. These interface properties have important effects on the precipitation kinetics of both homogeneous and heterogeneous nucleation. Possible shapes of grain boundary nuclei proposed by Johnson and co-workers were used to determine expressions for the critical Gibbs free energy changes for the formation of hydride nuclei on grain boundaries. It is evident from the model developed that the magnitudes of grain boundary energies are key factors in determining whether grain boundary nucleation is favoured over intra-granular nucleation. There is a threshold grain boundary energy at which grain boundary nucleation is the preferred mechanism. The authors found that the greatest reduction in the critical Gibbs free energy change for grain boundary nucleation under external stress – and, hence, increase in preferential orientation – is achieved, not surprisingly, when the habit planes of the hydrides on at least one side of the grain boundary are parallel to the externally applied uniaxial tensile stress direction. This prediction is consistent with the experimental observations of Une and co-workers and of those of the authors.

A different method to determine the hydride reorientation threshold to that based on the value of F_x was carried out by Leger and Donner on flattened material taken from Zircaloy-2 and experimental Zr-2.5Nb pressure tube material, the latter of which had been specifically manufactured to reduce their irradiation-induced axial elongations during time in service. Use was made of tapered specimens, cut such that their tensile axes were in the circumferential direction of the tube. Since these specimens were flatted from rounded sections of pressure tube they contained macroscopic regions of residual stress of opposite sign through the thickness (i.e., prior pressure tube wall) direction of the specimens which, overall, balanced to zero. After the reorientation tests, composite micrographs of the circumferential-radial plane of the entire tapered section of individual specimens were made. These composite micrographs showed that there is a fairly distinct boundary representing the locations where overall hydride orientation changes from being mostly circumferential to mostly radial. It was recognized that this boundary is the net result of two sources of stress: externally applied and internal residual. Comparison of the variation of this boundary through the cross-section of these specimens with the residual stress patterns obtained by Hardie and Shanahan in similarly flattened specimens showed that the residual stress pattern had a strong effect on hydride orientation. To account for these residual stresses in determining the threshold stress for hydride reorientation, Leger and Donner used two different methods as follows.

The first method (Method 1) takes account of the fact that the overall residual stress must balance to zero across the specimen's wall and that this distribution is the same along the entire tapered length of the specimen. As both residual and externally applied stresses are in the elastic range, the stress at any one location could then be assumed to consist of the sum of the local values of residual and externally applied stresses. The latter stress varies with distance along the tensile axis of the specimen whilst the former varies with distance across the wall of the specimen. It was then assumed that the local, through-wall residual stresses did not vary along the axial direction. The final assumption in this method was that hydride stress reorientation requires the attainment of a

threshold stress. The threshold stress could then be obtained as the stress for which the integrated areas of compressive and tensile stresses balance.

The second method (Method 2) of obtaining the hydride reorientation threshold stress involved a simpler procedure compared to Method 1. It consisted of plotting the fraction of the specimen's wall thickness containing 100% radial hydrides against the nominal applied stress on the cross section. The stress along the taper at which 50% of the thickness contains only radial hydrides was then determined as the reorientation threshold stress assuming that the residual stresses were distributed such that equal and opposite cross-sectional areas have equal and opposite residual stress values.

Comparison of the threshold stress values obtained with the two methods showed close agreement between them although the stress balancing method tended to give threshold stress values that were systematically higher by up to 7%. From the results of the residual stress distribution, Leger and Donner were able to determine the threshold stress in the transition zone at which radial hydrides made their first appearance. As expected, these (lower) threshold stress values were considerably reduced in magnitude – but were also less precise – than the (upper) threshold stresses at which all hydrides had become radially oriented.

The main conclusions from this study were *that there is a clear correlation between the threshold stress for radial hydride formation and the material's ultimate tensile strength in the axial tube direction showing that the threshold stress increases with increase in the material's longitudinal ultimate tensile strength.* On the other hand, small variations in texture, grain size and dislocation density were found to have no evident effect on threshold stress.

In a study by Hong and Lee to determine the temperature dependence of radial hydride stress reorientation in tube specimens, three different specimens were heated under an applied load to 200, 300 and 400°C, then cooled by 100°C in each case at a cooling rate of 4°C/min below which the load was removed and the specimens air-cooled to room temperature. For each of the three specimens the load was adjusted so that it was always at a value of ≈ 68% of the yield strength. Since the yield strength decreases with increase in temperature, this meant that the load was continuously reduced during heat up and increased during cool down. The combination of total hydrogen content in the samples and thermo-mechanical cycles was such that radial hydride precipitates formed in the presence of unreoriented hydrides. An analysis of the amount of hydrogen content available for reorientation, then, required the use of TSSP data relevant to such a physical situation. Only the TSSP data of Pan and co-workers on Zr-2.5Nb PT material provided such data.

The prediction from this analysis based on the TSSP data of Pan and co-workers was that the thermal cycle with the highest maximum temperature would have the largest predicted radial hydride ratio. These predicted results were, however, not in accord with the authors' experimental ones. It was argued by this writer that the reason for this disagreement could be the presence of a stress gradient across the wall of the tubular material.

A similar set of studies as those of Hong and Lee were carried out by Min and co-workers. The reorientation tests were carried out under a constant tensile stress of 150 MPa and under a variety of cooling rates. Both F_x and average radial hydride lengths as a function of cooling rate were measured. Regarding the effect of hydrogen content, the usual result was obtained; i.e., F_x decreased with increase in hydrogen content when it was greater than what is completely dissolvable at the maximum temperature of the thermal cycle (in this case, 400°C). A similar trend was followed by the average lengths of the hydrides. There was also an important effect of cooling rate on these two parameters with both increasing with decrease in cooling rate. *The authors interpreted this effect of cooling rate as having its origin in the temperature dependence of the threshold stress for* $F_x(\sigma,\%)$*, which is shown in the literature as increasing with decrease in maximum temperature. However, it is not made clear how such a result could then lead to a cooling rate effect on radial hydride fraction.* The most direct explanation for the cooling rate effect would seem to be that increasing the cooling rate increases the undercooling temperature (i.e., the reduction in temperature below the incoherent solvus) and, hence, the rate at which most hydride nucleation occurs. *It was demonstrated with the use of the Ells/Puls hydride nucleation model that an increase in undercooling results in an increase in the upper threshold stress (i.e., the stress at* $F_x(\sigma,\%) = 98\%$ *beyond which there is little further increase in this parameter).* For values less than this stress there is a sigmoidal variation of applied stress on the fraction of radial hydrides formed. *The effect of cooling rate based on the predictions of the Ells/Puls model would then appear to be two-fold. One is that as the tests were all carried out with the same constant applied stress, this stress could cease to be sufficient to achieve close to 100% radial hydride formation as the cooling rate (and, hence, undercooling) increases. The second is that the critical nucleus sizes increase with decrease in undercooling and, hence, cooling rate. Since the difference in formation frequency of radial to circumferential hydrides is proportional to the exponential of the volume of the*

critical nucleus times the hydride interaction energy difference, this means that the preference for radial compared to circumferential hydrides increases with decrease in undercooling.

In a study on hydride reorientation in Zircaloy-4 fuel cladding tubes, Desquines and co-workers used a C-shaped Compression Test (CCT) apparatus and specimen configuration to explore the effect of a wide range of hydrogen contents on the lower and upper threshold stresses for first appearance and for close to 100% radial hydride formation, respectively, in such components. Two maximum temperatures of 350 and 450°C were used for the thermo-mechanical cycles on specimens containing hydrogen contents ranging from 50 to 600 wppm. Threshold stresses for radial hydride reorientation were determined by superimposing on these metallographic sections the contours of circumferential stress as determined from finite element analysis through the thickness and along the circumference of these specimens.

The results show that the threshold stress for precipitating close to 100% of radial hydrides during the cooling stage of the thermo-mechanical cycle does not depend on the maximum temperature between 350 and 400℃*, although it is somewhat dependent on hydrogen content. On the other hand, the lower threshold stress for onset of radial hydride formation is influenced by both sample hydrogen content and maximum temperature of the thermal cycle.*

Using a linear combination of the minimum stress required for the onset of formation of radial hydrides and the minimum stress for formation of 100% of radial hydrides, a simple interpolation equation was derived quantifying the fraction of radial hydride formation in between these two limits. This equation is in good agreement with literature data except for results of pre-irradiated M5, although data for this material are very limited coming from only one type of test. *On the basis of the present knowledge, then, the test result for the M5 specimen suggests that there is a greater susceptibility for radial hydride formation. This could be the result of influences of either the metallurgical state of the M5 alloy, or of some specific effect of irradiation.*

In a recent study by Cinbiz and co-workers, hydride reorientation behaviour under multiaxial stress states was assessed based on metallographic examinations of double-edge notched tension ("plane-strain" and "near-equibiaxial") specimens combined with FE analyses of these test geometries. This study produced the surprising result – in terms of the predictions of the Ells/Puls model for hydride reorientation – that the stress for initiation of hydride reorientation, i.e., the lower threshold stress value, decreased with increase in stress biaxiality from stress states of uniaxial to near-equibiaxial tension.

Examination of the equibiaxial samples prepared, post-testing, for metallography shows that the lower threshold stress is only 75 MPa for the region where the ratio of principal stresses $\sigma_2/\sigma_1 > 0.83$. (The absence of radial hydrides near the specimen's edge is consistent with the uniaxial stress state at that location where the local σ_1 value is less than 155 MPa.) The value of 75 MPa for the lower threshold stress when the stress state is in near equibiaxial tension is significantly lower than that of 110 MPa for the lower threshold stress in near plane strain tension when $\sigma_2/\sigma_1 > 0.57$. Hence, these tests show that the lower threshold stress for radial hydride precipitation decreases from 110 MPa to ≈ 75 MPa as the stress biaxiality ratio increases from 0.5 to 0.83. *The consistent trend shown by all of these data is that increasing stress biaxiality decreases the lower threshold stress for hydride reorientation whilst – in all cases – the radial hydrides are oriented such that the platelet normals are aligned along the direction of the local maximum principal stress.*

Overall, the combined test data obtained from uniaxial and multiaxial tension specimens indicate that out-of-plane (radial) hydride precipitation is enhanced by the presence of a multiaxial stress state. Specifically, it was found that the minimum value of the major principal stress required for hydride reorientation decreases in a roughly linear manner with increasing stress biaxiality ratio. The effect of increasing stress biaxiality ratio on the lower threshold stress is significant, with the threshold stress decreasing from ≈ 155 MPa at $\sigma_2/\sigma_1 = 0$ to ≈ 75 MPa at $\sigma_2/\sigma_1 = 0.8$, which is a decrease byabout a factor of two of the lower threshold stress for hydride reorientation for this range of stress states. It is speculated that the reason for this effect of stress state on the lower threshold stress – which cannot be explained in terms of the Ells/Puls model for hydride reorientation – is the presence of stress gradients in these specimens as explained in the following.

A clue to finding an explanation for the effect found in this study of stress state on the lower threshold stress for hydride reorientation – is revealed by plotting the lower threshold stress values versus their corresponding stress biaxiality values. Note that in the determination of the threshold stress in these experiments, the lower threshold stress value is defined as the value of the maximum principal stress (σ_1) at which initiation of hydride reorientation starts. It is found that the lower threshold stress defined in this way correlates linearly with the corresponding stress biaxiality values. Because of this linear relationship and the fact that the lower threshold

stress for hydride reorientation was associated with the value of the maximum principal stress at that location, the mean (hydrostatic) stress, given by:

Equation 6-5: $$\sigma_m = 1/3\,(\sigma_1 + \sigma_2)$$

(assuming plane stress conditions for these thin specimens) is approximately the same at all threshold stress values, equal to 51 ± 7 MPa. The authors concluded from this result that "preferential hydrogen accumulation to regions of high stress biaxiality should *not* occur". However, there must clearly be regions of higher hydrostatic stress in each of the two types of specimens (containing notches or notches and holes) when subjected to uniaxial external tensile stress. In these regions of higher hydrostatic tensile stress the maximum principal stress would be greater than the threshold value and the fraction of reoriented hydrides would be greater than the observable limiting fraction. As a result of the presence of these, albeit small, hydrostatic stress gradients, the regions at which hydrostatic tensile stress values are highest would have slightly higher hydrogen concentrations upon application of an external load prior to reaching the solubility limit for hydride precipitation. Hydride precipitation during cooling would thus start at slightly higher temperatures in these regions in these specimens. Not clear is how and in what direction these very small hydrostatic tensile stress gradients could affect the limiting maximum principal stress below which the fraction of reoriented hydrides would be too small to be observable. Since the observed limit of reoriented hydrides occurred during continuous cooling, the isothermal version of the Ells/Puls model is too limiting to provide a theoretical explanation for the foregoing experimental finding. Theoretical models that – at the very least – account for continuous cooling, such as those of Massih and Jernkvist or those of Shi and co-workers based on PFM models would be needed to obtain at least a semi-quantitative measure of the resultant hydride distribution/ orientations produced upon completion of the thermo-mechanical cycles in these specimens.

6.5 Hydride reorientation tests of irradiated specimens

A comparative study of hydride reorientation for unirradiated and irradiated Zircaloy-4 fuel cladding material was carried out by Daum and co-workers. Two different sets of Zircaloy-4 tube material were used. The tests on unirradiated material were carried out on tubes taken from 900-mm long sections of tubes supplied by Framatom Advanced Nuclear Products (F-ANP). The irradiated material came from an assembly array that had been irradiated for seven cycles in the H.B. Robinson (HBR) Unit 2 reactor. Both materials were fabricated by a similar cold working and stress relieving route, but their original material sources were not the same.

Thermo-mechanical tests to reorient hydrides in the radial direction of the tube wall were carried out on the remnants of the hydrogenated F-ANP and HBR cladding segments, machined into 8-mm-long rings. The combination of rings and tensile grips were analysed using FE assuming an applied average hoop (circumferential) tensile stress of 160 MPa at the ring mid-plane normal to the loading direction. The loading arrangement was such that the top grip was pulled upward whilst the bottom was held rigidly in place.

The conclusion from this study was that irradiation does not appear to affect the threshold stress. This is opposite to what was found by Leger and Donner for unirradiated material having different yield strength values. The explanation given for the latter result was based on the supposition of a connection between the materials yield strength and the magnitudes of internal residual stresses generated during its manufacture resulting in material of increased yield strength also having an increased lower threshold strength value. On the other hand, the significant increase in yield strength produced in irradiated material would not be expected to affect the residual stress in the material, since it was created after manufacture of the tube. Hence, as observed, there would be no corresponding increase in the radial hydride lower threshold stress value compared to in unirradiated material since the residual stress in both materials would be similar.

A number of cladding materials removed from different reactors after long burn up were evaluated for hydride stress reorientation by Aomi and co-workers. Both fuel cladding from BWRs and PWRs were studied. Experimental parameters controlled were temperature, hoop stress, and cooling rate of the cladding specimens. Temperature conditions were chosen to correspond to the expected cladding temperatures in dry storage. The range of applied hoop stress was chosen to straddle the expected threshold stress for radial hydride reorientation at each temperature. The chosen temperature and the hoop stress values represented relatively moderate conditions for radial hydride reorientation compared to those previously reported.

From the results it was found *that there is an increase in the* $Fn(40)$ *(equivalent to* F_x *with* $x = 40°$*) and* $Fl(45)$ *(where* l *refers to the hydride lengths) ratios with increase in cooling rate.* A clue as to the physical reason for this result is that the specimen with the lower cooling rate has a lower volume fraction of hydrides in the cladding material and a correspondingly greater volume fraction of hydrides in the liner compared to the specimen with

the higher cooling rate. *Literature data show that the softer Zr liner material has slightly lower TSSD and TSSP concentrations at a given temperature than does the harder Zircaloy-2 cladding. Hence at temperatures where hydrides are present in both materials there would be some diffusion of hydrogen from the Zircaloy-2 fuel cladding to its liner. At constant temperature, diffusion of hydrogen would stop once the concentration in the liner reached that in the cladding. No precipitation of hydrides would occur in the liner at constant temperature as a result of this diffusion because of the large hysteresis between TSSD and TSSP. However, during cooling this small additional hydrogen in solution would eventually precipitate once the temperature is low enough. When this occurs additional hydrogen in solution would again diffuse into the liner and precipitate as hydride after a sufficient further drop in temperature, and so on with continuous drop in temperature. Given that the additional hydrogen in the liner cannot precipitate until a sufficient drop in temperature needed to reach the TSSP solvus at that concentration had been reached during the cooling, then the slower is the cooling rate the more hydrogen would be able to diffuse from the Zircaloy-2 cladding to the Zr liner. The result of this process is that with decreasing cooling rate there would be less hydrogen in solution in the Zircaloy-2 cladding to precipitate under stress during cooling and, hence, form radial hydrides.* Note that in the experiments of Min and co-workers the opposite result was obtained. In the experiments of these authors, however, the fuel cladding was not surrounded by a Zr liner. In that case all of the hydrogen in solution would have nowhere to go but remain in the cladding regardless of the cool down rate. *The opposite trend observed in the case of the tests by Min and co-workers, then, was attributed to the increase in stress orienting potency as the cooling rate decreases, resulting in lower effective undercooling from the incoherent solvus at which hydride nucleation has its peak steady-state value. The result is a larger critical nucleation volume during nucleation and, hence, greater amplification factor for stress orienting.*

A similar analysis as for the BWR material carried out for the Zr-4 fuel cladding of fuel rods removed from PWR reactors found that compared to the as-irradiated specimen the radial hydride ratio increased after a thermo-mechanical cycle at 300°C with cooling rate of 30°C/h under an applied hoop stress of 115 MPa. In addition, the sum of the lengths of radial hydrides per unit area increased with maximum temperature of the cycle. The increase in the hydride amount after a thermo-mechanical cycle over that in the as-irradiated specimens was closely proportional to the TSSD concentration at the maximum temperature of each cycle.

The effects of cooling rate was that the $Fl(45)$ values in the specimens cooled at 3°C/h (0.05°C/min) are slightly larger than those of specimens cooled at 30°C/h (0.5°C/min), whilst there was little difference compared with the specimens cooled at 0.6°C/h (0.01°C/min). The length of radial hydrides increased with decrease in cooling rate between 30 and 3°C/h (0.5 and 0.05°C/min) whilst the differences between cooling rates of 3°C/h and 0.6°C/h (0.05 and 0.01°C/min) were smaller. These results are qualitatively similar to those obtained by Min and co-workers for unirradiated Zr-Nib cladding material, in which the cladding was also surrounded by a Zr liner.

In analysing their results in relation to the predictions of the Ells model for hydride stress reorientation the authors accounted for the fact that not all of the hydrides present at room temperature would have been dissolved at the maximum temperatures of the thermo-mechanical cycles. To ensure that only the hydrogen in solution at the maximum temperature of the cycle is accounted for in the calculations of the radial hydride precipitate fraction formed under stress, the ratios given by $Fn(40)$ and $Fl(45)$ were re-evaluated to take this into account using a similar approach as that employed by Desquines and co-workers. The revised ratios were denoted by $Fne(40)$ and $Fle(45)$ and the corresponding effective ratios, $Rne(40)$ and $Rle(45)$ were derived from these.

From the mathematical form of the simplified Ells/Puls model, $R_{Fne}(40)$ was expressed in terms of fitting parameters A and B – with these constants assumed independent of temperature – by:

Equation 6-6:
$$R_{Fne}(40) = A \cdot exp\left(\frac{B\sigma}{T}\right)$$

$R_{Fne}(40)$ depends exponentially on applied stress, σ, as opposed to $Fne(40)$, which has a sigmoidal dependence on stress. *The model thus predicts that there should be a linear relationship between the logarithms of* $R_{Fne}(40)$ *versus hoop stress.* It was found that a reasonably good linear dependence was obtained for the data for specimens subjected to a thermo-mechanical cycle with T_{max} of 400°C. However, this was not the case for the thermo-mechanical cycle with T_{max} of 300°C. A difference is also visible in the reorientation behaviour between the regions at the inner and outer surfaces of the specimens. During the cooling stage, for relatively moderate thermo-mechanical cycle conditions such as at T_{max} of 300°C and hoop stress of 70 MPa, new hydrides precipitated in the radial direction in the Zircaloy-2 inner area near the Zr liner where the volume fraction of hydrides was sufficiently small that all of the hydrides would have been completely dissolved at maximum temperature of the thermo-mechanical cycle (i.e., the local hydrogen content would have been lower

7 Closing Remarks

The results of experimental and theoretical studies given in this text and elsewhere in the literature have shown that hydride precipitates have platelet-like shapes with the directions of their in-plane dimensions defining their orientations. The two orthogonal, in-plane directions of these plates are generally not of the same lengths with the length in the axial plate direction being longer than that in the radial or circumferential plate directions (for hydride platelets oriented in either the radial or circumferential directions, respectively). Hydride precipitates have plate- or needle-like shapes primarily because of the anistropic crystal structure of the matrix, this anisotropy resulting in hydride precipitates having anistropic transformation strains, surface energies and elastic or elastic-plastic constitutive properties, with the latter also differing slightly between hydride and matrix. The fundamental driving force governing how these hydride precipitates are oriented is derived from the difference in interaction energy for hydrides of different orientations with respect to internally or externally applied non-hydrostatic stresses. The reason for this difference is because – with the exception of needle-shaped γ–hydride precipitates – the dilatational transformation strains of the hydride precipitates have tetragonal symmetry with the strain components in the plate-face normal directions larger than those in the other two directions. Thus, application of a uniaxial tensile stress produces a negative interaction energy difference when hydride platelets are aligned such that their face normals are in the direction of the applied tensile stress. (Calculation of this interaction energy difference does not require knowledge of the exact shapes of the hydride precipitates.) A tensile stress in the hoop (circumferential) or, conversely, a compressive stress in the radial direction, favours radial hydride orientation when these form in matrix grains having their $\boldsymbol{c}$ axes in the hoop direction whilst the opposite is the case when there exists tensile stress in the radial direction in matrix grains having their $\boldsymbol{c}$ axes in the radial direction. This means that in tubes that are not subjected to any external stress, hydrides have circumferential orientations whilst when a sufficiently large tensile stress is applied in the tube-wall hoop direction these precipitates will form oriented in the radial direction during cooling from above the hydride nucleation temperature.

The hydride transformation strains are source strains, with their magnitudes and directions – for a given crystallographic orientation relationships between the two phases – arising from the difference in crystal structures and lattice parameter values between the two phases. Accurate calculations of these transformation strains in relation to the orientations and shapes of the hydride precipitates requires knowing the orientation relationships between the two phases for the observed habit planes and shapes of the hydrides and the lattice parameter values of the two phases in their stress-free states. Because of the latter requirement, accurately calculating the transformation strains of hydride precipitates of metastable hydride phase is problematic since macroscopic amounts of material consistings solely of a metastable hydride phase in its unstressed state cannot be produced. The crystal structures of the different stable and metastable hydride phases depend on the hydrogen composition of the precursor matrix phase. The hydrogen composition of these hydride phases could also vary with temperature. In addition, since the lattice parameter values of hydride and matrix phases generally vary with temperature, but at different rates, this will result in the transformation strains having both a dependence on hydrogen composition and on temperature.

The strains in embedded hydride precipitates and surrounding matrix are relaxed from their imposed transformation (source) strain values according to the elastic or elastic-plastic constitutive behaviour of matrix and hydride. When the precipitate sizes/shapes are below some critical value, these relaxed (constrained) strains are governed only bv the elastic properties of hydride and matrix (i.e., they remain fully coherent with the matrix), whilst at and above their critical sizes, the constrained strains are determined from both the elastic and plastic constitutive relations of the two phases. The constrained strains will depend on temperature as a result of the temperature dependencies of the elastic properties of hydride and matrix phases and, in the case of elastic-plastic deformation, also on the temperature dependencies of the yield strengths of hydride and matrix phases. Under an applied stress there will also be an additional (induced) component of transformation strain produced when there is a difference in elastic properties between hydride and matrix phases. In this case, since – at the very least – the elastic properites of the matrix phase are anisotropic, the induced strains will also be anisotropic, being greatest along the direction of the maximum applied principal stress.

The dilatational components of the transformation strains cannot be reduced by the elastic or elastic-plastic response of hydride and matrix; they can only be redistributed. In addition, in the realistic case of a finite solid, the dilatational source strains produced by the formation of a hydride precipitate in the interior of the material are recovered at the free surface of the material. Dilational source strains can only be reduced to zero by removal of material at the hydride-matrix interface – such as, for instance, could occur by vacancy diffusion – to make possible the stress-free formation of the hydride precipitate within the matrix. Removal of material around the

hydride-matrix interface in this way is unlikely to occur at temperatures of practical interest related to the application of zirconium alloys in the nuclear industry.

As demonstrated in this text, hydride orientation is determined during the hydride nucleation stage. In the derivation of a hydride orientation model, classical nucleation theory was used with the assumption that the nucleating phase would be the stable δ–hydride phase having hydrogen composition as a function of temperature given by the high-hydrogen concentration side of the Zr-H phase diagram. It was recognized, however, that, because of the large increase in hydrogen concentration required to form this phase, it might be unlikely that this would actually be the phase forming during the nucleation process. Therefore the results obtained with this model should be considered as indicative (semi-quantitative) only. In fact, recent experimental and theoretical studies reviewed in this text have suggested that the first stage in hydride precipitate formation is likely the precipitation of the recently observed, metastable ζ–hydride phase for which the stoichiometric composition is Zr_2H. Further growth is then thought to result in the conversion these ζ–hydride precipitates to metastable γ–hydride precipitates which would ultimately transform to stable δ–hydride precipitates with hydrogen concentrations straddling the stoichiometric composition $ZrH_{1.5}$ (Zr_2H_3) of this phase. It is expected that the γ–hydride precipitates would have reached a size range above which the imposed transformation strains could be locally relaxed by both elastic and plastic deformation. The assumption of the existence of the latter deformation mode is consistent with experimental observations showing that the experiementally observed γ–hydride precipitates were always surrounded by a network of dislocations that appear to have been emitted from the surfaces of these acicular (needle or sword-shaped) precipitates. Both the increase in the number of precipitates with decrease in temperature and the initiation of plastic deformation would mean, however, that formation and dissolution of γ–hydride precipitates would involve hysteresis and therefore would not be possible at constant temperature by thermal fluctuations alone. However, during continuous cooling the progressive reduction in temperature ensures the presenc of a chemical driving force making possible the phase transformation of hydride precipitates from their γ– to their δ–hydride phases, consistent with the experimental observations by synchrotron XRD given in this text that only δ–hydride precipitates were observed during heating or cooling.

The question arising from the foregoing considerations is how does this affect the hydride orientation predictions made in this text based on the assumption that the critical nuclei are of the δ–hydride phase with hydrogen concentrations corresponding to those given in Zr-H phase diagrams?

Experimentally it has been observed that hydride precipitates tend to collect in clusters with individual precipitates slightly offset from each other in a quasi-linear chain. Based on theoretical calculations and experimental observations, two types of chains are most likely to form. One type consisting of a chain of precipitates with each successive precipitate in the chain having closely similar orientation as of the preceding ones but with its trailing edge close to, and slightly offset from, the leading edge of the preceding precipitate. The other type has a row of short platelets all of similar heights stacked like domino stones, but angled – as if they are in the process of falling – towards the long direction of the matrix grain axes in which they had formed. This latter type of stacking sequence was proposed by Vicente Alvarez and co-workers but was deemed repulsive by Perovic and co-workers, a conclusion supported by this writer for reasons given in the discussion in this text comparing the proposed hydride stacking schematics of the two sets of authors. Both sets of authors proposed stacking schematics basesd on the assumption that the individual hydride platelets making up these stacks consist of the δ–hydride phase and having, from the start, hydride nuclei shapes that are platelet-shaped. Experimental examinations of the make-up of hydride precipitates and their distributions at different size scales have also indicated that they consist (or consisted) of clusters of smaller hydrides having similar stacking sequences, regardless of the sizes of the component platelets making up these clusters; that is, geometrically, the hydride clusters have the property of a fractal and there is self-similarity in the make-up of these clusters between size scales.

Extrapolating the evolution of the hydride clusters to the size scale just above that corresponding to the formation of critical hydride nuclei, then, suggests that the critical step determining the overall orientation of the hydride clusters formed as they increase in size are the orientations of the first hydride precipitates formed during the nucleation stage. These considerations, then, suggest that, despite the complex makeup of the hydride clusters observed at optical magnifications, it appears that the orientations of the hydride nuclei predicted from the classical nucleation model largely determine the overall orientations of the macroscopic hydride clusters formed from them and that the most likely stacking arrangements of the component hydride precipitates are such that the orientations of the clusters are closely similar to the orientations of the smaller hydride precipitates making up the macroscopic clusters.

It is important to establish whether the experimentally observed hydride clusters had formed in the way described in the foregoing since the orientations of the initial hydride precipitates making up the macroscopic hydride clusters would then be indicative of the effective transformation strains (i.e., the source strains) applicable to the overall shapes of these clusters. These macroscopic clusters are of a size scale from which engineering data are usually derived for the fraction of radial to radial-plus-circumferential hydride orientations. If the orientations of the transformation strains of the underlying microscopic hydride precipitates making up clusters of these size scales can be established, then it may be possible to also predict the stresses in these clusters. Determining these stresses is a necessary first step in developing viable models of component fracture initiated at reoriented bulk hydrides.

References

Alam A.M. and Hellwig C., *Cladding Tube Deformation Test for Stress Reorientation of Hydrides,* J. ASTM Int. 5, Paper ID JAI101110, 2008

Aomi M. et al., *Evaluation of Hydride Reorientation Behaviour and Mechanical Properties for High-Burnup Fuel- Cladding Tubes in Interim Dry Storage*, Journal of ASTM International, Vol. 5, Issue 9, Paper ID JAI101262, 2009.

Babayak W.J., *Hydride Habit in Zirconium and in Unstressed and Stressed Zircaloy-4,* Trans. Met. Soc. AIME 239, p. 252, 1967

Bai J. Gilbon J., Prioul C., Francois D., *Hydride Embrittlement in Zircaloy-4 Plate: Part II. Interaction Between the Tensile Stress and the Hydride Morphology*, Met. and Materials Transactions, Vol. 25A, p. 1199, 1994.

Bailey J.E., *Electron Microscope Observations on the Precipitation of Zirconium Hydride in Zirconium,* Acta Metall. 11, p. 267, 1963

Beck R. L., *Zirconium-Hydrogen Phase System*, Trans. ASM 55, 542–555, 1962.

Billone M., Bursteva T.A. and Liu L., Argonne National Laboratory Report, ANL-12-58, 2012

Blat-Yrieix M. et al., *Toward a Better Understanding of Dimensional Changes in Zircaloy-4: What is the Impact Induced by Hydrides and Oxide Layer?*, 15th Zirconium in the Nuclear Industry, ASTM, Sunriver, OR, June 2007 and Journal of ASTM International, Vol. 5, No. 9 Paper ID JAI101321, www.astm.org

Borisov V.T., Golikov V.M. and Scherberdinsky G.V., Phys. Met. Metall. 17, p. 80, 1964

Bouffioux P., *Réorientation des Hydrures – Synthèse des Résultats Acquis pour les Gaines en Zircaloy-4* AFA-2G, EDF Report HT25-C2002-191/PB, 2002

Cahn J.W. and Hilliard J.E., *Free Energy of a Nonuniform System. I. Interfacial Free Energy*, J. Chem. Phys. 28, p. 258, 1958

Cahn J.W. and Hilliard J.E., *Nucleation in a Two-Component Incompressible Fluid,* J. Chem. Phys. 31, p. 688, 1959

Cameron D.J. and Duncan R.G., *On the Existence of a Memory Effect in Hydride Precipitation in Cold-Worked Zr-2.5% Nb,* J. Nuclear Materials 68, p. 340, 1977

Carpenter G.J.C., *The Dilatational Misfit of Zirconium Hydride Precipitated in Zr*, J. Nuclear Materials 48, p. 264, 1973.

Carpenter G., Watters J. and Gilbert R., *Dislocations Generated by Zirconium Hydrides in Zirconium and Some of its Alloys*, J. Nuclear Materials 48, p. 267, 1973.

Christian J.W., *The Theory of Transformations in Metals and Alloys*, Pergamon Press, Oxford, p. 416, 1965

Chu H., Wu S. and Kuo R., *Hydride Reorientation in Zircaloy-4 Cladding*, J. Nuclear Materials 373, p. 319, 2008.

Chung H.M., *Understanding hydride- and hydrogen-related processes in high-burnup cladding in spent-fuel-storage and accident situations* in: *Proceedings of the 2004 International Meeting on LWR Fuel Performance*, Orlando, Florida, September 19-22, 2004

Cinbiz M.N., Motta A.T. and Koss D.A., *Hydride Reorientation in Zircaloy-4 under Different States of Stress as Studied with in-situ X-Ray Diffraction,* J. Nuclear Materials 477, p. 157, 2016

Colas K. B. et al., *In situ Study of Hydride Precipitation Kinetics and Re-orientation in Zircaloy using Synchrotron Radiation*, Acta Mater. 58, p. 6575, 2010.

Colas K. et al., *In-situ Study of Hydride Reorientation Kinetics using Synchrotron Radiation*, 16th ASTM Zr Symposium, Chengdu, China, 2011.

Colas K.B., *Fundamental Experiments on Hydride Reorientation in Zircaloy* , PhD. Dissertation, Pennsylvania State University, University Park, 2012

Colas K., Motta A., Daymond M.R., Almer J., *Mechanisms of Hydride Reorientation in Zircaloy-4 Studied in Situ*, in: *Zirconium in the Nuclear Industry: 17th International Symposium*, Comstock A.J., Barbéris P. (Eds.), ASTM International, West Conshohocken, PA, 10428-2959, U.S.A., STP 1543, 2014

Colas, private communication, 2017.

Coleman C. E. and Inozemtsev V. V., *Measurement of Rates of Delayed Hydride Cracking (DHC) in Zr-2.5 Nb Alloys – an IAEA Coordinated Research Project*, J. ASTM International 5, 2008, Paper ID JAI101091. (Based on IAEA Report, IAEA-TECDOC-1410, 2004), 2008.

Coleman C.E. et al., *Delayed Hydride Cracking in Zircaloy Fuel Cladding – An IAEA Coordinated Research Programme,* Nuclear Eng. & Technol. 41, p. 1, 2009

Daum R., Majumdar S., Liu Y., Billone M., *Radial-Hydride Embrittlement of High-Burnup Zircaloy-4 Fuel Cladding*, Journal of Nuclear Science and Technology 43, No.9, p.1, 2006.

Daum R., Chu Y. and Motta A., *Identification and Quantification of Hydride Phases in Zircaloy-4 Cladding Using Synchrotron X-Ray Diffraction*, J. Nuclear Materials 392, p.453, 2009.

Delobelle P., Robinet P., Geyer P., Bouiffioux P., *A Model to Describe the Anisotropic Behaviour of Zircaloy--4 Tubes*, J. Nuclear Materials 238, p. 135, 1996.

Desquines J. et al., *Influence of Temperature and Hydrogen Content on Stress-induced Radial Hydride Precipitation in Zircaloy-4 Cladding*, J. Nuclear Materials 453, p. 131, 2014.

Dutton R. and Puls M.P., *A Theoretical Model for Hydrogen Induced Sub-Critical Crack Growth*, in: *Effect of Hydrogen on Behaviour of Materials*, A.W. Thompson and I.M. Bernstein, Eds., Metal Society, 516-528, AIME, New York, 1976.

Dutton R., Nuttall K., Puls M.P., Simpson L.A., *Mechanisms of Hydrogen Induced Delayed Cracking in Hydride Forming Materials,* Metall. Trans. A 8A, p. 1553, 1977

Ells C.E., *Hydride Precipitates in Zirconium Alloys*, J. Nuclear Materials 28, p. 129, 1968.

Ells C.E., *The Stress Orientation of Hydride in Zirconium Alloys*, J. Nuclear Materials 35, p. 306, 1970.

Eshelby J.D, *The Continuum Theory of Lattice Defects*, in: *Solid States Physics*, Seitz F., Turnbull D.(Eds.), Vol. 3, p. 79, Academic Press, New York, 1956

Eshelby J.D. *The Determination of the Elastic Field of an Ellipsoidal Inclusion, and Related Problems,* Proc. Roy. Soc. A241, p. 376, 1957

Eshelby J.D., *Elastic Inclusions and Inhomogeneities,* in: *Progress in Solid Mechanics*, Snedden N. I. and Hill R., Eds., Vol. 2, p. 89, North Holland, 1961

Fielding L.C.D., *The Bainite Controversy,* J. Mater. Sci. & Techno. 29, p. 383, 2013

Flanagan T.P., Park C.-N. and Oates W.A., *Hysteresis in Solid State Reactions,* Prog. Solid St. Chem. 23, p. 291, 1995

Flanagan M.E., in: *Proc. 2008 Water React. Fuel Perf. Meeting,* Seoul, Korea, 2008

Glendening A., Koss D.A., Motta A.T., Pierron A.T., Daum R.S, *Failure of Hydrided Zircaloy-4 under Equal-Biaxial and Plane-Strain Tensile Deformation*, J. ASTM Int. 2, paper ID12441, 2005

Goldak J., Lloyd L.T. and Barrett C.S., *Lattice Parameters, Thermal Expansions, and Grüneisen Coefficients of Zirconium, 4.2 to 1130°K,* Phys. Rev. 144, p. 478, 1966

Guo X.H., Shi S.-Q. and Ma X.Q., *Elastoplastic Phase Field Model for Microsctructure Evolution,* Applied Phys. Lett. 87, p. 221910, 2005

Guo X.H.R., Shi S.-Q., Zhang Q.M., Ma X.Q., *An Elastoplastic Phase Field Model for the Evolution of Hydride Precipitation in Zirconium, Part I: Smooth Specimen,* J. Nuclear Materials 378, p. 110, 2008a

Guo X.H.R., Shi S.-Q., Zhang Q.M., Ma X.Q., *An Elastoplastic Phase Field Model for the Evolution of Hydride Precipitation in Zirconium, Part II: Specimen with Flaws,* J. Nuclear Materials 378, p. 120, 2008b

Haeffner D.R., Almer J.D. and Lienert U. *The Use of High Energy X-rays from the Advanced Photon Source to Study Stresses in Materials*, Mater. Sci. & Eng. A 399, p. 120, 2005

Ham F.S., *Stress-assisted Precipitation on Dislocations*, J. Appl. Phys. 30, p. 915, 1959

Hardie D. and Shanahan M.W., *The Effect of Residual Stresses on Hydride Orientation in a Zirconium-2.5% Niobium Alloy*, J. Nuclear Materials 50, p. 40, 1974.

Hardie D. and Shanahan M.W., *Stress Re-Orientation of Hydrides in Zr-2.5% Nb*, J. Nuclear Materials 55, p. 1, 1975

Hellouin de Menibus A. et al., *Hydrogen Contribution to the Thermal Expansion of Hydrided Zircaloy-4 Cladding Tubes,* J. Nuclear Materials 440, p. 169, 2013

Hielscher R. and Schaeben H., *A Novel Pole Figure Inversion Method: Specification of the MTEX Algorithm*, J. Appl. Crystall. 41, p. 1024, 2008

Holliger L., Legris A. and Besson R., *Hexagonal-based Ordered Phases in H-Zr,* Phys. Rev. B 80, p. 094111-1, 2009

Holt R.A. and Aldridge S.A., *Effect of Extrusion Variables on Crystallographic Texture of Zr-2.5wt%Nb*, J. Nuclear Materials 135, p. 246, 1985.

Holt R.A. and Zhao P., *Micro-texture of Extruded Zr-2.5Nb Tubes*, J. Nuclear Materials 335, 520, 2004.

Hong S.I. and Lee K.W., *Stress-Induced Reorientation of Hydrides and Mechanical Properties of Zircaloy-4 Cladding Tubes*, J. Nuclear Materials 340, p. 203, 2005.

IAEA, IAEA-TECDOC 1410., *Delayed Hydride Cracking in Zirconium Alloys in Pressure Tube Nuclear Reactors*, 2004

Ishia G. et al., *Quantitative Rietveld Texture Analysis of Zirconium from Single Synchrotron Diffraction Images*, J. Appl. Crystall. 38, p. 377, 2005

Johnson W.C. et al., *Influence of Crystallography on Aspects of Solid-Solid Nucleation Theory*, Metall. Trans. A 6A, p. 911, 1975

Kammenzind B.F. et al., *The Long-Range Migration of Hydrogen through Zircaloy in Response to Tensile and Compressive Stress Gradients,* in: *Zirconium in the Nuclear Industry: Twelfth International Symposium*, Moan G.D., Rudling P. (Eds.), ASTM International,West Conshohocken, PA, 10428-2959, U.S.A., STP 1354, p. 196, 2000

Kearns J. and Woods C.R., *Effect of Texture, Grain Size and Cold Work on the Precipitation of Oriented Hydrides in Zircaloy Tubing and Plate*, J. Nuclear Materials 20, p. 241, 1966.

Kearns J., *Terminal Solubility and Partitioning of Hydrogen in the α Phase of Zirconium, Zircaloy-2, and Zircaloy-4*, J. Nuclear Materials 22, p. 292, 1967.

Kese K., *Hydride Re-Orientation in Zircaloy and its Effect on Tensile Properties*, SKI Report 98:32. 1998.

Khachaturyan A.G. and Shatalov G.A., Sov. Phys. JETP (English transl.) 29, p. 557, 1969

Khachaturyan A.G., *Theory of Structural Transformations in Solids*, Dover Publications Inc., Mineola, New York, 2008

Khatamian D. and Roots J.H., *Comparison of TSSD Results Obtained by DSC and Neutron Diffraction*, J. Nuclear Materials 372, p. 106, 2008.

Appendix A Derivations of Critical Nucleation Energies for the Formation of δ–Zirconium Hydride Precipitates

In the following, analytical expressions of various approximations for the critical nucleation energy and volume of a δ–hydride precipitate formed in α–Zr matrix are derived. The derivations are based on classical nucleation theory. In this approach an initial general shape is assumed for the incipient nucleus and the objective is to determine the actual size and relative dimensions of the critical nucleus for this general shape. The starting shape is deduced on the basis of the experimentally observed habit planes and shapes of hydride precipitates examined at sizes well past those of critical nuclei. Hence it is assumed that there would be no changes in general shape and transformation strains during growth of incipient hydride nuclei from critical to first observable sizes and beyond. In choosing a general shape for the nucleus, one criterion is that this shape must be consistent with the difference in crystal symmetries of hydride and matrix phases and the observed habit planes. This difference in symmetry results in anisotropies of surface and strain energies. The shape chosen, then, should be one that minimizes both the surface and strain energy contributions to the Gibbs free energy of hydride nucleus formation whilst accounting for these anisotropies.

In the following, for ease of calculations of the strain energy contributions to the change in total Gibbs free energy, the shape of the incipient nucleus is approximated by an oblate spheroid of minor axis, c, and major axis, a. However, since an oblate spheroid is not a convenient shape to account for the possibility that there are abrupt differences in the surface energies depending on the orientations of the interfaces between the hydride precipitate and the matrix, the shape of the nucleus is approximated by a circular disc of radius, a, and thickness, $2c$, having different surface energy values for the faces (γ_c) and the edge (γ_i) of such a disc. The habit plane of the hydride nucleus is assumed to have the following orientation relationship: $(0\ 0\ 0\ 2)_{\alpha-Zr} \approx \| (1\ 1\ 1)_{\delta}$ and $[1\ 1\ \bar{2}\ 0]_{\alpha-\mathrm{Zr}} \| (1\ \bar{1}\ 0)_{\delta}$. Thus, for homogenous nucleation (hydride nuclei formed intra-granularly) it is assumed that these disc-shaped nuclei are oriented in grains such that their face normals are parallel to the basal pole direction of the α–Zr matrix in which they are located. The hydrides can achieve such orientation relationships through a pure lattice strain transformation mechanism of the α–Zr matrix. An analysis by Carpenter [Carpenter, 1973] based on this mechanism yielded positive values of the diagonal components of the transformation strain matrix, with the two orthogonal transformation strains in the plane of the disc having equal but slightly smaller values than the transformation strain in the direction of the face normal of the disc-shaped precipitate. As a result, the transformation strains have tetragonal symmetry.

A much larger tetragonal symmetry of the transformation strains is obtained when it is assumed that hydride formation occurs via an invariant plane strain transformation mechanism. In this case it was shown by Weatherly [Weatherly, 1981] for γ–hydride precipitates that this results in hydride habit planes lying on planes that deviate slightly (≈ 14°) from the directions of the $\{0\ 0\ 0\ 2\}_{\alpha-\mathrm{Zr}}$ planes. Although a similar sequence of steps required to achieve the foregoing habit planes by this mechanism could not be derived by Perovic and co-workers [Perovic et al., 1984] for δ–hydride precipitates, the fact that such habit planes were observed for hydride precipitates of this shape suggested to these authors that a similar transformation mechanism as was postulated for the formation of γ–hydride precipitates should be applicable also to δ hydrides.

In the following general derivation of the specific shape and size of a hydride critical nucleus it is assumed that the crystallographic directions of the transformation strains are along the same directions regardless of whether they were derived assuming hydride formation occurs via a pure lattice strain transformation, as done by Carpenter [Carpenter, 1973] or via an invariant plane strain transformation mechanism as done by Perovic and co-workers [Perovic et al., 1984]. In both cases, then, the directions for the diagonal components of the transformation strains, e_{11}^T, e_{22}^T, e_{33}^T are: $< 1\ 1\ \bar{2}\ 0 >$, $< 1\ \bar{1}\ 0\ 0 >$, $< 0\ 0\ 0\ 1 >$, respectively, with the disc-shaped hydride precipitate oriented such that the x_1 and x_2 coordinates are along the two orthogonal edge-face directions (also, the *a* axis of the oblate spheroid) and the x_3 coordinate is in the face normal direction (also, the *c* axis of the oblate spheroid).

Additionally, it is assumed that the disc face of the hydride precipitate is coherent with the matrix with surface energy, γ_c, regardless of whether it had been formed via a pure lattice strain or an invariant plane strain transformation, whilst the disc edge is assumed to be incoherent with the matrix with surface energy, γ_i. That is, it is assumed that the choice of transformation mode affects only the transformation strains of the hydride nucleus – and hence its strain energy – but not significantly the surface energies in the disc- and edge-face directions. The total Gibbs free energy change, ΔG, for nucleation of an oblate spheroid (*sph*) having volume, $V_{sph} = 4/3\pi a^2 c$ is, then, given by:

Equation A-1:

$$G = \frac{4}{3}\pi a^2 c\left(\Delta g_{chem}^{hyd} + \Delta g_{strain}^{hyd} + \Delta g_{int}^{hyd}\right) + 2\pi a^2 \gamma_c + 4\pi ac\gamma_i$$

where Δg_{chem}^{hyd} = change in chemical Gibbs free energy of the hydride phase from its equilibrium (incoherent) solvus composition (i.e. excluding energy contributions from coherency misfit strains between hydride and matrix) and when the H composition in the α–Zr phase is in excess of the equilibrium solvus composition

Δg_{strain}^{hyd} = change in strain energy of hydride precipitate and matrix produced by a misfitting, coherent hydride precipitate

Δg_{int}^{hyd} = interaction energy with internal or external stresses produced when a hydride precipitate forms or dissolves in the presence of these stresses

γ_c = coherent surface energy between hydride precipitate and matrix

γ_i = incoherent surface energy between hydride precipitate and matrix

All of the energies within the brackets of Equation A-1 are per unit volume whilst the surface energies are per unit area. Note that with the foregoing definition, Δg_{chem}^{hyd} is negative when the α–Zr lattice is supersaturated in hydrogen (i.e., has a greater value) at a given temperature with respect to its equilibrium solvus composition. For nucleation to be possible, this energy must be sufficiently negative to overcome the positive surface and self-strain energies of nucleus formation in addition to any positive net interaction energies.

The foregoing self-strain and interaction energies of the nucleus, expressed per unit volume, are generally given in the literature as partial molar quantities either per mole Zr or per mole H, denoted by this writer by $\Delta \bar{g}_{strain}^{hyd}$ and $\Delta \bar{g}_{int}^{hyd}$, respectively. In linear elastic derivations of these energy changes the strains are calculated from a reference state given by the hydrogen free, undistorted α–Zr lattice, the partial molar volume of which is given by $\bar{V}_{Zr}^{\alpha-Zr}$. Hence, these strain and interaction energies are most straightforwardly given per mole Zr. Dividing $\Delta \bar{g}_{strain}^{hyd}$ and $\Delta \bar{g}_{int}^{hyd}$ by $\bar{V}_{Zr}^{\alpha-Zr}$ when the latter are given as per mole Zr, then, converts these energies to those per unit volume. Account also needs to be taken of the H/Zr atom or mole ratio, r_H^{β}, in each phase, β, when converting the energies per atom (or mole) Zr to the more convenient form per atom (or mole) H. Thus the following conditions apply between the Gibbs free energy changes per unit volume in Equation A-1 and those expressed as per mole H (assuming here that β corresponds to the δ–hydride phase):

Equation A-2:

$$\Delta g_{strain}^{hyd} = \frac{r_H^{\delta}}{\bar{V}_{Zr}^{\alpha-Zr}} \Delta \bar{g}_{strain}^{hyd}$$

Equation A-3:

$$\Delta g_{int}^{hyd} = \frac{\Delta \bar{g}_{int}^{hyd}}{\bar{V}_{Zr}^{\alpha-Zr}}$$

The general form of the partial molar interaction energy, $\Delta \bar{g}_{int}^{hyd}$, in Equation A-3, applicable to an inclusion (a misfitting precipitate having the same lattice constants as the matrix) and based on the linear elastic expressions derived by Eshelby [Eshelby, 1957, 1961], is given for a hydride precipitate by:

Equation A-4:

$$\Delta \bar{g}_{int}^{hyd} = -\frac{\bar{V}_{Zr}^{\alpha-Zr} \sigma_{ij} e_{ij}^{T}}{r_H^{\delta}}$$

where σ_{ij} = stress matrix

e_{ij}^{T} = hydride transformation strain matrix

r_H^{δ} = hydrogen concentration in hydride given as ratio of H/Zr (atom or mole)

Conversion to this molar quantity is necessary for a one-to-one comparison with the partial molar interaction energy of hydrogen in solution.

Hence from Equation A-3 and Equation A-4, the interaction energy per unit volume is given by:

Equation A-5:

$$\Delta g_{int}^{hyd} = -\frac{\sigma_{ij} e_{ij}^{T}}{r_H^{\delta}}$$

In Equation A-4 and Equation A-5, the stress matrix, σ_{ij}, refers, in general, to any stresses that are from sources other than those produced by the inclusion or defect itself, and acting at the centre of the inclusion or defect, uniform over its volume. As shown further on, a similar expression as Equation A-5 applies to the interaction energy with external stresses of hydrogen atoms that are in solution in the α–Zr matrix, but in this case without the explicit inclusion of the factor, r_H, since the dimensionless transformation strains, e_{ij}^{T}, are replaced by the λ-tensor strains, which have units of transformation strain per r_H.

Hydride-matrix strain energy: To allow for an analytical solution in the minimization of the total Gibbs free energy given further on, a simple analytical expression, valid when $c/a \ll 1$, due to Christian [Christian, 1965] is used for Δg_{strain}^{hyd}:

Equation A-6:

$$\Delta g_{strain}^{hyd} = \frac{E}{1-\nu}\Delta^2 + \frac{E}{1-\nu}\frac{\pi}{2}\frac{c}{a}\left[\Delta \cdot \xi + \frac{1}{4(1+\nu)}\xi^2 + \frac{1}{8}\frac{(2-\nu)}{(1+\nu)}s^2\right]$$

where E = elastic modulus

ν = Poisson's ratio

Δ = isotropic component of hydride transformation strains

ξ = hydride transformation strain in the direction of the plate face in excess of the isotropic component

s = shear strain in the plane of the plate

From the foregoing, in the strain energy expression given by Equation A-6 the coordinate system with axes $x_1,\ x_2\ ,\ x_3$ is oriented so that the plate normal (also, oblate spheroid minor axis, c) is along the x_3 direction and the other two orthogonal directions are in the plane of the plate (also, along the oblate spheroid major axis, a). The following correspondences then apply between the misfit strains given in Equation A-6 and the non-zero components of the hydride precipitate's transformation strains, e_{11}^{T}, e_{22}^{T}, e_{33}^{T}, e_{12}^{T}:

Equation A-7:

$$e_{11}^{T} = e_{22}^{T} = \Delta$$

Equation A-8:

$$e_{33}^{T} = \Delta + \xi$$

Equation A-9:

$$e_{12}^{T} = e_{21}^{T} = \frac{s}{2}$$

All other shear transformation strains are assumed to be zero.

Appendix B Derivation of Relationship between Hydrogen in Solution in the α–Zr Phase at the Solvus and the Normalized Hydride Peak Intensities

The starting point for the following derivation is based on the experimental observation that at temperatures below about 50°C it is a good approximation to assume that almost all of the total hydrogen content in the solid has precipitated as hydrides and, hence, the amount of hydrogen in solid solution is approximately equal to zero. Thus the initial room temperature peak intensity represents the hydride volume fraction corresponding to the total hydrogen content in the sample. The hydride volume fraction, $f_v^\delta(T)$, at temperatures above ambient (taken here to be 25°C) can then be obtained, assuming a linear relationship between hydride peak intensity, $I(T)$, and volume fraction, $f_v^\delta(T)$, through the ratio:

Equation B-1:

$$f_v^\delta(T) = \frac{I(T)}{I(25°\mathrm{C})} \times f_v^\delta(25°\mathrm{C})$$

An expression for the solvus concentration as a function of temperature, $[\mathrm{H}]_{at}^{\alpha}$, corresponding to the experimentally determined value of $f_v^\delta(T)$ given by Equation B-1 is then derived making use of the law of conservation of mass (lever law).

From the lever law the following relationship is obtained between the solvus concentration $[\mathrm{H}]_{at}^{\alpha}$ and the atomic fraction of the δ–hydride phase, $f_{at}^\delta(T)$ where, for brevity, $f_{at}^\delta(T)$ in the following is denoted by f_{at}^δ:

Equation B-2:

$$[\mathrm{H}]_{at}^{\alpha} = \frac{[\mathrm{H}]_{at}^{tot} - f_{at}^\delta [\mathrm{H}]_{at}^\delta}{1 - f_{at}^\delta}$$

In Equation B-2 $[\mathrm{H}]_{at}^{tot}$ is the total hydrogen content in the sample and $[\mathrm{H}]_{at}^\delta$ is the hydrogen content of the δ–hydride phase. (All concentration units (denoted by square brackets) are in atom fractions.)

To obtain a relationship between the solvus concentration given by Equation B-2 from the δ–hydride volume fraction given by Equation B-1 requires deriving a relationship between f_{at}^δ and f_v^δ. This derivation is given in the following.

We start by recognizing that the total volume of a given amount of two-phase material, V^{tot}, can be expressed by the sum of:

Equation B-3:

$$V^{tot} = V^\alpha + V^\delta$$

where V^α = total volume of the α–Zr phase

V^δ = total volume of the δ–hydride phase in the sample

The volume fraction of the δ–hydride phase, f_v^δ, is then obtained from Equation B-3 by:

Equation B-4:

$$f_v^\delta = \frac{V^\delta}{V^\alpha + V^\delta}$$

The total volumes of the α–Zr and δ–hydride phases can also be expressed, respectively, by:

Equation B-5:

$$V^\alpha = f_{at}^\alpha \Omega_{Zr}^\alpha [\mathrm{Zr}]_{at}^\alpha = f_{at}^\alpha \Omega_{Zr}^\alpha (1 - [\mathrm{H}]_{at}^\alpha)$$

Equation B-6:

$$V^{\delta} = f_{at}^{\delta}\Omega_{Zr}^{\delta}[\mathrm{Zr}]_{at}^{\delta} = f_{at}^{\delta}\Omega_{Zr}^{\delta}(1 - [\mathrm{H}]_{at}^{\delta})$$

In Equation B-5 and Equation B-6, Ω_{Zr}^{δ} is the volume of the primitive cell of the δ–hydride phase, which means that it contains only one Zr atom; Ω_{Zr}^{α} is the volume of the primitive cell of the α–Zr phase which similarly means that it contains only one Zr atom; the concentrations $[\mathrm{Zr}]_{at}^{\delta}$ and $[Zr]_{at}^{\alpha}$ are the concentrations of Zr atoms in units of atom fraction in the respective α–Zr and δ–hydride phases. That is, they are defined by the relations:

Equation B-7:

$$[Zr]_{at}^{\alpha} = \frac{N_{Zr}^{\alpha}}{N_{H}^{\alpha} + N_{Zr}^{\alpha}}$$

Equation B-8:

$$[Zr]_{at}^{\delta} = \frac{N_{Zr}^{\delta}}{N_{H}^{\alpha} + N_{Zr}^{\alpha}}$$

whilst the H content in the α–Zr and δ–hydride phases, $[\mathrm{H}]_{at}^{\alpha}$ and $[\mathrm{H}]_{at}^{\delta}$, are defined by:

Equation B-9:

$$[\mathrm{H}]_{at}^{\alpha} = \frac{N_{H}^{\alpha}}{N_{H}^{\alpha} + N_{Zr}^{\alpha}}$$

Equation B-10:

$$[\mathrm{H}]_{at}^{\delta} = \frac{N_{H}^{\delta}}{N_{H}^{\delta} + N_{Zr}^{\delta}}$$

where, for a given amount of material, N_{H}^{α} is the total number of H atoms and N_{Zr}^{α} is the total number of Zr atoms in the α–Zr phase and similarly for the δ–hydride phase. With these definitions for the concentrations, then: $[\mathrm{Zr}]_{at}^{pha} + [\mathrm{H}]_{at}^{pha} = 1$ where *pha* stands for α or δ and, hence, one can replace $[\mathrm{Zr}]_{at}^{pha}$ with $1 - [\mathrm{H}]_{at}^{pha}$ in Equation B-5 and Equation B-6 for the respective phases, α Zr and δ hydride as was done in the far right hand side of the latter two equations.

From Equation B-4 to Equation B-6, the relationship between f_{at}^{δ} and f_{v}^{δ} is then given by:

Equation B-11:

$$f_{v}^{\delta} = \frac{\Omega_{Zr}^{\delta}(1 - [\mathrm{H}]_{at}^{\delta})f_{at}^{\delta}}{\Omega_{Zr}^{\alpha}(1 - [\mathrm{H}]_{at}^{\alpha})(1 - f_{at}^{\delta}) + \Omega_{Zr}^{\delta}(1 - [\mathrm{H}]_{at}^{\delta})f_{at}^{\delta}}$$

where f_{at}^{α} in the first term in the denominator in Equation B-11 has been replaced by $(1 - f_{at}^{\delta})$ since $f_{at}^{\alpha} + f_{at}^{\delta} = 1$. Equation B-11 can be used to calculate $f_{v}^{\delta}(25°)$ by replacing f_{at}^{δ} in this equation with its value at 25°C. The latter is obtained from the lever law relation, which can be given for the general case by:

Equation B-12:

$$f_{at}^{\delta}(T) = \frac{[\mathrm{H}]_{at}^{\alpha} - [\mathrm{H}]_{at}^{tot}}{[\mathrm{H}]_{at}^{\alpha} - [\mathrm{H}]_{at}^{\delta}}$$

Assuming that at $T = 25°\mathrm{C}$, $[\mathrm{H}]_{at}^{\alpha} \cong 0$, then Equation B-12 becomes:

Equation B-13:

$$f_{at}^{\delta}(25°\mathrm{C}) = \frac{[\mathrm{H}]_{at}^{tot}}{[\mathrm{H}]_{at}^{\delta}}$$

Appendix C References

Carpenter G.J.C., *The Dilatational Misfit of Zirconium Hydride Precipitated in Zr*, J. Nuclear Materials 48, p. 264, 1973.

Christian J.W., *The Theory of Transformations in Metals and Alloys*, Pergamon Press, Oxford, p. 416, 1965

Eshelby J.D., *The Determination of the Elastic Field of an Ellipsoidal Inclusion, and Related Problems,* Proc. Roy. Soc. A241, p. 376, 1957

Eshelby J.D., *Elastic Inclusions and Inhomogeneities,* in: *Progress in Solid Mechanics*, Snedden N. I. and Hill R., Eds., Vol. 2, p. 89, North Holland, 1961

Li J.C.M., Oriani R.A. and Darken L.S., *The Thermodynamics of Stressed Solids*, Z. Physik Chem. Neue Folge 49, 271-279, 1966.

MacEwen S.R., Coleman C.E. and Ells C.E., *Dilation of h.c.p. Zirconium by Interstitial Deuterium,* Acta Metall. 33, p. 753, 1985

Perovic V. and Weatherly G.C., *The Nucleation of Hydrides in Zr-2.5 wt% Nb Alloy,* J. Nuclear Materials 126, p. 160, 1984

Puls M.P., *Hydrogen-Induced Delayed Cracking: 2. Effect of Stress on Nucleation, Growth and Coarsening of Zirconium Hydride Precipitates,* Atomic Energy of Canada Limited Report, CNL, Chalk River, Ontario, Canada, AECL-8381, 1984a

Puls M.P., *Elastic and Plastic Accommadation Effects on Metal-Hydride Solubility,* Acta Metall. 32, p. 1259, 1984b

Puls M.P., *Effect of Stress on Hydride Reorientation in Zirconium Alloys,* in: *Solute-Defect Interaction: Theory and Experiment*, Saimoto S., Purdy G.R., Kidson, G.V. (Eds.), Pergamon Press, p. 426, 1986

Puls M.P., *Effect of Hydrogen and Hydrides on the Integrity of Zirconium Alloy Components: Delayed Hydride Cracking*, ISSN 1612-1370, Springer-Verlag, London, UK, 2012

Weatherly G.C., *The Precipitation of γ–hydride Plates in Zirconium,* Acta Metall. 29, p. 501, 1981

Zanellato O. et al., *Synchrotron Diffraction Study of Dissolution and Precipitation Kineticsof Hydrides in Zircaloy-4* , J. Nuclear Materials 420, p. 537, 2012

Zuzek E. et al., in: *Phase Diagrams of Binary Alloys: H-Zr (hydrogen-zirconium)*, ASM International, Ohio, p. 309, 2000

Acronyms and Abbreviations

DHC	Delayed Hydride Cracking
TSS	Terminal Solid Solubility
TSSD	Terminal Solid Solubility Dissolution
TSSP	Terminal Solid Solubility Precipitation
TSSP1	Terminal Solid Solubility Precipitation 1
TSSP2	Terminal Solid Solubility Precipitation 2
SAR	Stand Alone Report
PFM	Phase Field Methodology
ID	Inner Diameter
OD	Outer Diameter
SEM	Scanning Electron Microscope
TEM	Transmission Electron Microscope
XRD	X-Ray Diffraction
RXA	Recrystalized Annealed
RD	Rolling Direction of a plate
WD	Width Direction of a plate
TD	Transverse Direction of a plate
ND	Normal Direction of a plate
SRA	Stress Relieved Annealed
wppm	weight parts per million
hcp (h.c.p.)	hexagonal close packed
fcc	face centred cubic
EBSD	Electron Back Scattering Diffraction
PHWR	Pressurized Heavy Water Reactor
PWR	Pressured Water Reactor
RHT	Radial hydride precipitation Heat Treatment (also Radial Hydride Treatment)
HRT	Hydride Reorientation Treatment
CCT	C-shaped Compression Test
ASTM	American Society of Testing and Materials
CWSR	Cold Worked Stress Relieved
FE	Finite Element
2-D, 3-D	Two (2) or three (3) Dimension
RHF	Radial Hydride Fraction
F-ANP	Framatom Advance Nuclear Products
HBR	H.B. Robinson (reactor)
CTDT	Cladding Tube Deformation Test
RT	Room Temperature
BWR	Boiling Water Reactor
DSC	Differential Scanning Calorimeter
DEM	Dynamic Elastic Modulus
FWHM	Full Width Half Maximum
HAZ	Heat Affected Zone
ODF	Orientation Distribution Function
HT	Heat Treatment
PLTS	Pure Lattice Transformation Strain
PLST	Pure Lattice Strain Transformation (same meaning as PLTS)
IPST	Invariant Plane Strain Transformation
PSTS	Pure Shear Transformation Strain (same meaning as IPST)
CANDU™	CANada Deuterium Uranium
CCD	Charge Coupled Device
KS	Khachaturyan Shatalov
IF	Internal Friction

Nomenclature

Nomenclature used by this author:

J^*	time-dependent nucleation rate (the superscript * denotes quantities evaluated at the size of the critical nucleus)
Z	Zeldovich non-equilibrium factor
β^*	rate at which atoms are added onto the critical nucleus
N	number of atomic nucleation sites per unit volume
r_H	atom ratio H/Zr
β_{phas}	number of energetically equivalent interstitial H sites per Zr atoms in a phase, with $\beta_{phas} = 1, 1, 1.5, 2$ for $phas =$ α–Zr, γ–, δ– and ε–hydride phases, respectively
c_H	$= r_H / \beta_{phas}$
c_H^β	H/Zr mole (or atom) ratio of solute component (H in this text) in the critical nucleus (where β designates the precipitate phase, which for hydrides could be either the δ, γ or ε phase)
ΔG^*	Gibbs free energy of activation for critical nucleus formation
τ	nucleation incubation time
t	isothermal reaction (hold) time
$k_B T$	product of Boltzmann constant and absolute temperature, respectively
n	number of atoms in an embryo
n^*	number of atoms in the critical nucleus
ΔG^o	Gibbs free energy change for the formation of a cluster of n solute atoms
S^*	disordered area of the critical nucleus (i.e., the area of the nucleus over which single solute atoms could be added)
D	appropriate diffusivity
c_H^α	atom fraction of solute (H) in the α–Zr matrix phase ($\equiv r_H / \beta_{\alpha\text{–Zr}} = r_H$) since $\beta_{\alpha\text{–Zr}} = 1$
a^*	major axis of critical nucleus when modelled as having the shape of an oblate spheroid, or radius when modelled as a disc
c_H^o	H/Zr atom ratio of solute (H) in the supersaturated solution of the α–Zr phase; this is equivalent to c_H^α, but denoted here by c_H^o to indicate that in a closed system – cooling from a temperature at which all hydrides had been dissolved – it is the total hydrogen content in the solid
D_H^v	volume diffusion coefficient of the solute (H)
d	jump distance of solute (H) in the matrix (α–Zr) phase (≈ one lattice parameter)
$\boldsymbol{\sigma}$	applied and/or residual stress vector
$\Delta g_{chem}^{hyd}(\boldsymbol{\sigma})$	change in chemical Gibbs free energy of a solid under stress, $\boldsymbol{\sigma}$, of the hydride phase from its equilibrium (incoherent) solvus composition (i.e., excluding energy contributions from

	coherency misfit strains between hydride and matrix) when the H composition in the α–Zr phase is in excess of its equilibrium solvus composition
Δg_{strain}^{hyd}	change in strain energy of hydride precipitate and matrix produced by a misfitting, coherent, or partially coherent hydride precipitate
$\Delta \bar{g}_{strain}^{hyd}$	partial molar strain energy of Δg_{strain}^{hyd}
Δg_{int}^{H}	change in interaction energy with internal or external stresses produced when an H atom is added or removed in the presence of these stresses
$\Delta \bar{g}_{int}^{H}$	partial molar interaction energy of Δg_{int}^{H}
γ_c	coherent surface energy between hydride precipitate and matrix
γ_i	incoherent surface energy between hydride precipitate and matrix
a^*	semi-major axis of critical nucleus when modelled as having the shape of an oblate spheroid or radius of disc when modelled as a disc
c^*	semi-minor axis of critical nucleus when modelled as having the shape of an oblate spheroid or half thickness of disc when modelled as a disc
ε^*	$= c^*/a^*$
R	gas constant
T_n	absolute value of the hold temperature at which the nucleation rate is being determined corresponding to a chosen undercooling from the incoherent solvus
$\Delta g_{chem}^{'H}$	change in chemical free energy excluding the term(s) involving internally and/or externally applied stresses
$\bar{V}_{Zr}^{\alpha-Zr}$	partial molar volume of Zr in the α–Zr phase
$\bar{V}_{H}^{\alpha-Zr}$	partial molar volume of H in α Zr ($= N_A \Delta v \equiv \left.\frac{\partial V}{\partial n_H}\right\|_{T,P,n_j}$)
$\bar{V}_{H}^{\delta-hyd}$	partial molar volume of H in the δ–hydride phase
$c_H^{\alpha-Zr}(\boldsymbol{\sigma})$	H/Zr atom ratio in solution in the α–Zr phase as a function of externally applied stress, $\boldsymbol{\sigma}$
$\mu_H^{\alpha-Zr}(\boldsymbol{\sigma})$	chemical potential of H in solution in the α–Zr phase as a function of externally applied stress, $\boldsymbol{\sigma}$
μ_H^o	chemical potential of H in an arbitrary reference state
Δv	partial atomic volume of H in the α–Zr phase
N_A	Avogadro's number
n_H	number of moles of dissolved H atoms in the metal (Zr) with the derivative (see $\bar{V}_H^{\alpha-Zr}$ above) taken at constant temperature, T, pressure, P, and other mole numbers, n_j
V	volume of the metal in its single-phase, α–Zr state
ΔH_E	enthalpy of hydride formation or dissolution assuming no hysteresis between hydride formation and dissolution

Unit conversion

TEMPERATURE		
°C + 273.15 = K	°C × 1.8 + 32 = °F	
T(K)	T(°C)	T(°F)
273	**0**	32
289	16	61
298	25	77
373	**100**	212
473	**200**	392
573	**300**	572
633	360	680
673	**400**	752
773	**500**	932
783	510	950
793	520	968
823	550	1022
833	560	1040
873	**600**	1112
878	605	1121
893	620	1148
923	650	1202
973	**700**	1292
1023	750	1382
1053	780	1436
1073	**800**	1472
1136	863	1585
1143	870	1598
1173	**900**	1652
1273	**1000**	1832
1343	1070	1958
1478	1204	**2200**

Radioactivity	
1 Sv	= 100 Rem
1 Ci	= 3.7×10^{10} Bq = 37 GBq
1 Bq	= 1 s^{-1}

MASS	
kg	lbs
0.454	**1**
1	2.20

DISTANCE	
x (µm)	x (mils)
0.6	0.02
1	0.04
5	0.20
10	0.39
20	0.79
25	0.98
25.4	**1.00**
100	3.94

PRESSURE		
bar	MPa	psi
1	0.1	14
10	**1**	142
70	7	995
70.4	7.04	**1000**
100	10	1421
130	13	1847
155	15.5	2203
704	70.4	**10000**
1000	100	14211

STRESS INTENSITY FACTOR	
MPa$\sqrt{m}$	ksi$\sqrt{inch}$
0.91	**1**
1	1.10